

Nanoscale

Accepted Manuscript



This is an *Accepted Manuscript*, which has been through the Royal Society of Chemistry peer review process and has been accepted for publication.

Accepted Manuscripts are published online shortly after acceptance, before technical editing, formatting and proof reading. Using this free service, authors can make their results available to the community, in citable form, before we publish the edited article. We will replace this *Accepted Manuscript* with the edited and formatted *Advance Article* as soon as it is available.

You can find more information about *Accepted Manuscripts* in the [Information for Authors](#).

Please note that technical editing may introduce minor changes to the text and/or graphics, which may alter content. The journal's standard [Terms & Conditions](#) and the [Ethical guidelines](#) still apply. In no event shall the Royal Society of Chemistry be held responsible for any errors or omissions in this *Accepted Manuscript* or any consequences arising from the use of any information it contains.

Polymorphic phase transition among the titania crystal structures in solution based approach:

From precursor chemistry to nucleation process

S. Girish Kumar, K. S. R. Koteswara Rao*

Department of Physics, Indian Institute of Science, Bangalore-560012, Karnataka, INDIA

E-mail: ksrkrao@physics.iisc.ernet.in ; raoksrk@gmail.com

Abstract

Nanocrystalline titania has been the robust candidate for various functional applications owing to its non-toxicity, cheap availability, ease of preparation and exceptional photochemical and thermal stability. The uniqueness in each lattice structure of titania leads to multifaceted physico-chemical and opto-electronic properties giving different functionalities, thus influencing their performance in various green energy applications. The high temperature treatment for crystallizing the titania triggers inevitable particle growth and destruction of delicate nanostructural features. Thus, preparation of crystalline titania with tunable phase/particle size/morphology at low to moderate temperature from solution based approach has opened the grand research avenue. In this focused review, titania synthesis from hydrothermal/solvothermal, conventional sol-gel method and sol-gel assisted via ultrasonication, photoillumination and ILs, thermolysis and microemulsion routes are discussed. These wet chemical methods has broader visibility, since multiple reaction parameters such as precursor chemistry, surfactants, chelating agents, solvents, mineralizer, solution pH, aging time, reaction temperature/time, inorganic electrolytes, etc., can be easily manipulated to tune the final physical structure. This review sheds light on the stabilization/phase transformation pathways of titania polymorphs like anatase, rutile, brookite and $\text{TiO}_2(\text{B})$ under variety of reaction conditions. The driving force for crystallization arising from complex species in solution coupled with solution pH and ion species facilitating the orientation of octahedral resulting in crystalline phase is reviewed in detail. Besides titanium halide/alkoxide, nucleation of titania from other precursors like peroxy and layered titanates are also emphasized. The non-aqueous route and ball milling

induced titania transformation is briefly outlined. The lacunae in understanding the concepts and future prospects in this exciting field are suggested.

Acryonms

Acetylacetone	AcAc	Nuclear Magnetic Resonance	NMR
Acetic acid	AcOH	Oriented Attachment	OA
Anatase to Rutile Phase Transition	ART	Ostwald Ripening	OR
Anatase to Brookite Phase Transition	ABT	Polyethylene Oxide	PEO
Benzyl Alcohol	BA	Polypropylene Oxide	PPO
Brookite to Anatase Phase Transition	BAT	Peroxo Titanate Complex	PTC
Brookite to Rutile Phase Transition	BRT	Polyvinylpyrrolidone	PVP
Conduction Band	CB	Point of Zero Charge	PZC
Cetyltriethyl Ammonium Bromide	CTAB	Room Temperature	RT
Cetyltrimethyl Ammonium Chloride	CTAC	RT Ionic Liquids	RTILs
Critical Micellar Concentration	CMC	Titanium (IV) bis (ammonium lactate) dihydroxide complex	TiBALDH
Diethanolamine	DEA	Triethyl Amine	TEA
Energy of Activation	E_a	Tetra Butyl Ammonium Hydroxide	TBAOH
Differential Scanning Calorimetry	DSC	Tetra Ethyl Ammonium Hydroxide	TEAOH
Ethylenediamine	ED	Transmission Electron Microscopy	TEM
Fourier Transform-Infra Red	FTIR	Thermogravimetric Analysis	TGA
Ionic Liquids	ILs	Titanium n-butoxide	Ti(OBu) ₄
Isopropyl Alcohol	IPA	Titanium Tetra Isopropoxide	TTIP
Johnson-Mehl-Avrami-Kolmogorov	JMAK	TiO ₆ Octahedra	[TiO ₆]
Luarylamine Hydrochloride	LAHC	Tetra Methyl Ammonium Hydroxide	TMAOH
Methyl Cellulose	MC	X-ray Diffraction	XRD
Nanoparticles	NPs	X-ray Photoelectron Spectroscopy	XPS
Nanorods	NRs	Valence Band	VB

1.0 Introduction

The polymorphic TiO_2 is extensively studied nanomaterial envisaged because of its specific properties and important roles in alleviating environmental and energy crisis through effective utilization of solar energy. The landmark report on photocatalytic splitting of water using TiO_2 electrode has triggered in exploring its applications in diverse areas like photocatalysis, photovoltaics, batteries, photonic crystals, UV blockers, smart coatings, and filling materials in textiles, paints, papers, cosmetics and biomedical sciences.¹⁻⁵ Titania is blessed with numerous unique features such as high redox potential, inexpensiveness, non-toxicity, good stability towards adverse environment, hydrophilicity, humidity and gas sensing, dielectric character, favorable band edge positions, facile preparation with diverse morphologies, etc.⁶⁻¹⁰ Most of the fascinating properties of titania NPs originates from size quantization effect. By decreasing the particle size, bandgap widens as reflected by blue shift in the absorption edge. The shift of CB and VB towards more negative and positive potentials respectively favors redox process that cannot occur in their bulk counterparts.¹¹

Each crystalline forms of titania have been spotlighted in the spectrum of applications and lattice structure differences among the polymorphs quite often leads to multifaceted physico-chemical and opto-electronic properties that controls electronic structure and bulk diffusion ability of charge carriers. For instance, rutile has high refractive index, exceptional light scattering efficiency and UV absorptivity enabling its utility as filter in solar creams, pigments, opacifiers and optical communication devices (isolators, modulators and switches),¹²⁻¹³ while anatase is largely preferred in photocatalysis and photovoltaics. Though brookite and $\text{TiO}_2(\text{B})$ are rare polymorph in nature and are synthesized only under sensitive conditions, its importance was recently realized in photocatalysis, photovoltaics and lithium ion insertion.¹⁴⁻¹⁷ In addition, some structural features of a polymorph will be vital than others depending on application: size or surface area to volume ratio play a central role in

catalysis,¹⁸ while controlling their size and shape (exposed facet) is important for fabricating photonic crystals, providing more flexibility and options for the design of nanostructures to satisfy unique requirements.¹⁹ The mixed crystal framework of titania is also beneficial for green energy technologies, pointing to the possibility of achieving optimized performances via controlling the phase composition. The morphology at the polymorphic interfaces and surface states are critical for such synergistic effect and intimate contact between the phases exhibit “magic effects” on charge carrier transfer dynamics in light induced photoreactions. The different bandgap as well as the position of CB and VB edges results in the formation of stable heterojunction that allows absorption of wide spectral range and improves charge carrier dynamics-generation, separation and transfer process.²⁰⁻²⁵

The study on the phase transition of titania polymorphs is an active area of research from the view point of flourishing scientific interest and technological applications. Since, there is no equilibrium temperature between the polymorphs of titania, specific or particular temperature regime for the phase transition to occur is not well defined. It is unambiguously accepted that intrinsic parameters such as particle size, purity, nature of titanium precursor, surface energy, density of intrinsic and induced defects, aggregation tendency or particle packing, solution chemistry, crystal growth dynamics, etc, coupled with external factors like peptization, addition of modifiers/surfactant/chelating agents and annealing ambience governs the temperature and activation energy of any phase transformation pathways.²⁶⁻³³ Owing to such complexities, it is inevitable to find a simple method to control size-shape-phase conveniently. The defect richness and structural diversity in TiO₂ can be manipulated via careful monitoring of processing conditions. Between the several wet and dry methods, synthesis from homogeneous solution via wet chemical approaches seems to be very promising as multiple reaction parameters like precursor concentration, chelating agents, solvents, mineralizer, solution pH, aging time, reaction temperature, kinetics of precursor

hydrolysis etc., can be easily adjusted to tailor the intrinsic properties of final crystal structure. The solution approach offers the possibility to control over the reaction pathways on a molecular level during the transformation of precursor species into final products enabling the synthesis with well-defined crystal polymorph and morphologies without impurities.³⁴⁻³⁷ More importantly, it dispenses the impurity doping into titania matrix to achieve desired phase stabilization/transition. The wide focus from wet chemical approaches is reviewed to shed light on solution chemistry and complex species responsible for the nucleation of particular crystal structure.

2.0 Structural features of titania polymorphs

The TiO_2 exists in several crystallographic forms like anatase ($a=b=3.785 \text{ \AA}$, $C = 9.514 \text{ \AA}$; space group D_{4h}^{19} , $I4_1/amd$), brookite ($a=5.143 \text{ \AA}$, $b=5.456 \text{ \AA}$, $C = 9.182 \text{ \AA}$; space group D_{2h}^{15} , $pbca$), rutile ($a=b=4.593 \text{ \AA}$, $C = 2.959 \text{ \AA}$; space group D_{4h}^{14} , $P4_2/mnm$) and TiO_2 (B) ($a= 12.1787 \text{ \AA}$, $b= 3.7412 \text{ \AA}$, $c= 6.5249 \text{ \AA}$; space group C_2/m).³⁸⁻⁴⁹ The local order in each phase is represented by octahedron constituting oxygen ions in its vertices and titanium atoms at the center with different spatial arrangements sharing edges and corners in a different manner.⁴⁹⁻⁵⁴ There is a structural inter-relationship between anatase and rutile as evidenced from theoretical and experimental studies.⁵⁵⁻⁵⁷ The rutile is thermodynamically most stable at all temperatures and pressures, while metastable anatase and brookite are kinetic products. The rutile is composed of corner-sharing octahedra with each octahedron surrounded by ten octahedra; two are edge shared and eight are corner shared (Fig. 1).^{1e,54,57} The $[\text{TiO}_6]$ in anatase are surrounded by eight octahedra (four edge shared and four corner shared).⁵⁸⁻⁶⁰ Thus, fraction of edge-sharing octahedra required to form anatase is greater compared to rutile (50 % vs 20 % respectively). The two juxtaposed hydrolysis and condensation reaction between two octahedral is required to form for an edge shared bonding, while corner sharing octahedra demands hydrolysis and condensation reaction in the co-ordination sphere. The

body centered tetragonal anatase consists of edge-shared octahedra to form zigzag ribbons along [221], while octahedra in primitive tetragonal rutile lattice share two edges to form linear chains parallel to [001] and [TiO₆] chains are linked together via corner connections along [110] and $[\bar{1}\bar{1}0]$.^{47,61,62} The brookite adopts orthorhombic structure wherein octahedra share three edges with one of them determines the crystal distribution along [100] direction and other two along [001] direction,⁶⁰ with tunnels along c-axis. The octahedral chains are rotated at 90° in rutile and nearly 90° in brookite, but are not rotated to a larger extent in anatase. The lattice structure of brookite resembles anatase and its structural characteristics are in between anatase and rutile.^{46,62-66} For instance, refractive index of anatase, brookite and rutile are 2.52, 2.63, and 2.72, while the theoretical density is 3.84, 4.11 and 4.26 g/cm³ respectively.⁶¹ The optical (3.11 eV) and indirect band gap (2.85 eV) of brookite were found to lie between those of anatase and rutile,⁶⁷ while few suggests that optical gap is 0.06 and 0.16 eV higher than rutile and anatase respectively.⁶⁸ Thus, property of pure brookite without the co-existence of anatase or rutile remains as challenging task. The low density monoclinic TiO₂(B) has edge-and corner-shared [TiO₆] with pervoskite-like windows between sites and relatively open structure.^{46,69-71} The unit cell volume of TiO₂(B) is 35.27 (Å)³, whereas that of anatase, rutile, and brookite is 34.02, 31.12 and 32.20 (Å)³ respectively.^{43,72} It is obvious that rutile is more symmetric and compact compared to other titania polymorphs. The other rare crystal structure encountered are high pressure phase TiO₂(II) with α -PbO₂ structure,⁷³ TiO₂(R),⁴² Baddeleyite,⁷⁴ cubic TiO₂,⁷⁵ srilankite,⁷⁶ TiO₂-H (I4/m),⁴¹ and TiO₂-III (P2₁/c).⁷⁷⁻

78

3.0 Classical theories of phase transition

3.1 Parameters governing the phase transition- A well documented approach

(a) Types of nucleation process

The transformation among the titania polymorphs involves fundamental issues of both kinetic and thermodynamic aspects. The rutile configuration is thermodynamically favorable as its linearity allows relaxation of Ti-Ti bond. In contrast, right angle configuration cannot relax as easily, but statistically encourages the nucleation of anatase/brookite.⁶¹ During the crystallization, anatase type crystallite seems to form prior to rutile like, but when rutile crystallizes, anatase nucleation will be either inhibited or transforms to rutile.⁷⁹ The ART occurs in the wide range of 600 – 1100 °C, while brookite is generally regarded as by product in the synthesis. The preference of BAT⁸⁰⁻⁸¹ or BRT⁸²⁻⁸⁴ is largely ambiguous due to difficulties associated with obtaining pure brookite as it is farthest away from equilibrium under ambient conditions⁸⁵ and specific nucleus facilitating such transition is unknown. Few researchers argued that low solution pH and high concentration of chloride anions,^{82,86} presence of sodium cations⁸⁷⁻⁸⁸ and mechanical activation (ball milling conditions) strongly influences the brookite formation.⁸⁹ The brookite was observed as by-product when precipitated in acidic medium at low temperature, aging the precipitate from TiCl₄ and NH₃ for 15 months, and in pure form under hydrothermal method or by replication of metal organic framework.^{88,90-95}

The predilection of a particular polymorph to crystallize under the given conditions and phase transition rate has been explained by several acceptable models. In general, phase transition can be described as rutile ← anatase ↔ brookite → rutile. The anatase or brookite transforms directly to rutile, if rutile nucleus is already present in the system. The second pathway is that anatase and brookite nucleus are inter convertible and that anatase-brookite interface nucleation sites promote rutile nucleation.⁹⁶ The phase transition from rutile to anatase although thermodynamically irreversible, but was achieved via doping of rare earth ions into Degussa P 25 (anatase-rutile) that resulted in pure anatase.⁹⁷⁻⁹⁸ Unfortunately, mechanism pertinent to such transition is not investigated till date.

The E_a for ART are diverse ranging from 147 – 837 kJ/mol,⁹⁹⁻¹⁰² and the lowest reported so far is ~20 kJ/mol.¹⁰³ The latter was ascribed to high surface state density, uniformity of size and shape originating from diffusion controlled sol-gel synthesis. On the other hand, high activation energy was due to non-uniformity of morphology and wide particle size distribution.^{100,102,104} The reaction rate is expressed by standard first order kinetics and JMAK model with an Avrami exponent value of $n=0.62-0.66$ indicates that growth along defect sites like dislocations and vacancies. The first order kinetics resulted in E_a of 412 kJ/mol, while 429 kJ/mol was derived from JMAK model for this transition.⁶² The rate of ART is limited by density of potential nucleation sites along with the formation of twins and clusters having a rutile like character in anatase.^{47,105} The thermodynamics indicate that phase stability follows decreasing sequence of rutile, brookite and anatase,¹⁰⁶ which suggests that ABT takes place at a faster rate. The reconstructive ART involves an overall volume contraction of ~ 8 %, while BRT is accompanied by volume shrinkage of ~3.4 %.¹⁰⁷ Zhang and Banfield¹⁰⁸ reported that BRT has low barrier energy against ART as brookite is metastable with respect to rutile, but more stable than anatase. Thus, phase transition pathways among titania polymorphs followed the sequence: ABT (11.9 kJ/mol) > BRT (163.8 kJ/mol) > ART (>400 kJ/mol for bulk, as widely accepted).

Based on the phase transition in titania by high energy ball milling, it was proposed that anatase and brookite interfaces may form by OA of primary brookite and anatase {112} twin interfaces and other interfaces with different structures from that of bulk.^{47-48,109} Since {112} anatase twin interfaces contain an unit cell of brookite, it was concluded that brookite nucleates at twin planes and grow at the expense of anatase at low temperature,⁴⁸ and therefore ABT was facile compared to BRT. Such OA of primary particles between anatase and brookite results in the formation of planar defects, including twin planes and other interfaces.⁴⁷⁻⁴⁸ Anatase and brookite have a polytypic or reversible solid state transformation

rather than polymorphic structural relationship and their interconversion involves displacement of atoms into adjacent sites on two or four Ti planes.⁴⁸

The stable rutile nuclei maintain {101} facets during growth as a result of nucleation from layers of alternating anatase {112} twins. Since the unit cell of brookite also contains two anatase {112} twins, this form of TiO₂ is considered as a special case of {112} twin like anatase.¹¹⁰ In contrast, Zhou *et al.*¹¹⁰ concluded that OA is not necessary for the formation of {112} twin boundaries, rather {112} twin like anatase easily forms at surface and at the interface between two nanocrystals in an aggregate, leading to selective rutile nucleation at these locations among the twins and at the disordered surfaces.¹¹⁰ Subsequent to twin formation, emergence of small and isolated rutile particles among the twins, grow and shrink until a critical nucleus is formed. Despite the differences in the pathways of {112} twin formation, mechanism of rutile nucleation appears to be similar to that proposed based on experimental studies.⁴⁷ It was observed that rutile nuclei forms when half of [TiO₆] adjacent to anatase {112} twin boundary are displaced along <110> direction to form “straight” rutile like octahedral chains instead of “zig zag” anatase like chains. Simultaneous displacement of Ti octahedral along <110> direction, in every two out of four such planes leads to the formation of rutile {101} facet.¹¹⁰ The ability of {112} twin like anatase transforming to various polymorphs is apparent and might be tailored via a careful monitoring of experimental conditions.

(b) Thermodynamics and particle size effects

The main factor determining the transformation rate of phase ‘a’ to ‘b’ is the nucleation and growth mechanism (Δg_{a-b}) that represents the free energy difference between the phase ‘a’ and ‘b’. The transformation sequence among anatase, brookite and rutile is size dependent because energies of three polymorphs are sufficiently close, that they can be reversed even by small differences in surface energy. According to theoretical prediction,

anatase has lower surface and higher bulk Gibbs free energy compared to rutile.^{102,111-117} Anatase NPs were reported to be thermodynamically more stable than equal sized rutile in the size regime smaller than critical size, which is highly dependent on surface complexation conditions.^{105,108,112-117} From this standpoint, it is reasonable to assume that TiO₂ prefers to homogeneously nucleate in anatase form and rutile heterogeneously nucleates via aggregation of anatase NPs.^{47-48,118-119} The critical nuclei size for ART is governed by volume free energy, surface energy and strain energy which fluctuates with materials synthesis and processing conditions. Zhang and Banfield¹⁰⁸ concluded that anatase is stable for particle size <11 nm, brookite in the size regime of 11 – 35 nm and rutile is preferred >35 nm. Alternatively, Zhu *et al.*²⁷ reported that anatase, brookite and rutile is the most stable at the size <4.9 nm, 4.9 – 30 nm and >30 nm respectively.

If the size are equal, anatase transforms to brookite and then to rutile. If crystal sizes are unequal, transition pathways can be altered. Anatase (4.9 nm) with larger grain size transforms to rutile at a faster rate, compared to anatase with smaller grain size (2.6 nm) in anatase-brookite. In other words, anatase (4.9 nm) with smaller grain size than brookite (5.8 nm) transformed to rutile at a faster rate than the reversal trend (2.6 & 2.0 nm respectively). When the free energy of anatase is smaller than brookite, anatase is stabilized over brookite and their interface move towards brookite leading to BAT. In contrast, ABT prevails when the free energy of anatase is larger than that of brookite. The preference of ABT or BAT depends on the relative grain sizes and hence surface free energy between anatase and brookite. When the grain size of brookite is equal to critical size, anatase and brookite transforms to rutile; if the size is larger than critical size, ABT is preferred followed by BRT or directly ART occurs. However, when the size of brookite is smaller than critical size, BAT followed by ART or direct BRT will be observed.²⁷ Conversely, pure anatase with smaller crystallite size would undergo rapid ART compared to large crystallite due to the critical

nuclei size attainment of the former.¹²⁰ Therefore, thermodynamic stability is size dependent due to the balance of bulk and surface contribution.

Recent findings by Navorotsky's group,¹²¹ indicates that although bulk anatase is metastable relative to rutile, much lower surface energy of anatase reverses the thermodynamic stability for very small NPs. The analysis indicated that edge and corner atoms significantly influence the critical size at which rutile nanocrystals energetically dominates over anatase.¹¹⁰ The thermodynamic model based on surface free energies and first principle calculations revealed that anatase NPs are stabilized by surface adsorbates containing large fraction of hydrogen, while rutile particles become stable by surface adsorbates containing large fraction of oxygen.¹¹² However, this conclusion may be questioned because systematic studies on size effects in pure anatase NPs are unavailable and lack of knowledge on the surface studies that can be extended to all NPs. Thus particle size is not only the factor that influences the phase transition, but surface structure also contributes to the nucleation of particular polymorph. The size below which anatase becomes more stable than rutile (cross over diameter) is dependent on the environment of NPs. It is smaller in vacuum than those in water and continues to decrease with increase in temperature and phase stability in water is different from vacuum for NPs with same size.¹²²⁻¹²³ The ART is facilitated by enhanced ionic mobility at temperature near the melting point of NPs. The molecular dynamic simulations showed that rutile will be stable, if NPs are in vacuum and becomes smaller in size as temperature is elevated.^{123a} The grain size of three phases cannot be practically equal as the grain coalesces during the thermal treatment or phase transition. The grain size of initial powder is one of the most important parameters in governing the phase stability of titania especially in the nanometer scale region.¹⁰⁹ The structural feature that stabilize rutile in its bulk form are low tolerance to defects. Consequently, surfaces, edges and vertices induces much higher energetic penalty in rutile compared to anatase, since

these defects are relatively more abundant when particle sizes are small, stabilizing anatase at the nanoscale. The surface defects including edges and vertices also contribute to surface energies of the particles due to its uncoordinated nature that inverts the relative stabilities of anatase and rutile. The total surface energies are critically dependent upon defects associated with edges and corners of NPs at particles size ≤ 3 nm.^{26b}

Banfield *et al.*¹²⁴ found that creation of interfacial boundaries with the introduction of surface impurities suppressed the grain growth and shifted the ART temperature towards higher values. The interface nucleation model dominates for ART in anatase with denser particle packing and surface nucleation model for those with less dense particle packing.¹¹⁴ The rutile nucleates at the interface of necking anatase particles or on the surface of single anatase particle. The bulk nucleation is associated with growth processes during which rutile nuclei is formed within the anatase and grows in size eventually consuming the entire anatase.¹²⁵⁻¹²⁷ The concentration of crystalline particles in the system can impact on the rearrangement and packing of structural units. For instance, low concentration of particles results in anatase due to the lack of proper attachment or co-ordination of anatase particles reduces any chances for rutile nucleation. The densification in limited space at high particle concentration facilitates OA to promote ART.¹²⁸ Koparde and Cummings found that final sintering agglomerate transforms to rutile if one of the sintering NPs is rutile, while sintering of anatase and amorphous NPs resulted in brookite agglomerates.^{123a} A shear mechanism was found to be operative resulting in the formation of rutile lathes (plates) within anatase particles.¹²⁹ Shannon and Pask¹³⁰ suggested that most of the atomic arrangements likely to takes place within “psuedo” close-packed planes of oxygen in the respective structures. The oxide ion in anatase has fcc arrangement and changes to hexagonal packing during ART and this atomic rearrangement will be accompanied by the breakage of Ti-O bonds. *Thus, ART is classically defined as a “co-operative movement of titanium and oxygen atoms, in contrast to*

strict diffusion mechanism". The ART involves the breakage of two out of six Ti-O bonds in anatase or bulk anatase ruptures 7 out of 24 Ti-O bonds per unit cell and leads to the cooperative displacement of both titanium and oxygen.¹³⁰ This process will be accompanied by the formation of oxygen vacancies which accelerates Ti-O bond breaking and consequent structural rearrangement with drastic crystallite growth. The tuning of anatase or brookite to rutile via calcination is a difficult task, because transformation of metastable to stable polymorph proceeds at rapid rate. The delicate microstructure and surface property may be destroyed under high temperature or pressure. The abnormal particle growth of rutile during ART was accounted via three scenarios: (a) anatase particle sinter and forms a single crystal, which transforms into larger rutile particles; (b) single crystal of anatase transforms to rutile and that each rutile particle attaches to its neighbour forming new "bigger" rutile particle, which would have either single crystalline orientation or subgrain structure because of imperfect attachment; (c) anatase particles becomes attached to rutile particles and that former particle rotates acquiring a favourable crystallographic orientation for the transformation to proceed, thus forming a large single crystal of rutile (Fig. 2). An OA relationship of the type $[110]_A // [001]_R$ and $[112]_A // [110]_R$ was revealed by TEM.¹²⁹ The calcination temperature was found to have significant effect on ART. The annealing under oxygen ambience stabilized anatase, while rutile was favored under reducing/vacuum/nitrogen atmosphere.^{130,131}

3.2 Phase nucleation depending on solution chemistry

The ART during calcination in air proceeds via solid state interface nucleation,^{102,114} while in aqueous solution under hydrothermal treatment, it occurs through dissolution-precipitation pathway, via., dissolution of one phase by surface protonation (as in ART) or hydroxylation (as in ABT or BAT) followed by reprecipitation of most stable phase. In this

mechanism, phase with a higher free energy tends to dissolve and phase with lower surface energy precipitates out. In general, surplus TiO_2 growth units exist in solution. Considering the solution chemistry, Ti(IV) species in aqueous solutions are octahedrally coordinated using vacant 'd' orbitals of titanium ions to accept electron pairs from nucleophilic ligands such as $-\text{OH}$ group or H_2O forming species like $[\text{Ti}(\text{OH})_n(\text{H}_2\text{O})_{6-n}]^{(4-n)+}$.¹³² At the elevated temperature, mononuclear structure will dehydrate and condense to form amorphous $\text{TiO}_2 \cdot n\text{H}_2\text{O}$ oligomers containing metal-oxo-polymer (Ti-O-Ti) network.¹²⁰ The nature of ligand co-ordinated to central titanium is dictated by solution pH and presence of species acting as complexing agents.^{54,133} In the absence of any complexing species, pH of the medium plays a major role. For instance, $[\text{Ti}(\text{H}_2\text{O})_6]^{4+}$ undergoes a stepwise spontaneous hydroxylation forming $[\text{Ti}(\text{OH})(\text{H}_2\text{O})_5]^{3+}$, $[\text{Ti}(\text{OH})_2(\text{H}_2\text{O})_4]^{2+}$, $[\text{Ti}(\text{OH})_3(\text{H}_2\text{O})_3]^+$ and $[\text{Ti}(\text{OH})_4(\text{H}_2\text{O})_2]^0$ because of polarizability of Ti^{4+} ions. These reactions can be initiated by adding strong base or heating the solution. These complexes result in the formation of solid phase through the creation and growth of nuclei via ololation and oxolation pathways. In the presence of complexing agent that can react with co-ordination sphere of cation, solid phase is likely to result from different zero charge precursors leading to the nucleation of particular polymorph.

The formation of titania crystal via connection of octahedral by corner/edge sharing is generally discussed on the basis of '*partial charge model*',^{52,79,134-137} while linkage of $[\text{TiO}_6]$ units in TiO_2 is formed by the condensation of $[\text{Ti}(\text{OH})_n(\text{H}_2\text{O})_{6-n}]^{(4-n)+}$. If deoxolation does not occur, oxolation leads to linear growth along the equatorial plane of cations in the lower pH range. This reaction followed by oxolation between resulting linear chains leads to rutile. When deoxolation takes place at high pH, condensation can proceed along apical directions leading to skewed chains of anatase. Henry *et al.*¹³⁸ proposed that if deoxolation occurs before nucleation, condensation may orient towards cis-skewed chains of anatase.

Conversely, if deoxolation occurs after nucleation, trans-linear chain of rutile is formed. Gopal *et al.*⁵⁰ pointed out that when two octahedra join along an edge after initially sharing a corner during condensation, placement of third octahedron determines the final crystal structure. If a third octahedron bonds to other two octahedron forming a linear chain (basic structural unit for rutile), nucleus favoring rutile will be formed (Fig. 3). Alternatively, anatase or brookite may nucleate if third octahedron joins in such a way that a right angle is formed (basic structural unit of anatase/brookite). The competition between growth units of various polymorphs together with their relative stabilities from the aspects of surface/bulk energy and geometric configuration depends on the nature of growth units specific to processing conditions. During the anatase formation, rearrangements of these octahedra from the amorphous phase proceeds through solid state reaction, where water molecules form bridges between surface hydroxyl groups of different octahedra which share only one common vertex using two lone pairs of electrons on oxygen. Due to the size of water bridges, it is facile for the formation of two bridges between two octahedral, thus linking them by a triangular face. Having thus aligned the octahedral correctly, dehydration occurs resulting in two titanium ions linked by two further oxygen ion vertexes and thus sharing a face. The presence of small quantity of base increases the hydroxyl group density as well as number of potential bridging sites favoring anatase. In strong acidic conditions, hydroxide group in the pair of octahedra sharing one edge will be protonated. When a neighbouring octahedron attacks the pair of octahedra, electrostatic repulsion favours opposite edge sharing. Thus a 3-D linear chain sharing vertex results in rutile (Fig. 4).¹³⁹ In a mild acidic medium, hydroxide groups in neighbouring octahedra sharing an edge are partly protonated thereby promoting the formation of linear and spinal or zigzag chains, simultaneously leading to anatase, rutile or brookite. By adopting the partial charge model,¹⁴⁰ Aruna *et al.*¹³⁴ proposed that crystallization of TiO₂ starts with [TiO(OH)(OH₂)₄]⁺, which is evolved from Ti⁴⁺ via

$[\text{Ti}(\text{OH})(\text{H}_2\text{O})_5]^{3+}$ and $[\text{Ti}(\text{OH})_2(\text{H}_2\text{O})_4]^{2+}$ with increasing the solution pH. The $[\text{Ti}(\text{OH})_2(\text{H}_2\text{O})_4]^{2+}$ can yield $[\text{Ti}(\text{OH})_3(\text{H}_2\text{O})_3]^+$ via intramolecular deoxolation depending on the pH conditions. The deoxolation has much less probability to take place and oxolation among $[\text{TiO}(\text{OH})(\text{H}_2\text{O})_4]^+$ results in linear growth along the equatorial plane of cations at relatively low pH. This reaction followed by oxolation between resultant chains yields rutile. The condensation can proceed along apical directions via deoxolation leading to skewed chains of anatase at high pH values. Cheng *et al.*⁵⁴ explained pH effect from the view point of TiO_2 crystal structure: linking of $[\text{TiO}_6]$ units in TiO_2 is formed through oxolation (dehydration) between hydroxyl ligand in $[\text{Ti}(\text{OH})_n(\text{H}_2\text{O})_{6-n}]^{(4-n)+}$. As the formation of one-edge shared bonding requires two oxolation reactions between a pair of complex ions to occur simultaneously, high pH supports edge-shared bonding (anatase crystallization). At low pH (high acidity), edge shared bonding is suppressed to some extent and corner shared bonding is facile to form rutile. The brookite has both shared edges and corners and is midway between that of anatase and rutile in terms of edge shared bonding. This might attribute to brookite stabilization at intermediate pH. At pH values far below PZC of titania, NPs of rutile are more stable than anatase and vice versa at pH values above PZC.¹¹⁶

Due to different co-ordination ability and spatial steric effects of anions like F^- , Cl^- , NO_3^- , ClO_4^- , SO_4^{2-} and PO_4^{3-} , crystal phase of titania can be tailored through changing these mineralizers (acids), which affects the linkage of six-fold co-ordinated monomers in different bonding modes.¹⁴¹ These anions would replace $-\text{OH}$ or $-\text{OH}_2^+$ species to form $\equiv\text{Ti}$ -anion and its relative magnitude depends on bonding energy and anionic concentration. According to ligand field theory,⁵⁴ nucleation and crystallization into a actual crystallographic structure will be effectively influenced by ligands and dehydration reactions between partially hydrolyzed Ti^{4+} complexes existing in solution such as $\text{Ti}(\text{OH})_n(\text{A}_1)_m(\text{A}_2)_o$ (A :anion, $n+m+o=6$). Accordingly, Cheng *et al.*⁵⁴ suggested that the crystallization of TiO_2 should

proceed via dehydration between partially hydrolyzed $[\text{Ti}(\text{OH})_n(\text{Cl})_m]^{2-}$ ($n+m=6$, representing the acidity and concentration of chloride anion respectively in the solution) obtained from the hydrolysis of TiCl_4 . The phase formation/transformation is governed by the aggregation rate of octahedral complexes.⁵⁰ The high concentration of protons results in stronger repulsion among the particles and a slower aggregation rate leads to rutile and viceversa. The $[\text{TiO}_6]$ separated at acidic pH enhances the mobility of $[\text{TiO}_6]$ to benefit the formation of larger crystallites by depositing the discrete $[\text{TiO}_6]$ on the preformed nuclei. Alternatively, amorphous TiO_2 cannot be separated due to less protonation at high pH and $[\text{TiO}_6]$ units would be still in the aggregate form via hydrogen bonding. The aggregated amorphous TiO_2 will take part in face shared bonding via solid state epitaxial process during heat (hydrothermal) treatment.^{120,141} Barbe *et al.*¹⁴² also evidenced that low aggregation of anatase particles suppressed rutile formation. Thus, ART rate will increase dramatically when the interacting anatase is finely crystalline and aggregated due to increased contact sites between the NPs and are potential nucleation sites for rutile formation.^{116,143} In contrast, rutile can also co-precipitate with anatase in aqueous environment rather from structural rearrangement of aggregated anatase crystallites.^{123a}

3.3 Peptization and growth mechanism for NPs

The nucleation will be followed by growth of NPs via coarsening (classical growth) and aggregation (non classical growth).^{48,144} The grain growth in nanocrystallites can be regarded as movement of grain boundaries by atomic diffusion during the coalescence of smaller neighbouring grains. The processes such as coarsening and aggregation can compete with nucleation and growth in modifying the particle size distribution within the liquid medium. The phase transformation rate and particle growth dynamics are fundamental process that govern the final particle size, morphology and phase composition. The syntheses under the aqueous conditions are categorized into two regimes: synthesis at low and high

water-to-titanium ion ratio (r). In the former case ($r < 10$), relatively monodisperse aggregates of spherical nanocrystallites (0.5 – 1 nm) are obtained and growth kinetics of aggregates are determined by the stability of colloid. The nucleation and growth processes are completed within seconds ($r > 10$) due to rapid hydrolysis of titanium precursors.¹⁴⁵⁻¹⁵² As formed TiO_2 particles are unstable and precipitates to form large aggregates, which collapses to very small aggregates after peptization. This method is regarded as an efficient approach to obtain the crystalline phases at relatively low temperature.¹⁵³⁻¹⁵⁴ Kumar and co-workers¹⁵³⁻¹⁵⁵ concluded that less agglomerated samples obtained from peptization created an efficient packing of particles, whereas the unpeptized samples favored the formation of structures with greater porosity and larger pore size. The peptized sol will be uniformly packed and compact to favor rutile formation at low temperature compared to unpeptized sol in the course of thermal treatment. The pore sizes of peptized samples were monomodal and relatively narrow as compared to bimodal distribution for unpeptized ones.

As a peptizing agent, TEAOH promoted ART compared to TMAOH and TBAOH for $\text{Ti}(\text{O}i\text{Bu})_4$ under hydrothermal condition (200 – 240 °C, 2 h) and subsequent calcination (1050 °C, 1 h). The particle morphology changed from sphere to rodlike and asterisk like with increase in the concentration of TMAOH and TEAOH respectively, while it was unaffected with TBAOH. It was proposed that asterisk like morphology offered high density of potential nucleation sites to promote ART.¹⁵⁶ The hydrothermal processing of unpeptized titania precipitated from alkoxide precursor formed a highly crystallized powder in all the cases.¹⁵⁷ After peptization (precipitates were redispersed in HNO_3 and refluxed to obtain transparent sols), varying amount of anatase-rutile were obtained for ethoxide and isopropoxide and pure anatase from tertiary butoxide precursor. Thus obtained powders from hydrolysis of TTIP in water-HCl mixture (pH 1 – 2) was anatase-brookite and later transformed to rutile during calcination (500 °C, 1 h).¹²⁵ The rutile content was highest in the sample previously peptized

at RT compared to artificial peptization (50 °C and 70 °C).¹²⁵ Surprisingly, sample peptized at 70 °C showed no significant rutile enhancement even after calcination. This phenomenon was explained by the fact that peptization at high temperature resulted in smaller particle size even below the critical nuclei size due to high thermal energy (kT). Alternatively, peptized powders at high temperature when dried at RT showed high rutile content compared to those dried at 0 – 5 °C. The lattice defects and produced microstrains within the titania were reduced by cool-drying technique, which retarded rearrangement of parallel octahedral in the case of anatase to 90° rotated octahedral in rutile. Relatively smaller E_a (11 kJ/mol) was observed for the powder dried at RT compared to cool-drying process (21 kJ/mol). Due to very small crystallite size (~ 3.5 nm), temperature for ART followed within the regime of nanoscale transformation. The transformation E_a was calculated in the range of 7.5 – 11 kJ/mol and 11 – 21 kJ/mol based on peptization and drying temperature respectively. Furthermore, enthalpy change for crystallization was 10.4 ± 0.3 kJ/mol according to DSC analysis.¹²⁵ The peptization of gel with HNO_3 at 35 °C resulted in dominant anatase for all the concentration of TTIP. After calcination (400 °C, 1 h), anatase-rutile-brookite with dominant rutile was observed in the samples having hydrolysis ratio ($\text{Ti}^{4+}/\text{H}_2\text{O}$) of 30:1. The high concentration of Ti^{4+} leads to faster agglomeration and increasing the total contact area promoting ART.^{158a} On the other hand, peptization with HCl leads to the formation of rutile.^{158b}

During the peptization, aggregates will be broken down and electrostatically stabilizes the sol in which the particles attain positive charge as a result of protons adsorption. The particles are then repelled (double-layer repulsion) and stable sol results with a minimum degree of aggregation.¹⁵³⁻¹⁵⁵ The character of hydroxyl anion and large cation group of tetra alkyl ammonium hydroxide permit them to serve as catalysts in hydrolysis and as peptizers for the deagglomeration of precipitates.¹⁵⁹⁻¹⁶⁰

The driving force for crystal growth arises from surface energy reduction with specific morphological features.^{48,119} The coarsening or Ostwald ripening (OR) is a dissolution-reprecipitation growth mechanism by which smaller particles dissolve due to thermodynamic instability and larger particles continue to grow by consuming the dissolved species in the solution (Fig. 5). In other words, larger particles grow at the expense of smaller ones. In this case (OR), particles tend towards an isotropic growth, generating particles with regular and almost spherical shapes. Alternatively, secondary particles can also be produced by aggregation of primary particles.¹⁶¹⁻¹⁶⁶ In this mechanism (OA), primary particles aggregate first and then align crystallographically at specific locations to form mesocrystals. It favors the formation of anisotropic nanocrystal by the coalescence of two or more nanocrystals.¹⁶⁴⁻¹⁶⁵ Although primary particles in mesocrystals are not in direct contact with each other, they will be in crystallographic registry. Subsequently, mesocrystals transform to secondary crystalline particles or oriented aggregates.¹⁶⁶⁻¹⁶⁸ This mechanism is predominant in materials with very low solubility. In general, OR results in characteristic equilibrium morphology of crystal,^{112,117,119} while OA leads to irregular morphologies due to twists, tilts and shifts at attachment planes.^{48,119} Another growth mechanism that results in dislocations and tilts is repeated nucleation, where heterogeneous nucleation takes place on pre-existing crystallites in the system.¹⁶⁹⁻¹⁷⁰ It was also hypothesized that particle grows by coarsening and assembly as opposed to coarsening alone.¹⁷¹ The driving force for the assembly process once again stems from the reduction of surface energy as observed for a variety of metal oxides.^{118,172,173} The growth mechanism is quite complicated process, evolving a variety of attachment sites and local surface environments. The particle growth kinetics can be tailored by using different solvent or complexing agent that could enhance the solubility of titanium complexes in solution.

4.0 Hydrothermal/Solvothermal route

This route offers a promising approach owing to multiple merits like low reaction temperatures to obtain particles without agglomeration or reduced aggregation, fast reaction velocity, narrow particle size distribution, high surface area and tailored crystal structures with well-defined unique morphology. In this method, chemical reaction proceeds in aqueous media to form highly crystalline material under the simultaneous generation of heat and pressure. The reaction develops an anomalous dielectric constant, density and ionic strength that cannot be achieved under ambient pressure/temperature allowing unusual reactions to occur. By interplaying with reaction parameters like solution pH, precursor chemistry, solvents, temperature and time, phase composition with diverse morphologies can be tailored depending on chemical structure and electronic environment of Ti(IV) complex. The only disadvantage of this method is the longer aging time for crystallisation at low temperature.¹⁷⁴ The driving force for hydrothermal crystallization originates from the free energy difference generated by the relative supersaturation which occurs on increasing the temperature from room to hydrothermal conditions and follows dissolution-precipitation mechanism.⁷⁹ It is generalized that anatase is stabilized under basic solutions, while rutile prevails in acidic conditions and larger rutile particles are stable regardless of pH for this method. For instance, Cheng *et al.*⁵⁴ concluded that high acidity and concentration of TiCl₄ favor rutile formation, whereas solution with wide pH range of 3.4 – 8.2 promoted anatase.

4.1 Preparation of TiO₂ from titanium chlorides

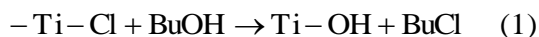
The crystallographic structure of titania formed at different concentration of TiCl₄ is concerned with co-ordination ability of Ti⁴⁺ complex ions.^{54,86} Nicholls *et al.*¹⁷⁵ found that Ti⁴⁺ exists as [Ti(OH)Cl₅]²⁻ and [TiCl₆]²⁻ in HCl. Hilderbrand *et al.*¹⁷⁶ revealed that corner-sharing titanium oxygen octahedral dimers and trimers exist in TiCl₄ (2.17 – 4.8 M) solution.

The hydrothermal treatment (200 °C, 24 h) of TiCl_4 resulted anatase-rutile for $[\text{TiCl}_4] < 0.5 \text{ M}$ and pure rutile above this concentration.⁷⁹ Surprisingly, brookite coexisted at intermediate concentration of 1 M and completely transformed to rutile at 2 M. The increase of hydrothermal treatment time from 18 – 42 h enhanced the rutile content, as anatase crystallites migrates and align themselves followed by in situ rearrangement of lattice to form larger rutile crystallites.¹¹¹ Based on microscopic model, this transformation was explained as follows; (i) low $[\text{TiCl}_4]$ contains large amount of dispersed $[\text{Ti}(\text{OH})_2(\text{OH}_2)_4]^{2+}$ monomers or edge-sharing dimmers at RT, while $[\text{TiO}(\text{OH})_5]^{2+}$ exists at high $[\text{TiCl}_4]$;¹⁷⁷⁻¹⁷⁸ (ii) after the attainment of reaction temperature, solution saturates and species in solution will be unstable and are prone to combine via oxolation or ololation forming a original nuclei. As these nuclei grow to exceed the critical size, they become stable and further growth continues. During the formation of original nuclei, $[\text{Ti}(\text{OH})_2(\text{OH}_2)_4]^{2+}$ monomers can form different structures of polymers by sharing equatorial or apical edges, while $[\text{TiO}(\text{OH})_5]^{2+}$ monomers can only form linear chain polymers by sharing equatorial edges.¹⁷⁹ Thus, rutile crystallite develops as solution contains only linear polymer chains at $[\text{TiCl}_4] > 0.4 \text{ M}$. The brookite-rutile prepared at high concentration of TiCl_4 (1.0 M) were dominant in spherical particles with minor portion of NRs, while increased proportion of rutile NRs was formed in dilute TiCl_4 (0.3 M) under hydrothermal condition (333 to 423 K, 12 h).¹⁸⁰ The excess H^+ under strong acidic conditions suppressed the hydrolytic process of TiCl_4 and thus fewer nuclei are formed in the concentrated acidic solution via layer-by-layer growth mechanism. The NRs with aspect ratio close to 10 were obtained with excess of chloride ions (3 M NaCl). The equilibrium between dissolution and precipitation of NPs under strong acidity is different from weakly acidic solution. The rutile NRs with $\{101\}$ facets was observed compared to $\{110\}$ plane. The surface energies of $\{011\}$, $\{110\}$, $\{100\}$ and $\{221\}$ facets are 1.85, 1.78, 2.08 and 2.02 J/m^2 respectively.¹⁸¹ The most stable surface is $\{110\}$ contains five and six co-ordinate species,

which in part may be the source of selective adsorption (physical, chemical or both) of chloride or anionic complex of Ti(IV) ions in the acidic medium. However, it is assumed that tips composed of high energy surface facet {101} adsorbs more anionic complex of Ti(IV) ions for lowering the surface energy. These Ti(IV) complexes dehydrate on the tips of NRs and form units of $[\text{TiO}_6]$ continuously, thus favouring anisotropic growth along c-axis.¹⁸⁰

The hydrothermal treatment (100 °C, 18 h) of TiCl_4 in mixed organic medium of alcohol and AcOH gave rutile, anatase and amorphous phase with ethanol, ethylene glycol and glycerol respectively.¹⁸² In contrast, treatment without AcOH resulted in anatase for ethanol and no crystalline product was observed for ethylene glycol and glycerol. However, rutile formation with glycerol was observed at 150 °C and no structural change took place for other two solvents. It was interesting to note that anatase-rutile was observed for ethylene glycol at 150 °C and no crystalline product was detected for glycerol without AcOH. This suggests that insitu generation of water as a reaction between alcohol and acid was instrumental in the nucleation of titania polymorphs. The formation of titania was mainly through hydrolytic process via water released from esterification of ethanol and AcOH, although non-hydrolytic pathway cannot be excluded. The HCl retained in the reaction system played a catalytic role to initiate the esterification reaction at elevated temperature and makes the hydrolytic process more feasible.¹⁸² The nature of titanium precursor and alcohol influenced the final phase formation under microwave assisted solvothermal process (190 °C, 30 min): pure anatase was observed for the reaction of TiCl_4 with propanol or butanol and rutile with octanol, while anatase-brookite, brookite-rutile and anatase-rutile was observed for TiCl_3 with aforementioned solvents respectively. Interestingly, only anatase was observed for TiCl_4 or TiCl_3 with ethanol.¹⁸³ Unlike TiCl_4 , solvent reaction with TiCl_3 involves oxidation and hydrolysis to form TiO_2 . It is known that residual alkoxy groups determine the crystallization behavior of titania precursor, which is influenced by initial ultrastructure of

amorphous phase.¹⁸⁴ The brookite nucleation might be related to unique formation of hydroxyl groups in the reaction of butanol with TiCl_3 . This formation may be due to the increased cationic character on the tertiary carbon atom of butanol that favored the nucleophilic attack of chloride ions:



In addition, varied morphologies were obtained; spheres, NPs and nano rod building spheres with ethanol, propanol and octanol respectively was found with TiCl_4 , while mixture of nanorod and nanoparticle was observed for TiCl_3 and butanol. The reaction between titanium chlorides and alcohol become less vigorous with increase in the number of carbon atoms in the alcohol, so does the evolution of HCl as the replacement of chloride ions in the precursor by alkoxy groups becomes more difficult. Consequently, reaction steps involve etherification of alcohols and water as byproduct. Accordingly, crystal structure changes from anatase to rutile or brookite with increasing the number of carbon atoms in the solvent. The solvothermal treatment of TiCl_3 (353 K, 24 h) and urea in HNO_3 showed rutile, anatase and varying amounts of anatase-rutile in aqueous, ethanol and water-ethanol respectively.¹⁸⁵ The hydrothermal reactions (250 °C, 4 h) of TiCl_4 with IPA-water resulted in anatase for 1 M [TiCl_4], while rutile (3 – 15 %) was favoured with increase in precursor concentration from 2 – 3 M after calcination (600 °C, 2 h).¹⁸⁶ The precipitate obtained by the hydrolysis of TiCl_4 and NH_3 were anatase, but amorphous with $\text{Ti}(\text{OC}_2\text{H}_5)_4$ and dry ethanol. However, hydrothermal aging (120 °C, 90 min) of amorphous powder with varied salt solutions (K_2SO_4 , Na_2SO_4 , KCl , NaCl) crystallized the anatase and totally different products were formed with NaF . The progressively lower amount of crystallization with chloride, sulfate and fluoride ions was attributed to increasing charge-to-size ratio, which adsorbs strongly on the titania surface and reduces surface/solution ion exchange and delays structure reorganization.¹⁸⁷ The solvothermal treatment (110 °C, 12 h) of TiCl_4 /acetone resulted in

anatase and rutile for the ratio of 1:15 and 1:10 respectively.¹⁸⁸ At the initial stage of reaction, Lewis acid TiCl_4 catalyzed the aldol condensation reaction of acetone to form diacetone alcohol, which easily dehydrates to form mesityl oxide and its isomers. The dehydrated dimers further condensates with remaining acetone to produce varying amounts of dehydrated trimers, tetramers etc.¹⁸⁹ Thus, water molecules produced from the dehydration of acetone oligomers triggers TiCl_4 hydrolysis to produce Ti-OH species and HCl . The dehydration of Ti-OH to form Ti-O-Ti continues leading to either anatase or rutile.

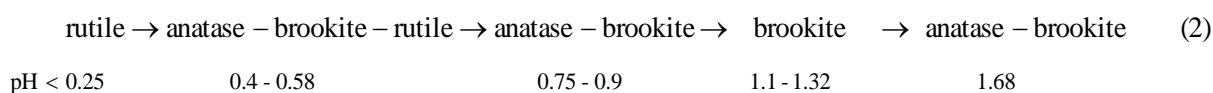
Hydrothermal treatment (220 °C, 3 h) of amorphous TiO_2 with HF and HNO_3 or HCl resulted in pure anatase, although rutile was observed at mild concentration of HCl or prolonging the reaction time (10 h).¹⁴¹ The TEM images revealed that broad size particle distribution indicating that crystallization of anatase from amorphous solid proceeds via solid-state epitaxial crystal growth with a slow nucleation process for hydrothermally treated amorphous TiO_2 at pH 9 without acids. In contrast, this transition preceded by face sharing polycondensation of protonated $[\text{TiO}_6]$ with acid as catalyst.¹⁸⁷ The addition of mineral acids disperse the aggregate $[\text{TiO}_6]$ and related species in the amorphous phase into discrete species by protonating the surface Ti-OH to Ti-OH_2^+ ,¹⁹⁰ that easily combines with $-\text{OH}$ groups of neighbouring $[\text{TiO}_6]$ to form Ti-O-Ti bridge accompanied by the elimination of water molecule (dehydration) through which crystal grows to larger size.^{141,191} Interestingly, pure rutile with rod like morphology was obtained with citric and nitric acid (pH 0.8 – 1.09) attributed to the prevention of surface sharing polycondensation through the chelation of citrates to $[\text{TiO}_6]$. Such chelation favours the edge sharing between $[\text{TiO}_6]$ rather than face sharing owing to the spatial inhibition effect of organic ligands. The increase of pH > 1.09 with citric acid promoted anatase along with rutile (150 °C, 22 h). The chelation of citrate to amorphous TiO_2 was affected by degree of protonation. If the acidity of suspension is high enough to achieve a discrete dispersion of $[\text{TiO}_6]$, amorphous phase can be uniformly

modified with citrate giving rise to pure rutile. Otherwise, chelation of citrate to amorphous TiO_2 will be incomplete due to the existence of aggregated amorphous masses resulting in anatase-rutile. The catalytic activity of HNO_3 and HF for anatase crystallization from amorphous is lower than HCl , since both acids have very poor nucleophilicity leading to the slow dispersion of amorphous aggregates into discrete $[\text{TiO}_6]$ and related species. The slow nucleation may induce competitive crystal growth leading to irregular faces of anatase titania. The competitive formation of chlorine atom-substituted octahedral similar to the partially hydrolyzed $[\text{Ti}(\text{OH})_n(\text{Cl})_m]^{2-}$ and related species like $\text{TiO}_2(\text{OH})_n^{n-}$ may explain the slow rate of rutile formation.¹⁴¹

The hydrothermal reaction (200 °C, 20 h) of TiCl_3 and NaNO_3 at alkaline medium ($\text{pH} > 10$) gave pure brookite, while addition of tartaric acid ($\text{C}_4\text{H}_6\text{O}_6$) facilitated BAT and complete anatase was observed for molar ratio of tartaric acid/ TiCl_3 at 0.75 (Fig. 6).¹⁹² As obtained brookite were aggregated by spindle like particles, while addition of tartaric acid changed the morphology to nanorod structure. The time dependent evolution of TiO_2 indicated the transition from amorphous to layered titanate (4 h) and later transformed to anatase and brookite. The brookite in its pure form was not observed for reaction system with $\text{pH} < 9$ and < 180 °C. When the $\text{C}_4\text{H}_4\text{O}_6/\text{Ti}$ molar ratio < 0.75 , insoluble amorphous $\text{Ti}(\text{OH})_4$ and soluble Ti-contained species $[\text{Ti}(\text{OH})_x(\text{C}_4\text{H}_4\text{O}_6)_y]^{z-}$ ($4 \leq x + 2y \leq 6$, $z = x + 2y - 4$) exists in the solution. The former transformed to layered titanate ($\text{Na}_{2-x}\text{H}_2\text{Ti}_2\text{O}_5 \cdot \text{H}_2\text{O}$) which further crystallizes to form brookite under certain concentration of Na^+ and OH^- ions. Due to the steric hindrance of carboxylic acid ligands, $[\text{Ti}(\text{OH})_x(\text{C}_4\text{H}_4\text{O}_6)_y]^{z-}$ should combine together by sharing equatorial or apical edges and arrange in zig zag chains to favor anatase.¹⁹³ The strong chelation between Ti center and $\text{C}_4\text{H}_6\text{O}_6$ reduces the condensation pathways between titania complexes resulting in relatively slow nucleation and growth of anatase embryos. Interestingly, anatase-brookite-rutile was transformed to pure anatase with exposed {001}

facets via addition of ascorbic acid and morphology changed from elongated NRs and nanoparticles to spindle like particles after hydrothermal treatment (180 °C, 10 h).¹⁹⁴

Anatase, rutile and brookite was selectively synthesized by the hydrothermal treatment (180 °C, 3 h) of TiCl_3 using $(\text{NH}_4)_2\text{S}_2\text{O}_8$, H_2O_2 , HNO_3 (or HClO_4) in the absence of mineralizers.⁶⁷ The three polymorphs showed distinct crystal shapes: rounded nanocrystals for anatase, nanoplates for brookite and NRs for rutile. Pure anatase was obtained with $(\text{NH}_4)_2\text{S}_2\text{O}_8$ irrespective of synthesis conditions (solution pH and initial Ti^{3+} concentration), while phase selective synthesis of anatase, brookite and rutile was achieved with other oxidants like H_2O_2 , HNO_3 and HClO_4 depending on $[\text{TiCl}_3]$ and solution pH. The unique transition sequence was observed for hydrothermal treatment of TiCl_3 (0.05 – 0.9 M) with oxidants like H_2O_2 , HNO_3 and HClO_4 in the pH range of $< 0 - 1.68$.



The chemically co-ordinated sulfate ion orients the precursor cations upon deoxygenation and oxygenation promoting anatase. The alkaline condition (pH 9.0) favoured anatase, low pH (0.44) resulted in rutile, while intermediate pH 1.32 stabilized brookite. Alternatively, very low (0.005 M TiCl_3) and high reactant (0.9 M TiCl_3) concentration stabilized anatase, while 0.0625 M showed pure brookite. The high reactant concentration results in rapid interactions among the precursor cations, which suppressed sufficient rearrangements of $[\text{TiO}_6]$ for brookite formation, while low precursor content decreased the growth/nucleation ratio.⁶⁷ Ovenstone and Yanagisawa¹⁹⁵ reported that powder with small crystallite size and trace brookite content undergoes ART at a faster rate compared to amorphous powder and pure anatase, suggesting that BRT was favored during calcination. The smaller crystallite would contain large number of lattice defects such as interstitial ions or ion vacancies. The atoms in

these defects have higher energy than those in the main lattice and can act as nucleation sites for rutile formation at the surface of anatase crystallites.¹⁹⁶⁻²⁰¹

Pure rutile NRs were obtained in the hydrothermal reaction (150 °C, 24 h) of TiCl₄ and water, while brookite co-existed with the addition of TEA as selective adjusting agent.²⁰² The TEA co-ordinates with Ti(IV) to form [TiO-N(C₂H₅)₃]²⁺, which could shield some charges and diminish the effects of electrostatic stabilization (repulsion). In the presence of excess TEA (> 7 mL), original transparent solution becomes opaque and adsorbed amine lowers the acidity of solution to benefit the brookite formation. The addition of 1.5 mL of TEA facilitated BRT, while reverse trend was observed for > 1.5 mL and pure brookite was observed for 9.0 mL.²⁰² The shape transformation from NRs to NPs was realized in the presence of MC and NaCl together with partial phase transition from rutile to brookite under hydrothermal conditions (160 °C, 2 h) using TiCl₃.²⁰³ As a hydrophobically modified cellulose derivative, MC completely dissolved in water entering the solution.²⁰⁴ At elevated temperature, hydrophobic association of MC chains became pronounced and was intensified further due to salt-out effect of NaCl.²⁰⁵ This assists the MC molecules in forming 3-D networks with high density hydroxyl groups exposed to water, where “hydrolyzed” Ti species were prone to settling in. The interactions between MC networks and Ti (species) facilitate the ololation and oxolation reactions, so that driving force for rutile nucleation is largely suppressed. Obviously, MC network density was raised as more MC is added in the solution and enhanced the brookite proportion. The hydrothermal treatment (200 °C, 3 days) of TiCl₃ at acidic conditions (pH 1) resulted in anatase-brookite-rutile. Upon calcination, both anatase and brookite transformed to rutile at 800 °C accompanied by the gradual formation of new corundum like titania phase at 500 °C that stabilized up to 900 °C.²⁰⁶ The stability of anatase and brookite was due to hydroxyl groups bonded to its crystalline structure during hydrothermal treatment. The preparation of TiO₂ from titanium chlorides is worthy of

investigation as it does not leads to the formation of any organic impurities in the final products.

4.2 Preparation of TiO₂ from titanium alkoxide precursor

Thermally stable anatase was obtained by solvothermal treatment (200 °C, 4 h) of Ti(OBu)₄ with 1-butanol in acidic medium.^{207a} This was due to capping action of n-butanol on the surface of titania, which inhibited the aggregation, reduced particle-particle contact area and hence suppressed pore collapse and ART during calcination. The aggregation and decomposition of surface alkoxy groups at > 800 °C facilitated complete rutile formation thereafter. Hydrothermal treatment (90 °C, 10 h) of amorphous powder obtained by TTIP and triblock copolymer EO₂₀PO₇₀EO₂₀ in the presence of AcAc transformed to anatase and was stabilized even after calcination up to 700 °C, attributed to small crystallite sizes in the inorganic domain.^{207b} However, rutile was formed at 700 °C for non-hydrothermally treated samples due to the collapse of pore structure. Thus amorphous phase can destroy the mesoporous framework during the calcination. The triblock co-polymer surfactant forms micelles in aqueous solution in the temperature range of 35 – 80 °C, because PPO block is more hydrophobic than PEO block and thus titania particles can only form at latter sites. The hydrolysis and condensation leads to the growth of larger NPs, which slowly aggregate and becomes microscopic to form well defined mesoporous with spherical shape particles. At this stage, it is supposed that micelle surrounds mesoporous titania facilitating the formation of spherical shape. After hydrothermal treatment and calcination, mesoporous titania particles with well defined spherical shapes were obtained.^{207b}

The solvothermal treatment (180 °C, 3 h) of toluene:HCl:Ti(OBu)₄ showed unique morphology of loosely aggregated NPs and NRs with random orientations.⁴⁹ The NPs were derived from anatase and brookite, NRs from rutile indicating that tricrystalline titania was

simultaneously nucleated by this protocol. The preferential growth of rutile nanorod along [001] direction (c-axis) arise from unique crystal structure of rutile itself. It is known that the rutile phase has 4_2 screw axes along the crystallographic c-axis. The screw structure will promote the crystal growth along this direction, leading to crystal morphology dominated by {110} facets.²⁰⁸ It was proposed that polar water from HCl formed a water/toluene interface hydrolyzed the titanium precursor. As temperature increases, water molecules diffuse away from high energy water/toluene interface to minimise the system energy and reacts with Ti^{4+} in toluene resulting in the formation of crystal nucleus from which mixed crystals were simultaneously formed.⁴⁹ The powder dominant with rutile was observed for toluene:HCl:Ti(OBu)₄ ratio of 15.0:4.0:2.0, while tricrystalline framework were obtained with varied concentrations. In any case, rutile content decreased first and increased later with varying concentration of toluene to HCl to Ti(OBu)₄, while brookite and anatase followed the reverse behaviour. In another study, hydrothermal treatment (160 °C, 4 – 8h) of Ti(OBu)₄ with HCl and toluene gave rutile microsphere on the glass substrate.²⁰⁹ The Ti^{4+} precursor will hydrolyze with water at water/glass interface resulting in the formation of first nanocrystalline layer. Thus, new interface between hydrophilic titania and toluene is formed with continuous hydrolysis and subsequent growth-crystallization takes place. Finally, hierarchical microspheres formation takes place adhered to glass substrate.²⁰⁹ Pure anatase was observed after hydrothermal treatment (573 K, 2h) of Ti(OBu)₄ in toluene with 25 cm³ of water even after calcining at 1073 K, while those prepared with 10 cm³ of water had anatase-rutile.²¹⁰

As obtained powder from hydrolysis of TTIP in water was amorphous and crystallised to anatase under acid free condition and to rutile with HNO₃ under hydrothermal condition (180 °C, 24 h).¹²⁰ The hydrothermal treatment of TTIP (water to TTIP mole ratio is 200, acidifying with HNO₃ at pH 1) at 200 °C showed anatase and brookite up to 60 h, while ART

was promoted for prolonging the aging times (140 h).¹⁷¹ The amorphous powder from TTIP transformed to anatase after calcination (450 °C, 2 h), while this crystallization was observed at low temperature via hydrothermal aging (80 °C, 24 h).¹²⁰ The anatase NPs (~10 nm) obtained (180 °C, 24 h) was stable up to 800 °C compared to the samples with crystallite size of 6 and 28 nm that was prepared at 80 and 240 °C respectively. The annealing induced slow grain growth of anatase with 10 nm size and inhibited to reach the critical size required for ART. In addition, loose packing of particles generated in hydrothermal conditions reduces the possibility for rutile nucleation. During the process, amorphous hydrous gels transforms into titania with further hydrolysis/polycondensation reactions accompanied by structural rearrangements and that mild environment is capable of yielding a better-defined structure with less surface impurities/defects to stabilize anatase. A lower aging temperature produces fine grain size (6 nm), but may not induce complete reactions of residual alkoxy/hydroxyl groups. These organic impurities serve as defect sites to promote ART. On the other hand, presence of non-equiaxed grains might have contributed to grain growth to reach the critical nuclei size for the sample with ~ 28 nm size.¹²⁰

Rutile was crystallized from acid peptized gel (HNO₃), while anatase from alkaline (TBAOH) gel via hydrothermal treatment at 210 and 270 °C respectively.²¹¹ The anatase NPs were more homogeneous with prismatic morphology and relatively narrower size distribution, while rutile exhibited bimodal distribution of particle size with larger rod like particles (60 – 80 nm) together with small spherical particles (5 – 10 nm) attributed to OR mechanism during the rutile crystal growth. The induction time of particle formation from alkaline peptized gel at 210 and 270 °C was 25 min, which is lower than acid peptized gel (34 and 30 min respectively) at the same temperature. It was noteworthy that smaller crystallites are produced at lower process temperatures from both acidic and alkaline gels.²¹¹ The hydrothermal treatment of amorphous powder under basic conditions leads to anatase (250

°C, 90 min), while rutile and brookite nucleated along with anatase under 0.5 M HCl (250 °C, 5h).¹⁸⁷ The mechanism for this reaction involves the protonation of surface amorphous titania, blocking the formation of kinetically favorable anatase. Li and Gray²¹² reinvestigated the influence of acidity on ART and concluded that rutile content in anatase-rutile do not increase monotonically with increasing acidity. The rutile fraction increased with change in HCl/Ti molar ratio from 0 to 10.5 and reverse trend prevailed from 10.5 to 35.2. The decline in rutile content was balanced by the increased proportion of brookite nucleus. At relatively low HCl/Ti molar ratio, precipitation process is slow facilitating rutile formation. In addition, rutile is stable under the influence of electrostatic repulsion in the charged environment. At high HCl/Ti ratio, more Cl⁻ or H₂O shields the positive charges and serve to lessen the effect of electrostatic repulsion. Thus, precipitation proceed via titanium hydroxo-chloro complexes such as [Ti(OH)₂Cl₃(OH₂)]⁻ and [Ti(OH)₂Cl₄]²⁻ favouring the formation of anatase or brookite.⁸⁶ Hydrothermal reaction (200 °C, 6 h) of amorphous powder (obtained from TTIP) with AcOH (1.5 M) resulted in anatase, while pure rutile (200 °C, 8 h) and brookite (175 °C, 7 h) was obtained at 4 M and 3 M HCl respectively.²¹³ It was proposed that anatase was dominated by surface energy effects, and rutile or brookite formation followed dissolution-precipitation pathway at high concentration of HCl (pH < 0). The nucleation of brookite and rutile under almost identical conditions (high acid concentration and same temperature) reflects that recrystallization process involve different precursor chemistry for each phase. The amorphous titania will be in equilibrium with soluble species of titanium (e.g. TiO²⁺ and chloro complexes) prior to crystallization. The asymmetric complexes [Ti(OH)₂Cl(OH₂)₃]⁺ predominates at RT according to speciation model for titania-chloro complexes in 3 M HCl, which inturn forms symmetrical chlorine rich complex [Ti(OH)₂Cl₄]²⁻ with increase in acidity. Homogeneous nucleation is assumed to involve zero charge complexes; hence it is liable that eventual precursor for nucleation consists of

two or more complexes combined with water as ligand. The chlorolysis-oxolation process leads to brookite in the case of asymmetric chloro-complex, while rutile nucleates from symmetric complex.²¹³ This was supported by their similarity in crystal structure, where in both brookite and rutile are formed by straight $2\mu_2$ polyhedron chains linked through corner sharing. An important difference between them is that the symmetry of octahedral in rutile is higher compared to brookite and that the linking of $2\mu_2$ chains occurs through trans-oxo bridges and via cis-oxo bridges in brookite. Finnegan *et al.*¹¹⁶ concluded that as obtained titania (85 % anatase, 15 % brookite) transformed to rutile at pH 1, while such transition was not significant at pH close or above the PZC of titania under hydrothermal conditions (200 °C, 500 h). At pH > 12, brookite transformed to anatase. Interestingly, no phase transformation was observed at 105 °C as thermal fluctuation were not enough to overcome the activation barrier for rutile formation and or dissolution of anatase, which was otherwise observed at 250 °C. Pure anatase was achieved for the treatment of amorphous powder obtained by $\text{Ti}(\text{OC}_2\text{H}_5)_4$ precursor after dry, vapor and hydrothermal conditions (250 °C, 1 h).¹⁸⁷ The powder treated in dry atmosphere had less crystallinity compared to powder treated in either vapor or hydrothermal conditions, suggesting that water adsorbs on amorphous titania and rearranges the $[\text{TiO}_6]$ to favour crystallization process. The use of low acid concentration in the reaction medium suppressed the anatase crystallization, since H_3O^+ cannot bridge because of only one lone pairs of electrons on oxygen. As the acid concentration is increased, surface of titania becomes protonated and titania becomes solubilised that allows dissolution-precipitation mechanism to operate resulting in rutile.

Sabyrov *et al.*²¹⁴ reported that hydrothermal treatment (250 °C, 20 h) of anatase with particle size of 3.1 and 3.7 nm transformed to rutile at a faster rate compared to those with 6.0 and 12.7 nm at acidic medium (pH 1) via dissolution of anatase and precipitation of rutile.



At pH 3, solubility of anatase is order of magnitude lower compared to pH 1 and hence aggregative mechanism contributes to partial ART.^{47,116,215,216} In contrast, suspension containing 3.7 nm particles transformed rapidly to rutile compared to particle with 3.1 nm size. The cryo-TEM revealed the particle densities of suspension with 3.1 nm had more open, fractal like structures, whereas aggregates of 3.7 nm crystals had denser and compact structures. Thus, increased compactness of aggregates triggered the effective concentration of particle-particle contacts and favoured ART.^{47,115} The HCl promoted brookite formation for hydrothermal treatment of powder with amorphous and anatase.^{217,218}

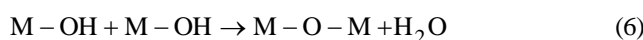
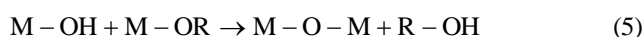
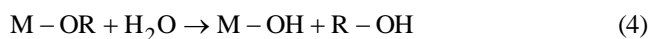
The sol-gel products that was not previously dialyzed was sensitive to BAT compared to dialyzed samples under the hydrothermal conditions (200 °C, 4 h).²¹⁷ The former particles are strongly agglomerated that favored phase transformation,²¹⁹ while side products and anions are removed to reduce the ionic strength resulting in strong electrostatic repulsions because of increased electrical double layer thickness in the latter case. In another study, brookite formation was favoured with increase in pH from -0.5 to 3.0. However, brookite content at their respective pH values decreased after hydrothermal aging (200 °C, 48 h) and the tendency of BAT was highest at pH -0.5. This was attributed to solubility of small size brookite NPs compared to anatase. The particle growth mechanism at pH -0.5 was dominated by coarsening, while both coarsening and oriented aggregation was observed for particles obtained at pH 3.²²⁰ The refluxing of TTIP with NaNO₃ (2 M) leads to anatase, while hydrothermal aging (200 °C, 48 h) triggered ART.²²¹ In contrast, anatase-rutile was observed with NaCl (2M) and anatase fraction increased with hydrothermal aging at pH -0.6. The anatase-brookite was observed at pH 3 after refluxing and further hydrothermal aging did not influenced the final phase composition. The brookite content was suppressed with increase in the ionic strength when the salts were added during synthesis, while reverse trend was observed when the salts were added during reflux and hydrothermal aging (pH 3). The role of

chloride ions in initial step of hydrolysis-condensation process, rearrangement of titanium complexes in solution and changes in surface energy was not clear.

The sample without ED treatment in the preparative step showed brookite (400 °C, 4 h) at the initial stage of calcination and later transformed to anatase (600 °C) and completely to rutile (800 °C). In contrast, brookite was stable up to 800 °C and anatase-rutile was observed at 900 °C for the sample with ED treatment.²²² The synthesis involved three stages: (i) hydrolysis of titanium precursor in acid medium resulting in aggregated amorphous phase; (ii) addition of CTAB during hydrothermal process (120 °C, 36 h) under basic condition effectively dispersed the agglomeration and further induced the assembly of as prepared crystallites. The strong electrostatic attraction between CTA⁺ and negatively charged titania surface resulted in the dispersion of NPs together with phase transformation from amorphous to crystalline and further induced assembly to form mesoporous titania,²²³⁻²²⁵ (iii) during refluxing with ED, titania nanocrystals will have strong interaction with amine groups of ED similar to ammonia.²²⁶ Thus, synergistic interaction between ED and TiO₂ as well as CTAB and TiO₂ stabilizes the porous framework, rendering outstanding thermal stability; (iv) XPS revealed nitrogen containing species in the titania matrix retained the anatase even at high temperature. Due to high pressure in sealed reaction vessel, in situ monitoring and growth analysis of NPs under hydrothermal conditions are very difficult and hence detailed sequence of hydrothermal reaction during particle formation/growth and phase transformation remains unclear. The additional problem such as high energy consumption and low throughput is yet to be solved.

5.0 Sol-gel route

The aqueous sol-gel process is defined as conversion of precursor solution into a solid via inorganic polymerization reactions by the introduction of water. It involves the formation of metal-oxo-polymer network from molecular precursor such as metal alkoxides or metal salts.



This method constitutes hydrolysis-condensation reactions catalyzed in the presence of an acid, governed by hydrolysis ratio and nature of co-ordinating groups in titanium precursor.^{34,132,136,227-235} The hydrolysis leads to the formation of original nuclei or basic unit of TiO₂, while the condensation leads to the growth of crosslinked network system of original basic units. The faster sol-gel reaction leads to the formation of amorphous and non-uniform particles, whereas slow rate has the potential to produce the ordered structure. With the use of bulky and branched alkoxy groups such as butoxides, hydrolysis rates can be reduced to favour the formation of fine particles with more uniform size distribution.¹²⁰ This method provides large amounts of powders with a high level of chemical purity (chemical homogeneity) and possibility of deriving unique metastable structures. The adsorption of water on the surface sites of oxide powder will be physical mode and organic species adsorption via chemical mode.

5.1 Preparation of TiO₂ from titanium alkoxide/chloride precursors

The alcohol washing of precipitated powders in ammoniacal medium suppressed the anatase crystallization from amorphous, while promoted ART attributed to the organic impurities (oxo-alkoxide) on the particle surface (Fig. 7).²³⁶⁻²³⁷ The crystallization of anatase from amorphous at 390 °C was shifted to 467 °C after washing with alcohol. Upon further calcination, rutile fraction was 5 and 58 % for water and alcohol washed samples respectively

(Fig. 8). The crystallization from amorphous is combined effects of dehydration and structural relaxation and thus alcohol rinsing might have affected the dehydration step as it lowers the water content and hence suppressed crystallization.²³⁸ The alcohol washed powders showed a wider ART temperature range from 550 – 925 °C against the water washed samples (800 – 1100 °C).²³⁷ The alcohol rinsing reduced the particle agglomeration and that residual organics served as nucleation sites for rutile formation.²³⁹ The H₂O and –OH groups remaining after anatase crystallization induces breaking of Ti-O bonds or creating oxygen vacancies.²⁴⁰⁻²⁴¹ The ART for alcohol rinsed powders obeys first order kinetics, while water washing showed no unique value of reaction order. The brookite nucleus precipitated at low pH (< 5) promoted ART during calcination (Fig. 9).^{242a} The interaction of brookite with anatase reduces the pressure on anatase grains and consequent decrease in strain energy promotes rutile formation.¹⁰⁵ In this study, brookite was not intermediate phase during ART, since it was not observed for powders synthesized at pH > 5 under heat treatment.^{96,242a} In addition, interface between brookite and anatase with robust interfacial energy provides high density of potential nucleation sites to favour ART. In anatase rich or brookite rich titania NPs, ABT is preferred at ≤ 600 °C due to thermodynamic stability of brookite. Both ART and BRT dominated as a result of particle growth at ≥ 700 °C. The increased particle-particle contact sites of anatase favoured aggregation and promoted ART over BRT.^{242b} The TGA analysis revealed that BRT takes place at 1104 K.²⁴³

The sample precipitated from Ti(OBu)₄ at pH 4.5 showed pure rutile (850 °C), while those precipitated at pH 6.5 converts to rutile at much lower temperature (650 °C). The unreacted butoxide group of precursor and larger concentration of oxygen vacancies accelerated ART in the latter case.²⁴⁴ The gel obtained by hydrolysis of TTIP with ethanol showed 20 % anatase, while 55 % with IPA after calcination (500 °C, 3 h).²⁴⁵ The slow hydrolysis with latter was due to its long carbon chain which avoided the rapid precipitation

of rutile. Generally, induction period is observed in which slow particle growth will be followed by rapid precipitation of titanium particle from the aggregation of titanium clusters.²⁴⁶ The induction period is dependent on carbon chain length in alcohol solvent, with ethanol showing the low induction period and butanol displaying the longest. The less steric hindrance in ethoxy groups facilitates both primary nucleophilic reaction and polymerization process to result in larger particles. The induction period is very short at alkaline pH compared to acidic medium. At pH 3, hydrolysis reaction is catalyzed by acidic protons through protonation of leaving groups (alkoxy groups). At the same time, protonation of hydroxyl groups on Ti cluster inhibits the nucleophilic attack and retards the condensation pathways.²⁴⁷ The positive surface charge of clusters/colloids hinders the aggregation due to repulsive forces. Thus, slow polycondensation rate results in the formation of sol at acidic pH. In alkaline medium, strong nucleophiles are produced via deprotonation of hydroxo ligands resulting in increased condensation rates.²⁴⁶ The hydrolysis of TTIP with HCl promoted the amorphous to anatase and ART, while hydrolysis with NH_4OH retarded both the transition pathways irrespective of their concentration.²⁴⁸ The powders hydrolyzed with acid and base showed small and large average grain size respectively during calcination. This decrease in crystallite size with acid, increased the nucleation sites and consequently accelerated the phase transformation.²⁴⁹ In addition, XRD and Raman studies concluded that molecular structure of titania precursor resembled that of crystalline anatase, as it was stable than amorphous at low pH conditions.^{250,251} The gel obtained at pH 4 (also at pH 2) through the hydrolysis of TiCl_4 in NH_4OH showed anatase-rutile after calcination ($450\text{ }^\circ\text{C}$, 2h) and complete rutile at $600\text{ }^\circ\text{C}$.¹³⁶

The aging of gel (12 – 48 h) promoted ART to occur at high temperature compared to unaged samples.³¹ The large agglomeration number for unaged samples induces more number of anatase crystallites and crystallite-crystallite contact with each cluster to promote rutile via

interface nucleation. The E_a of ART for aged and unaged samples were 426-506 kJ/mol and 205 kJ/mol respectively.³¹ In contrast, aging of gel for 3 – 4 weeks at RT favored the formation of rutile, while aging the gel for 3 weeks followed by firing (200 – 300° C, 2 h) resulted in anatase-brookite-rutile, with brookite disappearing at > 400 °C.⁶¹ The method of drying the gel was found to influence ART: hydrogel obtained by $TiCl_4$ dried under infrared light after refluxing with water retained anatase, while the sample without refluxing showed anatase-rutile.²⁵² The gel dried by azeotropic distillation with n-butanol showed pure rutile, while those dried by reacting with acetic oxide shifted ART to high temperature. Depending on pH of the gelling solution, only anatase was obtained in the samples gelled at pH 5 (or 9), while anatase-brookite-rutile and anatase-brookite was observed at pH 3 and 7 respectively followed by calcination (400 °C, 12 h).²⁵³

The sol-gel synthesis of TiO_2 using triblock copolymer $EO_{20}PO_{70}EO_{20}$ (P123) resulted in mesoporous anatase-rutile for $H^+/Ti^{4+} \geq 1.0$ and only anatase for $H^+/Ti^{4+} < 1.0$.²⁵⁴ The acid influenced the interaction between inorganic framework and organic template to hinder the gelatination of titania oligomers thereby promoting the crystallite growth. For low acid concentration, oligomers adsorbing on positive charge repelled each other and condensation was suppressed,²⁵⁵ while association between titanium species and PEO moiety were strengthened. Under high acid concentration, more protons were adsorbed on the surface of titania oligomers and repulsive force became stronger suppressing the condensation and consequent mesoporous structure formation. The addition of triblock copolymer Pluronic F127 ($PE_{106}PPO_{70}PEO_{106}$) as structure-directing agent to titania sol and followed by calcination (400 °C, 6 h) promoted ABT.²⁵⁶ The local pressure produced by the fast combustion of copolymer adsorbed on the surface during calcination favored more dense structure of brookite. In contrast, addition of DEA suppressed the brookite formation. The modified sol-gel method using TTIP in absolute ethanol with cellophane membrane stabilized

the anatase up to 900 °C, despite the drastic grain growth (15 to 108 nm) upon calcination (400 – 900 °C, 3h).²⁵⁷ The cationic surfactant CTAC assisted sol-gel hydrolysis of TiO₂ using Ti(OBu)₄ showed brookite-anatase after aging (100 °C, 24 h).²⁵⁸

Scotti *et al.*²⁵⁹ suggested that rutile fraction increased with increase in H₂O/Ti molar ratio at a faster rate compared to HCl/Ti ratio using triblock co-polymer (EO₂₀PO₇₀EO₂₀) as a templating agent. The anatase configuration is statistically favored since octahedral units share several edges to form right angle array and is thus preferred at high reaction rates.²⁵⁹ Thus, increased random organization of octahedral units at high concentration of titanium ions favoured anatase and ordered arrangement of octahedral units at lower concentration promoted rutile. The presence of triblock polymer co-ordinates to metal ion precursor and slows the reaction rate to favor rutile.²⁵⁹ The extraction of PVP at refluxing step with ethanol-HCl, changed the phase composition; anatase was formed with initial stages and switches to rutile with further increasing the acid concentration.²⁶⁰ The non-ionic surfactant template has an amphilic character derived from the presence of hydrophilic amide group and hydrophobic methylene and methine groups. The highly polarized amide groups make the carbonyl active to complex with titanium cations²⁶¹ and hydrophilic / hydrophobic interactions lead to the formation of mesostructure. It was also found that increase of PVP content (up to 3.0 g) enhanced the surface area and later decreased. When the concentration of PVP reaches to CMC, surfactant organization into micelles takes place and sufficient balance between hydrolysis-condensation process of titanium precursor and self assembling reactions will be established.²⁶⁰ The sol-gel process using LAHC/TTIP modified with AcAc showed anatase-rutile after thermal treatment (700 °C).²⁶² The LAHC served as template to mesoporous formation and also as gel-formation assisting agent, while AcAc slowed down the hydrolysis of titanium precursor. The organic-inorganic hybrid powder obtained by sol-gel hydrolysis with PEO and AcAc were spherical in shape and transformed to anatase/rutile core/shell

double structure at 800 °C.²⁶³ The anatase surface transformed to rutile via surface nucleation and growth mechanism. During heating, partial ART starts and with subsequent air quenching, anatase core and rutile shell separate from each other due to difference in their thermal coefficient of expansion. The anatase core shrinks more in the course of cooling since thermal expansion coefficient value of anatase and rutile are 10.2 and 7.14×10^{-6} /K respectively. The crystal volume shrinkage via rutile formation as well as removal of PEO (and AcAc) trapped inside the cores would result in further shrinkage of core and formation of nanopores, which accounted for 5 – 10 % diameter difference between shell and core. The structural feature of core and shell are different; core is nanocrystalline and nanoporous, while shell is microcrystalline and dense. The nanoporosity of the cores arises from decomposition of PEO and AcAc and subsequent gas evolution during the heat treatment. The sol-gel synthesis assisted by surfactants is used to synthesize nanoporous titania with large surface area.²⁶⁴⁻²⁶⁸ Both ionic and non-ionic surfactants have been used because their amphiphilic character provides electrostatic interactions and hydrogen bonding between surfactant micelles and TiO₂ framework.

The ART was influenced by hydrolysis rate through varying the H₂O/Ti⁴⁺ ratio in the reaction system. Higher the water content, larger rutile particles will be formed after thermal treatment and vice versa.⁶¹ Sahni *et al.*²⁶⁹ reported that increasing water content enhanced the hydrolysis rate and formation of larger particles thermodynamically favoured ART. The important significance is that gelation time is effectively reduced by increasing the water concentration as it accelerates the cross-linking process.²⁷⁰ At high water concentration, some liquid is formed after gelation and macromolecular networks form rapidly through hydrolysis-condensation to have very low inter connectivity. Consequently, network is rather loose and solvent drifts out of network. In contrast, a system with low water content will form dense and compact structure network that can incorporate a high solvent concentration. The

rutile was formed at much lower temperature (300 °C) for higher water content and complete ART was observed at (600 °C), which was otherwise observed at 500 and 800 °C respectively for lower water content.⁶¹ The hydrolysis temperature influenced the phase formation of titania; transition from amorphous to anatase was observed at 300 °C and ART at 600 °C for the gel hydrolysed at 0 °C, while this transition temperature was increased to 100 °C for the gel hydrolyzed at 80 °C. When water concentration will be very high, effect of hydrolysis temperature on phase transition becomes quite insignificant and residual alkyl (halides) groups will be relatively small which does not affect the phase transition pathways. In contrast, large amount of unhydrolyzed alkyls remained in the powder for very low water concentration during hydrolysis prevents the crystallization from amorphous state.²⁷¹ Ding *et al.*²⁷² synthesized titania powders from titanium secondary butoxide by controlling the amount of water during the hydrolysis reaction. The grain size of powder prepared at low water concentration was smaller compared to those prepared at high water concentration. As a result, ART takes place at low temperature in the former powder than that of latter. The anatase-brookite was formed during the sol-gel hydrolysis of $\text{Ti}(\text{OBU})_4$ with HNO_3 and ABT was observed in preference to ART during calcination, indicating brookite is more stable than anatase.²⁷ Above 500 °C, both brookite and anatase directly transformed to rutile or anatase transforms to brookite and then to rutile. Interestingly, absence of HNO_3 during the hydrolysis step favored more anatase (70 %) and little brookite (30 %) and that BAT was observed during calcination, suggesting that anatase was stable than brookite. In either the case, BRT was faster compared to ART attributed to the presence of more nucleation sites for rutile formation within the brookite grain.²⁷ The sample with 44.7 % brookite transformed to rutile at a faster rate compared to sample with 30 % brookite, indicating that brookite plays a major role in rutile formation. The brookite content increased from 13 to 33 with increase in ratio of $\text{Ti}/\text{H}_2\text{O}$ from 1:700 to 1:4 and with increase in sol-gel pH (0 – 3) in HNO_3 medium

via sol-gel route. In addition, no systematic change in brookite content was observed from changing the temperature during the sol-gel synthesis. In contrast, synthesis with HCl resulted in amorphous along with anatase, indicating that chloride inhibits nucleation and particle growth.²¹⁷ The hydrolysis with high concentration of chloride (2 M) and low pH (-0.6) resulted in nanosized rutile.²²¹ The hydrolysis of TTIP at RT followed by drying at 382 K showed anatase-brookite. The maximum brookite (41.8 %) was observed after thermal treatment at 472 K and anatase (68.7 %) at 672 K. The anatase-brookite-rutile co-existed at 872 K with rutile as minor content. After 872 K, brookite disappeared and anatase-rutile coexisted. The complete transformation to rutile was observed at 1172 K.²⁷³

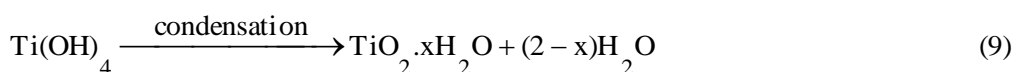
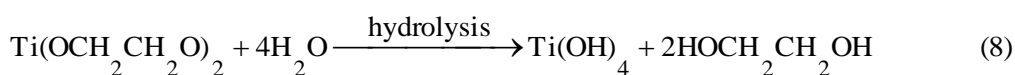
The gel obtained by TTIP and AcOH at pH 3 – 4 stabilized the anatase up to 1000 °C, while those obtained at pH 5 – 6 transformed to rutile at 800 °C.²⁷⁴ This was reasoned to strong chelating effect of AcOH, which declines with increase in pH of the reaction solution. At low pH, condensation reaction is slow compared to hydrolysis because of charge-charge repulsion between hydrated metal cations which facilitates branching to occur before particle growth to produce strong cross linked gel. The further increment in pH perturbs the well organized cross-linked network structure. The gel containing polymeric chains with little branching and cross linking and also a smaller void region, is structurally weak and thus collapses rapidly on calcination forming rutile at low temperature.²⁷⁵ Likewise, addition of water during the hydrolysis of TTIP with formic acid also promoted the rutile formation at low temperature. In contrast, increasing the volume of formic acid retained the anatase even at high temperature treatment. This result suggests that addition of water critically affects the chelation effect of anchoring groups to titania and thus ART.²⁷⁶⁻²⁷⁷ The formate group favored a bridging (syn-anti or syn-syn) mode of chelation depending on the reaction conditions (Fig. 10). The syn-anti bonding hinders the cross-linking of gel network resulting in a weak structure, while syn-syn mode of binding produce ordered gel networks. The

addition of water favoured syn-anti mode of binding and destabilized the system by collapsing the highly cross-linked network structure that facilitates hydrolysis and rutile formation. The addition of carboxylic acids like AcOH, propanoic acid and butyric acid during the hydrolysis step showed surprising results in crystallization behavior.²⁷⁸ In this study, precursor was modified with carboxylic acid prior to hydrolysis, while water and alkoxide are reacted without dilution in the hydrolysis step. Both AcOH and propanoic acid exerted similar effects on amorphous to anatase and ART as quantity of carboxylic acids was similar. However, both the transition was found to accelerate for butyric acid attributed to creation of defects by disrupting the ordering of hydrolysate structure. During annealing, organic residues undergo combustion and these defects will be destroyed accompanied by the release of stored energy which overcomes the activation barrier for the nucleation of crystalline phase. As the quantities of residual butanoate groups are greater than acetate and propionate groups, net effect in butyric hydrolysates is to decrease the energy required to induce crystallization and phase transformation.²⁷⁸ The presence of mixed complexing agents DEA-polyethylene glycol (**A**) in the hydrolysis of TTIP showed brookite, while other complexing agents like AcAc (**B**), DEA (**C**), polyethylene glycol (**D**), AcAc-polyethylene glycol (**E**) and AcAc-AcOH (**F**) showed pure anatase after calcination (600 °C, 1h). Interestingly, only (**B**) and (**F**) stabilized anatase, while the rest showed rutile at 800 °C.²⁷⁹ The in situ water produced in esterification via modified sol-gel method favoured anatase-TiO₂(B). The monoclinic phase initially appeared (400 °C, 6 h) followed by gradual transformation to anatase (550 °C). The steric effects induced from large stable acetate and sulfates may be beneficial to the formation of loose zig zag chains of octahedral in TiO₂ (B) as compared to linear chains of octahedral in rutile.²⁸⁰

The hydrolysed product of titanium glycolate crystallized to anatase (400 °C, 2 h) and later to rutile (850 °C).²⁸¹ The formation of glycolate precursor is expressed as:



On adding acetone, glycolated precursor undergoes a slow hydrolysis and spherical titania particles are tuned through homogeneous nucleation and growth process. Acetone is believed to accelerate the hydrolysis of glycolated precursor.²⁸² The water content in acetone influenced the final size of particles: inhomogeneous spherical particles were formed for water content > 0.4 % and titania particles were not generated at all for < 0.05 %. Thus, oxygen deficient spherical NPs with low dispersion was obtained at optimized water content (~0.3 %). The hydrolysis process and formation of titania can be expressed as:



The nucleophilic substitution reaction between ethylene glycol and $\text{Ti}(\text{OBu})_4$ produce titanium glycolate. The bridging occurs through chelating alkoxy ligand with ethylene glycol unit and it is more stable to moisture compared to alkoxide.

Typically, sol-gel derived precipitates are amorphous in nature, requiring further heat treatment for crystallization as well as to remove organic compounds on product surface which inevitably results in partial agglomeration and collapse of initial nanostructures accompanied by phase transition. Depending on pH and concentration of Ti^{4+} ions, large number of oligomeric species is formed making the aqueous chemistry quite complex. The counter ions co-ordinates to Ti^{4+} form a molecular precursor with different chemical reactivity towards hydrolysis and condensation and are impossible to predict. Since hydrolysis and condensation of molecular precursor are too fast, loss of morphology and structure of oxide material are very often. Another problem is the protocol developed for bulk metal oxide cannot be extended to its nanoscale counterparts.

5.2 Ultrasonication assisted sol-gel synthesis

Sonochemistry has become an effective technique for nanomaterials synthesis as unique reactions can be realized by irradiating the liquid at RT.²⁸³ This system offers a potential to produce inorganic materials of high purity, cause novel chemical reaction and physical changes, uniform and narrow particle size distribution with controlled shape. The sonochemical effect arises from acoustic cavitation, formation, growth and implosive collapse of bubbles in the liquid medium.²⁸⁴⁻²⁸⁶ After several compression cycles, cavitation bubbles collapse violently and adiabatically to generate localized hot spots with transient temperature of 5000 K, pressure of about 500 atm, heating and cooling rates $>10^9$ K/s.^{284,287} Therefore, application of ultrasound to enhance the reaction rate and to shorten the time has become synthetic technique for many homogeneous and heterogeneous chemical reactions.²⁸⁴⁻²⁸⁹ The turbulent flow and shock waves produced by acoustic cavitation drives the metal particles together at high velocities.²⁹⁰ A high speed collision produces localized high temperature region to accelerate the condensation reaction among hydroxyl groups on adjacent TiO₂ sol particles.²⁹¹ It was proposed that,²⁹²⁻²⁹³ there are three regions in aqueous sonochemical process: (a) gas phase region (5000 K, 180 atm) within the cavitation bubble; (b) interface zone (1900 K) between gas phase and bulk solution; (c) region of bulk solution. It is assumed that formation and growth of titania nuclei are accelerated at the interfacial region because of low vapor pressure of reactants.²⁹⁴ Thus, more growth units will be formed and titania nucleus grows at high velocity.

Anatase, rutile and anatase-rutile was obtained after ultrasonication (3 h) TTIP, TiCl₄ and its mixture respectively.¹⁷⁴ The hydrolysis of TTIP with 0.2 M HCl under sonication resulted in anatase-rutile and with only TTIP (303 K, 3 h) showed anatase-brookite. This indicated that ultrasound irradiation induces crystallization, while nature of precursor and acidity governs the phase transition pathways. The particle size of rutile was almost twice

than anatase; TiCl_4 hydrolyzes rapidly in water and part of titanium hydroxide precipitates before dissolving in the acidic solution. In the mean time, some of titanium ions that exist as titanate are further co-ordinated by chloride anions. In contrast, hydrolysis of TTIP is rather slow in water resulting in nearly neutral, partly condensed and more homogeneous gel. In the latter case, ultrasound irradiation creates more localized hot spots within the gel, outside which polycondensation of $\equiv\text{Ti-OH}$ species will be accelerated. This causes the homogeneous formation of large number of seed nuclei with smaller particle size. It was proposed that interaction caused by sonication amongst the titanium species in the gel is stronger compared to mixture containing $\equiv\text{Ti-Cl}$ species which results in less condensed metastable anatase.¹⁷⁴ The hydrolysis of $\text{Ti}(\text{O}i\text{Bu})_4$ with H_2SO_4 and Na_2SO_4 via ultrasound irradiation (358 K, 3 h) gave anatase, while rutile was formed with HCl (1.3 – 4.0 M).¹³⁹ The variation in the concentration of NaCl and KNO_3 in the synthesis step showed no influence on titania polymorphs. The anatase-brookite-rutile was observed for 1 M HNO_3 , while both anatase and brookite was transformed to rutile at 2 M HNO_3 . The anatase-brookite co-existed at 0.5 M HCl , while ART and ABT were observed at 0.8 M, followed by pure rutile at 1.3 M. Thus, sulfate anion promoted anatase, while chloride and nitrate favoured different polymorphs depending on its concentration. The sulphate anion reacts with octahedral hydroxyls by static electricity. Because of its steric effect, third octahedron attacks along the converse direction to reduce the steric repulsion and orientation of third octahedron is more conducive to favour anatase (Fig. 11). The ultrasonication of TTIP in ethanol-water (40 °C, 3 h) was amorphous and crystallized to anatase by increasing the reaction temperature (90 °C).²⁹⁵ The anatase was stabilized for ultrasonicated samples, while samples without ultrasonication transformed to pure rutile after calcination (800 °C, 2 h). The latter suffered from interparticle agglomeration and the particles were uniformly distributed in the former case.²⁹⁶ The ultrasonication (20 min) induced brookite formation at low temperature (25 °C), compared to

samples without ultrasonication (70 °C) during the hydrolysis of TTIP in ethanol-water. The BAT was dominated up to 500 °C and ART was observed thereafter (500 – 800 °C, 2h) in the former case. For the sample without ultrasonication, ABT was observed up to 400 °C, followed by BAT up to 500 °C, while ART prevailed at later stages. The pure anatase was observed at 500 °C in both the cases.²⁹⁷

Mesoporous anatase TiO₂ with worm-like framework structures was obtained using long-chain organic amine as structure directing agent via ultrasonication (6 h). The large surface area and high stability was achieved with increase in the alkyl chain length of amines, without change in morphology. The strong hydrogen bonding between amines and titanium precursor attributes to the formation of mesoporous structure.²⁹⁸ The ultrasound (3 h) initiated hydrolysis of TTIP for a short period of time followed by calcination (673 K, 1 h) resulted in 3-D and thermally stable mesoporous anatase titania without the use of any templates.²⁹⁹ The AcOH was used as a modifying agent to slow down the hydrolysis rate and as ligand to change the chemical identity of titanium alkoxide at molecular level. The AcOH inhibited the hydrolysis rate of TTIP by forming Ti(OPr)_x(OAc)_y, as AcOH is negatively charged ($\delta_{\text{AcOH}} = -0.7$) and PrOH is positively charged ($\delta_{\text{IPA}} = +0.1$). When this precursor is added to water, less electronegative alkoxide groups are hydrolyzed preferentially, whereas strongly bound complexing groups are difficult to remove. The remaining complexing groups acts as terminating agents that decrease the tendency towards condensation. It was proposed that monodispersed TiO₂ sol particles are initially formed by ultrasound assisted hydrolysis of AcOH modified TTIP. The mesoporous spherical or globular particles with a narrow pore size distribution are produced by controlled condensation and agglomeration of these sol NPs. The high thermal stability of mesoporous titania was attributed to its thick and robust inorganic walls.²⁹⁹ Ultrasound assisted synthesis of mesoporous TiO₂ using TTIP with triblock copolymer (EO₂₀PO₇₀EO₂₀) for 3 h increased the brookite content, which partially

transformed to anatase after calcination (673 K, 1 h).³⁰⁰ The hybrid inorganic/organic precursor formed between triblock polymer and TTIP promoted the brookite formation. In addition, ultrasound irradiation accelerated the crystallization of titania and also enhanced the extraction of triblock polymer from hybrid inorganic/organic precursor. Thus, hydrolysis, crystallization of amorphous and extraction of surfactant can be accomplished in one step. Although, presence of strong acid or base or alkali ions was essential for brookite formation,^{86,88,301} it was achieved under neutral pH conditions without alkali ions. The ultrasonication of TTIP in ethanol-water (molar ratio is 10) transformed to anatase upon calcination (400 °C, 1 h), while anatase-brookite was observed with pure water. The addition of ethanol inhibited crystallization and brookite formation by adsorbing on TiO₂ surface.³⁰² The increase of calcining treatment (600 °C, 1 h) showed anatase-brookite-rutile and that brookite disappeared completely at > 600 °C for the samples prepared in pure water. In contrast, high rutile content was observed with ethanol under same conditions. The ultrasonic (30 min) assisted sol-gel hydrolysis of titanium ethoxide in AcOH followed by calcination (773 K, 3 h) showed only anatase.³⁰³ The phase transformation pathways was found to depend on mode of ultrasonication via tip-type (irradiation carried out inside a reactor with a probe tip) and bath-type (irradiation from outside reactor); in the former case, ART and ABT dominated during initial stages (60 min), followed by BAT (90 min) and BRT (120 min).³⁰⁴ In the latter case, only ABT was observed in the entire reaction time (60 – 120 min) after calcination (500 °C, 3 h). The tricrystalline anatase-brookite-rutile, with anatase as dominant phase was observed in both cases. Based on a series of experiments, parameter effects was summarized as follows: (i) increase of ultrasonic power density in tip-type (18 – 42 W/L) favored ABT, with less preference to ART; (ii) increasing the reactor size in bath-type promoted ABT and ART upto 500 mL, while BRT and BAT was preferred at 1000 mL; (iii) ABT was observed accompanied by the disappearance of rutile with increase in water content

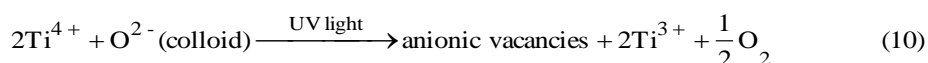
(H₂O/TTIP ratio) from 10 – 175 in bath-type. (iv) increase of hydrolysis temperature (5 – 40 °C) favoured ABT in tip-type.³⁰⁴ The rutile fraction increased initially with increase in ultrasonic irradiation amplitude (up to 40%) and later decreased after calcination (750 °C, 3 h).³⁰⁵ At this optimal amplitude, there would be an ideal balance between high temperature and high energy collapse which would limit the local volatilization of 2-propanol and heat energy would be utilized solely for phase transformation. At higher amplitudes, acoustic shielding or acoustic dampening effect together with volatilization of solvent predominates, leading to low yield for the reaction and ill crystallinity for the samples. In addition, cavity diameters will be too high to generate any cavitation that would be useful for titania synthesis.³⁰⁵

The operating variables such as ultrasonic power density, reactor size, stirring effect, rise in local temperature and mode of applications (tip- or bath-type) strongly influence the properties of titania. The cavitation process must be as efficient as possible in order to optimize sonochemical driven reactions. This would result in minimum loss of energy and optimum frequency of bubble oscillation and collapse, since the topology of acoustic pressure field depends on the type of reactor and source of ultrasound.³⁰⁴⁻³⁰⁵

5.3 Photo-illumination assisted sol-gel synthesis

Beside applying for photoreduction of metal ions onto the semiconductor surface, UV irradiation is used to densify and crystallize sol-gel derived powder as an alternative to calcination. The photo illumination (8 h) applied during the hydrolysis of TTIP with HCl and heat treatment (100 °C) gave anatase, while it was amorphous for non-irradiated samples.³⁰⁶ Since amorphous to anatase transition involves an overall shrinkage of 8 % with a cooperative movement of ions, removal of oxygen ion and/or oxygen defects generated by UV light was found to accelerate this transformation. In addition, pure rutile was formed at 600

and 700 °C for photoilluminated and non-irradiated samples respectively suggesting that former reduced the ART temperature to an extent of 100 °C (Fig. 12). The rutile particles were regular polyhedron and small grain size distribution without agglomeration in the former case, while deformed and agglomerated particles was observed for typical sol-gel powder.³⁰⁷ The UV-illumination can generate Ti³⁺ defect sites on TiO₂ surface through a surface reduction process of Ti⁴⁺ to Ti³⁺ similar to that induced by Ar sputtering, electron beam exposure and high energy UV-light.³⁰⁸⁻³⁰⁹ These surface Ti³⁺ defects are accompanied by the removal of surface oxygen atoms or most likely bridging oxygen atoms³¹⁰ generating surface oxygen vacancies to promote crystallization at low temperature. The possible reaction to induce formation of oxygen vacancies is;



In addition, photo-irradiated samples exhibited a new absorption band at wavelength longer than 400 nm, which suggests its possible applications under visible light.³¹¹ The production of Ti³⁺ also resulted in the formation of TiO₂-Ti₂O₃ binary oxides.³¹²⁻³¹³

The photoirradiation (15 h) of gel obtained from TTIP resulted in enhanced crystallinity and rutile formation at high water content after calcination (353 K, 4 h).³¹⁴ The UV light can excite the weak Ti-OR bonds and promotes the hydrolysis, replacing alkoxy groups by hydroxyl groups.³¹⁵⁻³¹⁷ Thus, olation is expected to occur at a faster rate at various hydrolysis ratios. The growth of rutile at high water concentration stems from enhanced surface hydroxylation combined with the highly distorted bulk atomic arrangements.³¹⁸ The surface of titania becomes protonated in acid medium facilitating dissolution-precipitation pathway to operate and resulting in rutile.^{187,319-320} In contrast, rutile nucleated at intermediate water content (r=H₂O/Ti=7), anatase at extreme ends (r=4 and 10) for the samples prepared by conventional sol-gel method. Surprisingly, brookite was formed at a value of r=20. At low hydrolysis ratio (r=4), more isopropoxy groups retain since the hydrolysis is usually

incomplete and that alkoxy groups are difficult to get removed.^{157,321-322} The oxolation leading to linear chain will be unfavorable because of steric hindrance and accordingly, oxolation will be preferred to form the skewed chains. When hydrolysis ratio increases ($r=7$), condensation proceed by oxolation or ololation pathway and competition of these two processes leads to anatase-rutile. The promotion of hydrolysis ($r\geq 10$) facilitates more hydroxyl groups favoring anatase. In contrast to previous report,³⁰⁷ ART was not faster in photo irradiated samples compared to traditional sol-gel powder, due to the absence of Ti^{3+} formation as evidenced by XPS technique. The crystalline anatase at very low temperature (80 °C) was observed via combined non-hydrolytic/UV illumination (30 – 100 min) utilizing $TiCl_4$ and tertiary butyl alcohol via alkyl halide elimination process.³²³ The surface hydroxyl group and oxygen vacancies are enriched under UV light which transforms the semicrystalline to crystallized anatase accompanied by the ‘self-oxidation’ photochemical effect. The large surface area, high crystallinity and less carbonaceous species can be achieved by photoassisted sol-gel method that benefits the titania for better applications.

6.0 ILs assisted sol-gel synthesis

The ILs are RT molten salts consisting of virtually bulky organic cations and weakly co-ordinating anions, widely studied as a new kind of reaction media in the context of green chemistry due to their unique features such as low volatility, low flammability, wide liquidus, no combustion, non-toxicity, good chemical-thermal stability, unusual solvent power for both organic and inorganic compounds, strongly designable structures, high ionic conductivity and wide electrochemical window.³²⁴⁻³²⁷ The high vapor pressure of organic solvents used in conventional sol-gel methods, causes gel shrinkage followed by loss of pore volume and surface area during solvent evaporation.³²⁸ In contrast, low or negligible vapor pressure of ILs reduces the problem of gel shrinkage during sol-aging and gel-drying avoiding the loss of

surface area.³²⁹ In addition, RTILs with hydrophobic regions and high directional polarizability from extended hydrogen bond systems in the liquid state results in a highly structured self-assembly of RTILs. The ILs containing small amount of water can be well blended with alcohol solvents to reduce the rate of hydrolysis reaction to yield better porous structure. The RTIL can capture protons or hydroxides through hydrogen bonds or electrostatic function acting as acid-base pair and accelerate the polycondensation pathway in the sol-gel process.³³⁰ However, the amount of RTIL has no obvious effects on average pore diameter of TiO₂. The strength of hydrogen bonds on the anion part of IL with water is essential to form mesoporous structure, while the alkyl chain length of cationic part determine the pore size and volume of nanoparticles. Since RTIL can cap the surface of nanocrystals, it affords low agglomeration tendency, good dispersibility and has potential to tailor the surface properties.

The addition of [cmim] [HSO₄] changed the morphology from rutile NRs to nanoflowers and induced high degree of crystallization under hydrothermal condition (180 °C, 3 h).³³¹ The following peculiar properties of [cmim] [HSO₄] enhanced the growth of rutile flowers containing a bunch of aligned NRs; (i) it promotes the ionic strength by dissolving in solution and thus enhances the solubility of Ti species; (ii) [cmim] [HSO₄] served as surfactants by dissolving in solution and then cap the nanocrystal facets to enhance the orientation of particles after rutile formation. (iii) it favored the formation of small crystals through electrostatic screening which is not available in traditional surfactants.³³² The anatase-brookite formed by thermolysis of 0.15 M TiCl₄ (100 °C, 24 h) transformed to rutile with the addition of [emim] [Br] up to 0.602 M, due to different structures of anatase (101) and rutile (110) planes.³³³ The structure of rutile (110) plane is very close to the bulk truncated geometry and the most stable crystal face.^{51,334} In this way, (110) plane unit cell contains one 2-fold co-ordinated bridging oxygen atoms above the (110) truncated plane. The

space between $[\text{emim}]^+$ ions after anchoring onto (110) plane via rutile (110)-c(2x2)- $[\text{emim}]^+$ will be 0.592 nm. Fortunately, $[\text{emim}]^+$ ions are separated in various directions according to mutual π -stacking distance (0.6 – 0.7 nm) between the aromatic rings.³³⁵⁻³³⁶ Thus, $[\text{emim}]^+$ ions was allowed to anchor onto rutile (110) plane to form relatively tight coverage layer (Fig. 13). The $[\text{emim}]^+$ substitutes H^+ ion resulting in the formation of $[\text{emim-O-Ti}]$ that favoured linear chains via edge shared $[\text{TiO}_6]$ based on mutual π -stacking between aromatic rings in the acidic medium. However, anatase (101) plane is toothed and distance between bridging oxygen atoms is not in the space range of mutual π -stacking between aromatic rings. Among the usual crystal plane of anatase, none of them was found to be suitable for forming coverage layer by this $[\text{emim}]^+$ ion adsorbing model.

Hydrothermal treatment of TiCl_4 and $[\text{bmim}] [\text{Cl}]$ promoted ART, while the presence of hard bases F^- or SO_4^{2-} stabilized only anatase.³³⁷ The fluoride ion selectively adsorbed on $\{001\}$ facets, leading to highly truncated bipyramid shaped primary NPs, while SO_4^{2-} was less selectively adsorbed leading to truncated pyramid and parallelepiped shaped nanocrystals. The nucleation and growth of rutile after prolonging the reaction time with bmim^+Cl^- and water were determined by the aggregation manner of anatase nanocrystals and OR respectively.³³⁸ The yellow solid $[\text{bmim}^+]_2[\text{TiCl}_{6-x}(\text{OH})_x]^{2-}$ was initially formed by mixing TiCl_4 and bmim^+Cl^- . The adsorbed bmim^+ cation layer served as steric protection shell to slow down the random aggregation process. The observed phase transformation was explained as follows: (i) hydrolysis of $[\text{bmim}^+]_2[\text{TiCl}_{6-x}(\text{OH})_x]^{2-}$ facilitates the substitution of hydroxyl groups through the attack of water molecules and formed Ti-oxo species acts as monomers for nucleation and growth; (ii) concentration of Ti-oxo species increases rapidly due to fast hydrolysis. According to LaMer model, nucleation burst occurs if the degree of supersaturation is high enough to overcome the energy barrier for nucleation. Thus numerous anatase nanocrystals are formed and Ti-oxo species concentration reduces rapidly; (iii)

aggregation of anatase NPs results in rutile or interface structure having rutile like character favours ART. The increase of acidity, Ti precursor concentration and water content favored the rutile fraction due to weaker adsorption of bmim^+ on TiO_2 surface leading to faster aggregation of nanocrystals. In addition, increase of temperature also promoted the rutile growth as a result of increase in the concentration of Ti-oxo species and activation of Ti-O bonds.

Mesoporous anatase with narrow pore size distribution was obtained at very low temperature (60 – 100 °C, 24 h) under hydrothermal conditions with [bmim] [BF₄] and was thermally stable up to 900 °C.³³⁹ The [bmim] [BF₄] consists of large imidazolium cation and BF₄⁻ ion adsorbed on the surface of octahedron through hydrogen bonding creates a steric barrier for brookite and rutile formation.³⁴⁰ In addition, RTIL has low interface tension and high ionic strength resulting in high nucleation rates to facilitate anatase formation.³²⁷ The IL extraction using acetonitrile followed by annealing (100 °C, 2 h) were amorphous, while thermal annealing of the product followed by acetonitrile extraction showed anatase.³⁴¹ The ILs play an important role in driving the surface crystallization of amorphous to anatase by retaining a suitable amount of water through dissolution-crystallization mechanism. The anatase crystallization induced from ILs was not observed at very low H₂O/TTIP molar ratio, due to association of IL as tight ion pairs.³⁴¹ At other H₂O/TTIP molar ratios, amorphous hydroxylated titanium compound could be formed due to rapid hydrolysis or IL induced water dissolution of condensation product. The ILs served as water adsorption agent and as steric stabilizer to the amorphous phase. The self-organization ability of ILs drives the formation of anatase through dehydration of hydroxyl group in the hydroxylated titanium compound in the subsequent thermal step. It has been reported that water-IL mixture cannot be considered as homogeneous, but rather as nanostructured system.³⁴² Liu *et al.*³⁴³ and Zhu *et al.*³⁴² found that most of ILs were self associated as tight ion pair in system rich in IL.

Whilst, most of water molecules were also self associated in water-rich system. Besides these two extreme cases, ILs are hydrogen bonded to water molecules. This specific characteristic of water-IL system might make the anatase crystallization behavior dependent on H₂O/TTIP molar ratio in ionothermal (sol-gel method containing IL) system. The increase in the volume of IL increased the crystallite size of titania, attributed to increased viscosity and decreased diffusion co-efficient.^{330,344}

The titanium precursor was hydrolyzed and condensed around the self-assembled [C₄mim] [BF₄] or [bmim] [PF₆] combined with water at a controlled rate resulting in porous anatase (80 °C, 12 h or 100 °C, 2 h).³⁴⁵⁻³⁴⁷ Further heat treatment improved the crystallinity and thermal stability without significant pore collapse due to their sponge-like mesoporous structure, constituting narrow size distribution and no large pore indicating the homogeneity of IL in the titania matrix.³⁴⁶ The possible mechanism for the formation of these titania NPs might be an effective aggregation of titania particles with a self assembled IL in the sol. The reduced hydrolysis with IL renders longer aging time for the formation of stable sol-gel network with an ordered array of Ti and O, without accompanying any shrinkage and collapse of gel network. The particle possesses disordered mesostructure without long-range order in the pore arrangement and no micropore was present. The water molecules in IL preferentially reacts with [PF₆]⁻ strongly through hydrogen bonding whereas imidazolium ring do not interact with water.³⁴⁸ Accordingly, [bmim]⁺ should array in the opposite direction to [PF₆]⁻ bonded with water and then start to pile up and stack, possibly by π - π interactions or other non covalent interactions between imidazolium rings. This indicates that IL can be used as self-assembling template like long chain surfactants without the formation of ordered micelles by hydrophilic and hydrophobic molecular chains.^{327,348-349} Consequently, titanium precursor is hydrolyzed and condenses around the self-assembled IL structure combined with water at a controlled rate, resulting in the formation of highly porous

crystalline TiO₂. The [bmim] [PF₆] assisted hydrolysis of TTIP stabilized anatase even up to 800° C, while unmodified titania completely transformed to rutile at the same temperature.^{344,345} The IL assisted sol-gel synthesis was crystalline anatase at 100 °C, while unmodified titania was still amorphous. At least 3 moles of IL are necessary to form crystalline titania for each mole of titania precursor at this temperature. Among the various ILs like [bmim] [PF₆], [bmim] [PF₄], [bmim] [CF₃SO₃] and [hmim] [PF₆], only [bmim] [PF₆] was effective in inducing mesoporous structure.³⁴⁴ However, role of water in [bmim] [PF₆] is complex, and its structure-chemical reactivity is different from those of bulk water as it is tightly bonded and activated in the hydrogen bond system of ILs.^{348,350-352} The [bmim] [PF₆] acts as capping agent for preventing direct hydrolysis of TTIP due to its water immiscibility and makes a localized anhydrous or water poor area between ILs and titanium precursor. This water poor condition suppress the formation of hydroxide and oxyhydrate (amorphous species) as limited amount of water drive the mass balance to completely condensed and directly crystalline systems.³⁴⁷ Also, in conventional sol-gel route employing excessive amount of water (surface tension, $\gamma = 72 \text{ mJ/m}^2$ at 293 K), nucleation of TiO₂ is slow, while low interface energy ($\gamma = 46 \text{ mJ/m}^2$ at 293 K) and adaptability of [bmim] [PF₆] results in high nucleation rate generating NPs.^{327,347,353} The NMR and FTIR studies revealed that IL was entrapped in the growing covalent titania network rather than being chemically bound to the inorganic matrix. The water immiscibility of [bmim] [PF₆] initiates the formation of Ti-O-Ti framework and TiO₂ particle would be homogeneously dispersed in hydrophobic [bmim] [PF₆] resulting in the formation of highly porous TiO₂. The ultrasonication of [C₃mimOH] [Tf₂N] with TTIP resulted in pure anatase, which transformed to rutile after calcination (800 °C, 5 h) with E_a of $13.87 \pm 0.5 \text{ kJ/mol}$.³⁵⁴ The other ILs like [P₆₆₆₁₄] [Tf₂N], [N₁₈₈₈] [Tf₂N], [C₄Py] [Tf₂N] and [C₄mim] [Tf₂N] resulted in anatase-brookite. The ultrasonication of TiCl₄ with [N₁₈₈₈][Tf₂N] showed anatase-rutile, while anatase and rutile were observed with urea

and HCl respectively (Fig. 14). Interestingly, [C₃mimOH][Tf₂N] under hydrothermal treatment (170 °C, 20 h) resulted in anatase, while microwave irradiation had anatase-brookite. The morphology of anatase was controlled by IL cation; nanospheres was observed with [C₃mimOH][Tf₂N], [P₆₆₆₁₄][Tf₂N] and [C₄Py][Tf₂N], while NRs with [N₁₈₈₈][Tf₂N] and spindle shape for [C₄mim][Tf₂N]. The TiO₂ (B) content in anatase-TiO₂ (B) was tuned by varying the ratio of surfactant to IL (C₁₆mimCl + C₄mimBF₄).³⁵⁵ The maximum TiO₂ (B) content was observed for very low ratio of ~ 10 %, while low content for a mixture of CTAC and C₄mimBF₄. Finally, systems where the solvent was based on ammonium group and independent of surfactant structure, only anatase was formed irrespective of surfactant to IL ratio. The mixture with C₁₆mimBF₄ + C₄mimBF₄ resulted in TiO₂ (B) for very high concentration ratio of > 10 %. Therefore, TiO₂ (B) was observed only with IL based on imidazolium moieties and the peculiar charge distribution and polarization pattern created by the self-assembled surfactant.

The use of ILs in the synthesis of metal oxides is very simple; reaction is performed under atmospheric pressure in a glass vessel, without harsh conditions and highly crystalline products together with tailored composition and large surface area can be obtained. The titania synthesis via photo-illumination, ultrasonication and with IL template has important implications, as this not only save energy and cost of synthesis procedure by avoiding calcination step to induce crystallization, but also allows a wider selection on the type of support materials to immobilize crystalline material at low temperature.

7.0 Thermolysis / Thermohydrolysis

7.1 Influence of water

The orthotitanic acid was formed by hydrolysis of TiCl₄ in water (TiCl₄: H₂O = 1:10), followed by boiling for 2 h gave anatase-rutile.³⁵⁶ The anatase-brookite obtained by the

hydrolysis of TTIP in hot water, transformed completely to rutile at 600 °C.²⁵⁶ Anatase, rutile and brookite was tuned in the thermohydrolysis (100 °C, 48 h) of TiCl₄ in various proportion of water. The rutile content gradually decreased, while anatase increased with change in TiCl₄/H₂O ratio from 1:5 to 1:150. The brookite was observed at 0.25 M TiCl₄ (TiCl₄/H₂O of 1:35) and their fraction was scarcely affected with water. Conversely, increasing the aging time to 48 – 76 h, brookite content increased at the expense of anatase and rutile irrespective of TiCl₄/H₂O ratio. The anatase-brookite-rutile, anatase-brookite and anatase-rutile were observed in the region of 0.25 – 0.09, 0.06 M and 0.81 – 0.34 M respectively and pure rutile at 1.48 M TiCl₄.³⁵⁷ Mesoporous rutile without amorphous content was obtained by simple hydrolysis of TiCl₄ in water (40 °C, 48 h) with octyl phenolpolyethylene oxide as surfactant, which was later removed by extraction with acetone and UV illumination.³⁵⁸ It was suggested that formation mechanism obeys self-assembly of nano rutile crystals, instead of inorganic/PEO contained polymer assembly mechanism. In the absence of surfactant, these nano rutile crystals are aligned together along one direction to form needle-like crystals with an appropriate ratio due to strong acidic conditions. The hydrophilic PEO moieties of surfactant are strongly absorbed on the surface of nanorutile crystals and hydrophobic moieties are directed to solution. Thus, formation of needle-like titania sample by aligning together with rutile crystals was hindered. When the concentration of surfactant is above CMC, rutile crystals with hydrophilic moieties are self-assembled to form mesoporous structure by self-assembly formation of hydrophobic moieties.³⁵⁸

7.2 Influence of alcohol

The hydrolysis of TiCl₄ ethanolic solution (50 °C, 24 h) in water gave pure rutile nanorod superstructures, while presence of KCl and TTIP instead of TiCl₄ showed anatase indicating that strong protonated condition from ethanolsis and hydrolysis of TiCl₄ favoured

rutile.³⁵⁹ When KCl was replaced by HNO₃ or H₂SO₄, rutile and anatase was formed respectively. The direct hydrolysis of TiCl₄ with water in the absence of ethanol resulted in fewer rod-like rutile NPs suggesting that ethanol was vital in the formation of nanorod superstructure. The TiCl₄ dissolves in C₂H₅OH to form [TiCl_m(OC₂H₅)_{6-m}]²⁻ and HCl, followed by reaction with water to give [Ti(OH)_nCl_m(OC₂H₅)_{6-m}]²⁻. The high acidity and large amount of chloride ions reduced the number of hydroxyl ligands to promote vertex shared bonding to form rutile.³⁵⁹ The thermohydrolysis of TiCl₄ in HCl-ethanol aqueous solution (40 – 90 °C, 30 min) resulted in rutile with well defined rod-like shapes, while irregular shapes with high polydispersity were observed in the absence of alcohol.³³² Anatase was formed via alcoholysis of TiCl₄ with ethanol (<100 °C, 72 h) and rutile nucleated after calcination (700 °C, 2 h). The critical size for ART was in the range of 32 – 42 nm.³⁶⁰ The reaction of TiCl₄ and ethanol leads to [TiCl_x(OCH₂-CH₃)_{4-x}], whose structural units are similar to anatase lattice.³⁶¹ The grain growth kinetics for anatase NPs can be described by:

$$D^2 = D_0^2 + 3.86 \times 10^4 \times t^{0.286(9)} e^{-32(2)/RT} \quad (11)$$

The FTIR revealed large degree of surface hydration by hydrogen bonds with a wide set of energetically non-equivalent surface hydroxyl groups due to the presence of different anatase crystal planes and various types of surface defects. The surface hydration increases with decrease in anatase particle size accompanied by volume contraction. The heating of hydrated particles (100 °C, 2 h) allows for the removal of small amount of water with only a small increase in particle size. However, removal of surface water below a certain threshold value, leads to significant grain growth. The rapid precipitation of rutile particles was observed with increase in the volume of 2-propanol to water ratio, while it was decreased for ethanol and methanol.³³² The acidic hydrolysis of TiCl₄ in IPA-water resulted in brookite, anatase and rutile at 0.3 M, 1.0 M and 1.4 M HCl respectively (83 °C, 15 h) under alcohol rich conditions. Further calcination (200 °C, 2 h) did not result in any change in crystalline structure, but

induced the crystalline growth.³⁶² The thermohydrolysis (373 K, 16 h) of TiCl_4 in water rich condition (70:0) formed anatase-rutile, while increasing the ethanol content (50:20) favored brookite formation at the complete expense of anatase. Surprisingly, brookite initially increased and later was hampered when anatase starts to reappear at the expense of rutile with decreasing water content (20:50).³⁶³ Finally, pure anatase was observed under alcohol rich conditions (10:60). The co-operative effect of excess chloride ions as structure directing agent and ethoxide suppressing the instant hydrolysis of precursor was responsible for brookite formation.³⁵⁷ At high concentration of ethanol, ethoxide adsorbs on Ti^{4+} cations precludes the corner sharing and facilitates edge sharing to promote anatase. Furthermore, ethanol facilitates the formation of spherical NPs and lowers the agglomeration by effectively acting as surface stabilizing agent.

7.3 Influence of mineral acids

The hydrolysis of TiCl_4 (80 °C, 2 h) in strong acidic conditions followed by calcination (100 °C) gave rutile.³⁶⁴ During peptization, there will be competition between the two growth units; anatase and rutile. At high proton concentration, more oxolation bonds among titanium atoms are broken and generated $-\text{OH}$ groups facilitates the movement of titanium atoms that was otherwise confined to its adjacent neighbours before peptization. The condensation among titania hydrates takes place among several titanium species, leading to structural rearrangement towards the formation of corner-shared octahedral chains.^{137,365} Thus, H^+ in the solution rearranges the amorphous precipitate and forms rutile. The anatase-brookite-rutile precipitated during the thermolysis of TiCl_4 and HClO_4 (1 – 5 M) and transformed to pure rutile after one month of thermal aging (100 °C).⁸⁶ The perchlorate ion co-ordinated to Ti(IV) cation complexes are not very stable and hence do not have any specific role in the crystallization process.³⁶⁶ The thermohydrolysis (95 °C, 24 h) of TiCl_4 in 1

M HNO₃ resulted in anatase (72 %)-brookite (6 %)-rutile (22 %).³⁶⁷ After 7 days of aging, anatase predominantly transformed to brookite and rutile. At this condition, fraction of anatase, brookite and rutile were 25, 25 and 50 % respectively. The brookite showed weak signature of increase in particle size, because of disappearance of anatase particles. Anatase was main product for lower to intermediate concentration of HNO₃ (0.5 –2.0 M), while brookite content prevailed under strong acidic condition (2 – 5 M). This specificity of HNO₃ to stabilize brookite nucleus originates from the low solubility of TiO₂ and its ability to form complex with Ti(IV) ion like [Ti(OH)_a(NO₃)_b(OH₂)_{6-a-b}]^{(4-a-b)+}, which gives neutral species [Ti(OH)₂(NO₃)₂(OH₂)₂]⁰ during thermolysis that acts as precursor for brookite nucleation. Therefore, nitrate ion played a central role in nucleating different polymorphic structure of titania despite of its weak complexing ability to Ti(IV) ions.³⁶⁷ The hydrolysis of TiCl₄ using NH₃ gas precipitator at low temperature (30 – 60 °C, 2 h) showed pure rutile at pH≤1 and anatase for pH≥4. The aging promoted NH₄Cl formation, without affecting titania crystal structures.³⁶⁸ The heating of aqueous TiCl₄ (50 °C, 150 min) under vigorous stirring resulted in rutile and anatase-rutile under refluxing conditions.²⁵² The formation of rutile was attributed to low pH and high concentration of chloride ions. The hydrolysis of TiCl₄ (100 °C, 24 h) with HCl showed pure rutile up to 2.0 M and later transformed into anatase with increase in [HCl] above it.³³³ When [HCl] ≤ 2.0 M, [TiO(OH₂)₅]²⁺ monomer dominates in TiCl₄ solution, which is prone to condense via olation. This results in edge sharing linear nuclei and forms rutile. If [HCl] ≥ 3.0 M, an intermediate species [Ti(OH)₂Cl₂(OH₂)₂]⁰ prevails and combines with each other to form anatase. In the case of 6 M HCl, brookite nucleated along with anatase. The thermolysis of TiCl₄ in 3 M HCl (100 °C, 48 h) showed brookite-rutile, although anatase was formed at very initial stages of hydrolysis (5 h).⁸⁶ The relative proportion of brookite (~ 80 %) did not vary beyond 48 h of aging, but were dependent on acidity of the medium (2≤[HCl]≤4 M) and concentration of titanium ions (0.15

M). Irrespective of acidity, brookite was formed by lowering the concentration of titanium ions to 0.05 M. Interestingly, pure rutile was present for 1 and 5 M HCl at 0.4 M Ti ions. It was proposed that non-electrically charged complex $[\text{Ti}(\text{OH})_2\text{Cl}_2(\text{OH}_2)_2]^0$ is solely responsible for brookite formation (Fig. 15). The presence of aquo and hydroxo ligands in the co-ordination sphere of this complex facilitate condensation or olation, which involves the elimination of aquo ligands (chloride ions being more strongly bound groups) and formation of dimmers and small chains of octahedra. When all water molecules are removed, further condensation will proceed by oxolation reaction with HCl elimination and formation of μ_3 -oxo bridges between octahedra. This process removes all chloride ions from the reacting species and yields oxides. Thus, high concentration of chloride ions in the thermolysis medium appears to be necessary for brookite formation and also to avoid recrystallization of brookite to rutile during aging. The Cl:Ti ratio should be between 17 and 35 for obtaining maximum fraction of brookite.⁸⁶

The hydrolysis of TiCl_3 in HCl (60 °C, 24 h) showed varied polymorphs depending on solution pH. Rutile was formed at strongly acidic conditions (pH 0.5), while brookite nucleated along with rutile (pH 1 – 3) followed by pure rutile at later stages (pH 3.5 – 4.0).³⁶⁹ At pH > 4, anatase crystallizes with brookite at the expense of rutile. Thus phase transition with increased pH (1 – 7) followed the sequence:



pH ~0.5 1 – 3 5 – 6 > 6 – 7

During thermolysis, preferential oxidation of Ti(III) compared to hydroxylation leads to acidic Ti(IV) complexes. At these acidic conditions, zero charged complexes $[\text{Ti}(\text{OH})_4(\text{H}_2\text{O})_2]^0$ are relatively formed at slow rate to yield rutile. The brookite formation either due to mixed complexes Ti(III)/Ti(IV) or partial oxidation of Ti(III) takes place along with proper ratio of Cl/Ti. At pH > 4.5, oxidation will be very fast and initial solid oxidizes

quickly and leads to the formation of amorphous TiO_2 , followed by crystallization into anatase after continued heating. The hydrolysis of TiCl_4 with H_2SO_4 or H_3PO_4 followed by refluxing (80°C , 1 h) and precipitation at alkaline medium was anatase, while hydrolyzing with HCl or CH_3COOH or HNO_3 exhibited anatase-rutile. Both sulfates and phosphates have tetrahedral geometry with negative ends at the oxygen atoms which co-ordinate to $[\text{TiO}_6]$ via mono, di and tridentate mode by a well known chelate effect. The bondings of these ions occupy a full face of octahedral and inhibit the growth of chain along opposite edges and inhibit rutile formation. The basic unit $[\text{Ti}(\text{OH})_2(\text{H}_2\text{O})_4]^{2+}$ can exist in cis and trans isomers, which grow into larger unit to crystallize titania polymorphs. Although, deprotonation of $[\text{Ti}(\text{OH})(\text{H}_2\text{O})]^{3+}$ can give $[\text{Ti}(\text{O})(\text{H}_2\text{O})]^{2+}$, oligomer growth units with titanyl $\text{Ti}=\text{O}$ bond is not evidenced so far and hence its role is excluded from the formation mechanism itself.³⁷⁰

7.4 Aging effects on phase transition

As obtained TiO_2 gel was amorphous, while aging by simple boiling for 12 – 48 h promoted the anatase and crystallinity was enhanced with increment in aging time. The hydroxyl ion existing in anatase lattice reduces the oxygen vacancy concentration and hence inhibits the grain growth during sintering. As a result, ART shifted to high temperature with increasing aging time. Contrarily, sample without aging underwent faster crystallite growth to reach critical size for ART (800°C).³⁷¹ Aging is a process by which the physical properties of gels changes as a consequence of polymerization, coarsening and phase transformation. The changes in structure and properties of gels that occur in the course of aging have a profound effect in the sintering process.³⁷² The hydrolysis of TiCl_4 in ice-bath conditions resulted in TiOCl_2 and pH was regulated by the addition of NH_4HCO_3 . The solution was then aged (40°C) on oil bath to get rutile (pH 0.4) and anatase-brookite (pH 2.7 – 4.0), while addition of sulfate gave anatase (pH 0.4).³⁷³ However, at pH 7 amorphous powder was obtained

($\text{TiO}_2 \cdot x\text{H}_2\text{O}$) and remained same even after aging for two weeks (40 °C) despite the presence of chloride ions. The amorphous phase transformed to anatase and brookite after reducing the pH to 2.6 – 5.0 and aging at 40 °C (4 days), while drying the slurry at RT did not crystallize even after aging for one week. Ding *et al.*³⁷⁴ reported that amorphous titania was converted into anatase and rutile after aging at RT for one year. Bosc *et al.*³⁷⁵ assigned the structure of dispersed alkoxide-derived colloids to anatase after aging for 3 h, while the precipitate obtained for longer aging (> 5 h) corresponds to anatase-rutile. The hydrolysis of TiCl_4 at RT was amorphous, while anatase crystallized after 0.5 h of aging and gradually transformed into rutile after extended aging (8 h) according to OR mechanism (373 K).³⁷⁶⁻³⁷⁹ The anatase crystallite size remained stable up to 2 h of aging. Thus, thermal effects in aqueous suspension and amorphous TiO_{2-x} were responsible for such phenomenon.³⁷⁸⁻³⁷⁹ These results suggests that ART was not governed by calcination but rather by interaction of defective anatase with other components of aqueous suspension.³⁷⁶ It was hypothesized that amorphous titania and very defective anatase are initially formed and their mutual strong interaction leads to the progressive covering of anatase surface by amorphous phase, impeding the crystal growth and favors slow ART. The interaction of acidic and basic hydroxyls promotes the formation of Ti-O-Ti bonds between amorphous and anatase which increases the aggregation of NPs. These interactions destabilize anatase crystals and favor ART as the solution aging progresses.

7.5 Thermolysis with other titanium precursors

The modified thermolysis (90 °C, 4 h) of mixture containing titania powder, HCl, urea and PEG 10000 showed unique flower like brookite agglomerates with an average diameter of 400 – 500 nm composed of single brookite nanocrystals (4 – 5 nm).⁴⁶ Further calcination (200 °C, 3 h) resulted in amorphous phase along with anatase-brookite-rutile. The co-existing

anatase rapidly grows out by the crystallization of amorphous fraction to anatase at 500 °C. The annealing of brookite resulted in gradual conversion to rutile and anatase in the range of 200 – 800 °C, with brookite being stabilized up to 500 °C before anatase (700 °C). Thus, anatase inhibited direct BRT during thermal treatment.⁴⁶ The thermal hydrolysis (160 °C, 24 h) of TiBALDH with 0.1 M urea yields pure anatase, while anatase-brookite for 0.5 – 5.0 M.³⁸⁰ At high concentration (≥ 6.0 M), high quality brookite nanorod was observed (Fig. 16). The brookite did not transform through intermediate anatase, rather brookite seed was self nucleated from TiBALDH complex and continues to grow in the solution until reaching the appropriate size.³⁸¹ Urea hydrolyzes slowly at RT but rapidly at > 90 °C releasing hydroxide ions.³⁸²⁻³⁸³ At low urea content, in situ generated hydroxide ion dosing is sufficient for slow hydrolysis of TiBALDH leading to anatase NPs. The increase in hydroxide ion capacity at high urea content facilitates the thermal hydrolysis of TiBALDH and formation of anatase-brookite seeds. Thus, it can be concluded that in situ hydroxide ion dosing favours the brookite formation. This was supported by coexistence of brookite along with anatase even at high concentration of NH_4OH (8 N). It was speculated that high concentration of urea effects the spatial confirmation of TiBALDH complex so that the resulting complex resembles the architecture of brookite. This assumption was based on rationale that complexation of urea with Ti(IV) appears to be unlikely due to their low stability as compared with lactate. Even if urea chelates to Ti(IV) as bidentate ligand, it forms four membered ring that is less stable than a five membered ring formed by lactate. The thermolysis of 0.9 M TiOSO_4 (90 °C, 4 h) leads to anatase, as sulfate species served as directing agent to favour anatase.³⁸⁴ The sulphur species strongly bonds to titania surface and increase the energy of crystallization and rutile formation, which however is difficult to remove by conventional washing.³⁸⁵ Koelsch *et al.*²¹⁸ proposed that sulphate acts as bidentate ligand in $[\text{Ti}(\text{OH})_2\text{SO}_4(\text{H}_2\text{O})_2]^{10}$ from which anatase will be nucleated. In addition, Ti^{4+} in H_2SO_4 has shown the occurrence of 1Ti:1 SO_4 and

1Ti:2SO₄ species, with the predominance of 1:1 complex. These complexes exist in low amounts, suggesting the role as catalyst or structure directing agent for anatase formation. The formation of sulfate species in the vicinity of cation may favour the condensation of opposed coplanar edges to form anatase.³⁸⁶⁻³⁸⁷ The ill crystalline and slight decrease in anatase crystallinity in the presence of chloride and nitrate anion, was attributed to their strong and weak complexing tendency with Ti⁴⁺ respectively. Interestingly, varying the concentration of [C₂O₄]²⁻/Ti⁴⁺ (R) resulted in anatase-rutile for R=0.2 and pure rutile at R=2. At intermediate concentration of R=1, Ti₂O₃(H₂O)₂(C₂O₄).H₂O was identified. Thus, oxalate ion either act as ligand with the stabilization of oxalate hydrate phase or as chelating agent to stabilize rutile depending on concentration. The titanium oxalate hydrate decomposes to either anatase³⁸⁸ or brookite. The brookite so formed at 300 °C transformed to rutile at > 600 °C. The brookite was embedded in large micrometer size particles and exhibited a high surface area (255 m²/g), because of mesoporosity arising from water removal in the above oxalate species. The facile synthesis and low stability of Ti₂O₃(H₂O)₂(C₂O₄).H₂O makes it suitable precursor for the preparation of brookite.³⁸⁸

An alternate to thermohydrolysis, solid-state metathesis uses exothermally driven chemical change to rapidly synthesize crystalline solids from simple starting materials. The TiBr₄ dissolved in hexadecane and Na₂O₂ resulted in anatase-rutile after heating near to reflux point of hexadecane; fast heating from RT to 288 °C within 15 min under constant stirring and holding at this reflux temperature for 2 or 6 h.³⁸⁹ In contrast, pure anatase was observed for slow experimental condition; precursor mixture was heated over a period of 4 h with constant stirring from RT to reflux and holding at reflux for 2 h. The same reaction with TiCl₄ produced amorphous, while Na₂O with TiBr₄ resulted in poorly crystallized titania phases. The isolated crystalline titania powders are either anatase or anatase-brookite mixture, depending on how quickly the reagents are heated to flux (Fig. 17). Locally

exothermic solution-surface events are likely responsible for titania formation directly from solvothermal reaction without any thermal treatments. These powders were resistant to thermal conversion to rutile at high temperature. Since one reagent is dissolved, its reaction with solid peroxide surface should be facile and may locally self propagate to form crystalline oxide regions.³⁸⁹ The direct crystallization to rutile from aqueous TiOCl_2 was observed after boiling (100 °C, 4 h). The addition NbCl_5 , NiCl_2 and FeCl_3 stabilized rutile and ZrOCl_2 facilitate anatase, while AlCl_3 promoted anatase-rutile.³⁹⁰ The similar ionic radius of Nb^{5+} and Fe^{3+} seems to stabilize the pristine phase, while Zr^{4+} and Al^{3+} having higher and lower ionic radius respectively suppressed the precipitation process to form anatase. Interestingly, similar ionic radius of Ni^{2+} compared to Ti^{4+} resulted in minor anatase fraction. The aging of titanatrane isopropoxide in HNO_3 (40 – 50 °C, 12 – 24 h) showed pure rutile.³⁹¹ The amorphous titania dissolved to a transparent titania gel in stirred acidic solution (HCl or HNO_3) reprecipitated as rutile after a long time (48 h) aging at RT. The crystallization temperature was about 385 and 110 °C lower than those of calcination in air (407 °C) and hydrothermal route (130 °C) respectively. Before reprecipitation, titanium exists as a six fold co-ordinated hydrated ion $[\text{Ti}(\text{H}_2\text{O})_6]^{4+}$, which dehydrate and polymerizes to $[(\text{H}_2\text{O})_4\text{Ti}(\text{OH})_2\text{-Ti}(\text{H}_2\text{O})_4]^{6+}$ and $[(\text{H}_2\text{O})_4\text{Ti}\dots\text{O}_2\dots\text{Ti}(\text{H}_2\text{O})_4]^{4+}$ followed by $[\text{TiO}_6]$ formation. The mole fraction of rutile decreased with increase in treatment temperature and pure anatase was obtained at > 150 °C. It was suggested that stable rutile nucleus with compact structure is formed by very slow reprecipitation rate at a temperature of < 60 °C, while anatase was formed at high temperature due to larger reprecipitation rate.³⁹² In a modified dissolution-reprecipitation process, rutile particles dissolved in H_2SO_4 and reprecipitated with NH_3 showed anatase-rutile after calcination (450 – 900 °C, 1 h).³⁹³

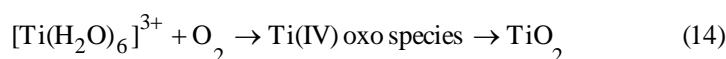
8.0 Micro-emulsion method

As a “soft template” reverse microemulsions, the organized assemblies formed by water, oil and surfactant have compartmentalized water-in-oil liquid structure composed of dispersed bubbles in the dispersion medium with features of micrometer or nanometer sealed reactors for the generation of NPs.³⁹⁴⁻³⁹⁶ A microemulsion is thermodynamically stable, optically isotropic and transparent solution of two immiscible liquids (water and oil) substituted by an interfacial film and separated by thin surfactant monolayer and can be either water in oil, oil in water or bicontinuous.³⁹⁷⁻³⁹⁹ For water-in-oil microemulsion, aqueous phase is dispersed as microdroplets surrounded by a monolayer of surfactant molecules in the continuous hydrocarbon phase. The formation of particles is controlled by the reactant distribution in the droplets and by the dynamics of interdroplet exchange. The surfactant stabilized by micro cavities provide a cage-like effect that suppress the particle nucleation, growth and agglomeration.⁴⁰⁰⁻⁴⁰¹ The size of particles formed in the reverse micelles is known to be larger than the thermodynamic size of reverse micellar droplets in which particles are formed.⁴⁰² This is due to partial cluster formation of micellar droplets, which is affected by temperature and micellar size. The water nucleus is the only region where titanium precursor could be hydrolyzed and thus the growth of particles in water nucleus is restricted leading to small size and high surface area for microemulsified particles.

The microemulsion assisted preparation with $\text{Ti}(\text{OBu})_4$, cyclohexanol, CTAB, TEA and acetone resulted in amorphous, anatase and rutile for as obtained, calcined at 550 and 700 °C (2h) respectively. The finely dispersed anatase (15 nm) particles was obtained compared to those prepared through sol-gel method (50 nm) with apparent agglomeration.⁴⁰³ By changing the volume ratio of oil to water in reverse microemulsion, rutile changed its morphology from nanocluster to nanospherules, then grew into nanodumb bells and finally nanorod was obtained.⁴⁰⁴ The TiO_2 prepared via reverse micro emulsion with Tween 60 and

Brij 58 surfactant stabilized the anatase up to 500 °C and promoted the rutile formation at 600 °C.⁴⁰⁵ When Brij series was used as surfactants, crystallite size decreased from 17 to 10 nm with an increase of hydrophilic group chain length. It is known that formation of water pool in a reverse micro emulsion occurs from the dispersion of water by hydrophilic group of surfactant. With decrease in hydrophilic group chain length, formation of water pool in the reverse micro emulsion becomes loose and then crystallite size increases by the rapid hydrolysis of water and titanium alkoxide. Interestingly, crystallite size also decreased from 12 to 9 nm with an increase of hydrophobic group chain length in the Tween series, as size of reverse micelles decreases because the hydrophobic chain prohibits the access of water near the micelles.⁴⁰⁵ The precipitate obtained by this route must be washed to remove the contaminated oil and surfactant (co-surfactant) from the particles.⁴⁰⁶ In this course, calcination was indispensable due to: (i) residual water and organic compounds must be removed via evaporation followed by thermal decomposition to form pure products; (ii) amorphous precipitate should be transformed to crystalline oxide at high temperature. The removal of impurities will be incomplete at low calcination temperature and grain growth was common due to the loss of microreactors at high temperature. Thus, further improvement was achieved by hydrothermally treating the microemulsified particles.

The anatase-rutile ratio was tuned by microemulsion-mediated solvothermal method (180 °C, 12 h) using TiCl_3 and urea.⁴⁰⁷ The TiO_2 showed gradual evolution of rutile to anatase with increasing urea content for series I (urea dissolved in water) and pure anatase was obtained after the addition of 1.8 g of urea. However, anatase-rutile coexisted even after the addition of 1.8 g of urea for series II samples (urea dissolved in HCl). At acidic pH, reactions are as follows;



The $[\text{Ti}(\text{OH})(\text{H}_2\text{O})_5]^{2+}$ is first produced by hydrolysis of $[\text{Ti}(\text{H}_2\text{O})_6]^{3+}$ and get oxidized by dissolved oxygen to form Ti(IV) oxo species. This species is assumed to be an intermediate between TiO^{2+} and TiO_2 consisting of partly dehydrated polymeric Ti(IV)hydroxide which undergoes corner shared bonding to form rutile.⁴⁰⁸⁻⁴⁰⁹ With increasing the concentration of urea in reaction medium, acidity would decrease as urea produces hydroxyl anion via hydrolysis at $> 85^\circ\text{C}$. Thus degree of hydrolysis increases resulting in more number of $-\text{OH}$ coordinated to Ti centres.



The increase of hydroxyl anion leads to the formation of zero-charge complex $[\text{Ti}(\text{OH})_3(\text{H}_2\text{O})_3]^0$, which subsequently oxidizes to $[\text{Ti}(\text{OH})_4(\text{H}_2\text{O})_2]^0$. The $[\text{Ti}(\text{OH})_x(\text{H}_2\text{O})_{6-x}]^{3-x}$ monomers can form different structures of polymers by sharing edges or corners leading to different crystalline polymorphs of titania.⁴⁰⁷ In another study, anatase fraction increased with increase in the concentration of $(\text{NH}_4)_2\text{SO}_4$ at the aqueous phase.³⁴⁰ Anatase-rutile was tuned by varying the concentration of acid in the aqueous phase; pure anatase was observed for 0.5 M HNO_3 and pure rutile at ≥ 1.0 M HCl , with anatase-rutile at 1.0 M HNO_3 and ≤ 0.5 M HCl . Pure rutile was not observed by increasing the $[\text{HNO}_3]$ at any temperature for any reaction times. In this study, water/Triton X-100/hexanol/cyclohexane microemulsion was used as constrained microreactor for controlled growth of titania particles under hydrothermal conditions (120°C , 12 h).⁴¹⁰ The TiCl_4 reacted with ammonia in water/(Triton X-100 + n-pentanol)/cycloheptane to form anatase hollow spheres.^{411a} The FTIR indicated that water interior of reverse micelles has a multilayered structure, consisting of interfacial, intermediate and core-water.⁴¹²⁻⁴¹³ The interfacial layer is composed of water molecules that are directly bonded by polar head groups of Triton X-100. Thus, hydroxyl anion released from NH_4OH penetrates to the interface, facilitating the reaction of Ti^{4+} with hydroxyl anion near the interfacial layer (bound water layer) of spherical emulsion droplets to form TiO_2 nuclei

surrounding the spherical aggregates and finally forms hollow TiO₂ microspheres. The low and high concentration of TiCl₄ results in hollow spheres with thin and thick shell respectively.^{411a} Due to their unique physical and chemical properties such as low density, high surface area and effective light-harvesting property, hollow nanostructures are extensively used in photocatalysis.^{411b-e} An unusual orthorhombic crystal structure of titania was obtained during the controlled hydrolysis of TiCl₄ due to chemical pressure generated within the constrained volume of aqueous core of reverse micellar droplets.³⁹⁴ Further heating up to 900 °C, these metastable spherical crystals are converted into relatively more stable NRs via making and breaking of Ti-O-Ti bonds without any further phase transition. However, when the sample was dispersed in water-acetone mixture, nanorod structure is destroyed and granular particles are formed due to hydrolysis of Ti-O-Ti to Ti-OH. The presence of HCl in hydrothermal treatment (120 °C, 13 h) of microemulsion gave rutile, while anatase with HNO₃.³⁹⁷ The droplet size templating effect was present during the solution mixing at RT and was completely absent at > 40 °C, which was contrast to previous study.⁴¹⁰ The turbidity and conductivity measurements suggested that microemulsions do not serve as template under hydrothermal conditions, but rather as initial size template during the mixing step prior to hydrothermal treatment.

9.0 Preparation of TiO₂ from various titanium precursors

9.1 Crystallization from inorganic titanium precursors

The nature of titanium precursor often plays a key role in determining the morphology and crystallization of titania. The formation and organization of polynuclear complexes essential for nucleation and growth of various polymorphs is determined by both anionic species and proton/hydroxyl ion concentration.^{79,141,414} The commonly used titanium precursors like titanium chloride/halides are quite expensive, corrosive and sensitive to

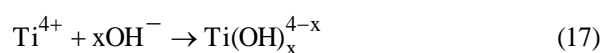
moisture as they readily hydrolyze in water or even with moist air. Thus care is required in handling these chemicals such as submerging it in ice-cooled water bath or handling under inert gas that makes titanium chemistry very complicated. Moreover, complex assembly of nanoclusters are usually difficult to obtain from these precursors as they have predisposition towards the evolution of aggregated amorphous titania, invariably requiring thermal treatment for crystallization. To this end, few other titanium precursors are reported to tailor the phase composition of titania as well as to obtain hierarchical nanostructures.

The hydrothermal aging (200 °C, 24 h) of water soluble titanium complexes with citric acid, tartaric acid and malic acid showed anatase, while rutile with glycolic acid and anatase-rutile from lactic acid.⁴¹⁵ The hydrothermal treatment (180 °C, 12 h) of TiB₂ in acidic medium (1 M HCl) containing 3 mM Na₂SO₄ resulted in nanocone rutile and transformed to truncated bipyramidal anatase after reducing the acid concentration (0.5 M). Alternatively, spherical brookite were obtained with HNO₃.⁴¹⁶ The evolution of titania polymorphs involved three stages: (i) dissolution of TiB₂ increases the concentration of soluble titanium species from nil to critical point for TiO₂ nucleation at the initial stage (0 – 2 h); (ii) TiO₂ nucleus co-existed with TiB₂ due to gradual release of titanium source from TiB₂ bulk as the treatment time proceeds (2 – 5 h); (iii) for the reaction time > 5 h, dominant solid phase in the mother liquor is titania, which undergoes further crystallization and ripening.⁴¹⁷ In comparison to Ti (III)/(IV) halide or alkoxides, crystalline TiB₂ has advantage of slow hydrolysis, non-toxic nature and non-corrosive byproducts. The choice of TiB₂ was attributed to specific bonds, intrinsic chemical stability and controlled release of titanium species from the bulk crystalline precursor enabling to obtain phase tunable titania. The TiOF₂ prepared by microwave assisted hydrothermal route (200 °C, 20 min) using Ti(OBu)₄ and HF transformed to anatase (400 °C, 2 h) and was thermally stable up to 900 °C.⁴¹⁸ The dual role of adsorbed fluoride ion in lowering the anatase surface energy and suppression of grain growth during

calcination inhibits the rutile formation.⁴¹⁹⁻⁴²¹ The microwave assisted hydrothermal synthesis is superior as it leads to reduction of heating time during the synthesis process because of rapid crystallization.⁴²² Although rutile was observed in both conventional (195 °C, 2 – 32 h) and microwave assisted hydrothermal route (195 °C, 5 – 60 min), latter produced a nanostructural spherical crystals (fine aggregates) and former generated larger acicular crystals.⁴²³

Pure rutile was synthesized at hydrothermal reactions (150 °C, 12 h) from water soluble TiBALDH at neutral pH conditions.⁴²⁴ The Ti cation in TiBALDH complex is octahedrally co-ordinated, containing two bidentate lactate ligands in x-y plane and two hydroxyl groups along z-axis. Thus, hydrolytic stability of TiBALDH complex in aqueous solution and lactate ligand affords the stability to the complex within x-y plane is enough to initiate condensation along the z-axis to form rutile (Fig. 18). The carboxylic functional group allows for a conjugate system, which reduces the Lewis basicity of bonding oxygens and thus lowers the charge donation to metal centres.⁴²⁵ Another reason for the stability of lactate ligand on TiBALDH at near neutral pH (stored in water) is likely due to its 5-membered ring, which reduces strain within the ring and not being sterically crowded around the metal centre.⁴²⁵ In addition, condensation occurs primarily through two existing hydroxyl group along z-axis allowing corner-shared bonds. Under alkaline medium, hydroxide cleaves the organic from Ti complex by nucleophilic addition to either Ti cation or lactate group forming ammonium lactate as by product.⁴²⁶ The rise in pH cleaves the organic ligands from Ti complex, thereby enabling hydrolysis-condensation process through edge shared bonding to form anatase.^{52,114} The co-existence of anatase-rutile suggests that nucleophilic cleavage of organic ligands and condensation reactions of two hydroxyl groups along z-axis are competing reactions. At pH 9, rate of lactate group cleavage is slower compared to pH 10 – 11, enabling the formation of corner shared bonds to yield minor quantity of rutile. The

growth of rutile rods appears to be driven by OA mechanism, due to lower solubility of Ti species. This reduces the dissolution of crystallites, thereby minimizing the amount of titanium ions available for growth via ion-by-ion addition (OR),^{48,119,427} while anatase crystallites continues to grow by OR mechanism at pH > 10. This study concluded that the hydrolysis rate of precursor with respect to pH determines the nucleation of titania crystal structure.⁴²⁴ The rutile/anatase core/shell structure was evolved from TiO_xC_y/C composite calcined at various temperature.⁴²⁸ Such structures were obtained by two stages: (i) hydrothermal treatment (160 °C, 12 h) involved semicrystalline TiO₂ embedded in caramelized sucrose matrix; (ii) thus formed TiO_xC_y/C calcined in nitrogen atmosphere (700 – 1300 °C, 4 h) transformed to crystalline titania. It was found that rutile exists within anatase particles and depth of rutile core in the anatase shell particles can be adjusted by tuning the thickness of TiO_xC_y (x<y) and TiO_xC_y (x>y) in TiO_xC_y/C composite through varying calcination temperature (Fig. 19). The concentration gradient of carbon atoms by its diffusion to bulk TiO₂ leads to the formation of TiO_xC_y (x<y) in the outer shell of particles and TiO_xC_y (x>y) in the middle of particles together with some non-reacted TiO₂ particles in the core. The migration of rutile core deep inside the anatase shell was evidenced by photoluminescence and UV-visible absorption spectroscopy studies.⁴²⁸ Hydrothermal treatment of water soluble TiS₂ (200 °C, 24 h) with NaOH (> 0.5 M) favored ABT and pure brookite was observed at 1.2 M NaOH. With further increase in the concentration of NaOH (1.5 – 2.0 M), sodium titanate was observed.⁴²⁹ When TiS₂ is added to NaOH, hydrolysis reaction occurs leading to the formation of Ti(OH)_x^{4-x} complex;



The appearance of brookite at high concentration of NaOH was due to rapid thermal hydrolysis of TiS₂. The time dependent experiments confirmed that TiS₂ with NaOH initially

leads to layered titanate, which transforms to anatase and brookite after increasing the hydrothermal reaction time (≥ 6 h). Interestingly, both anatase NPs and brookite nanoplates was not inter converted even after increasing the reaction time up to 24 h (Fig. 20). The formation of sodium titanate at very low concentration of NaOH was due to lower bond energy of Ti-S (418 ± 3 kJ/mol), in contrast to 10 M NaOH commonly used for TiO₂ because of high bond energy (672 ± 9 kJ/mol). Pure anatase was observed for hydrothermal treatment (220 °C, 48 h) of TiOSO₄ with 0.21 M NaOH below pH 7 and transforms to titanates at neutral pH, followed by brookite nucleation with low concentration of defects at alkaline medium (pH 10.5 – 12.5). Thus, brookite nucleation takes place directly from layered titanate rather than from anatase.⁴³⁰ In this system, Na⁺ or H⁺ ions located in the interlayer spaces of layered titanate could be gradually released, which disturbs the static interaction and introduces the internal structural tension. With an increase of this tension, layered titanate would become unstable and finally transformed to anatase in acidic or brookite under basic conditions. In the subsequent process, spindle and flower like brookite titania was formed, which undergo preferential coarsening of NPs as governed by surface charges and surface energy. Once brookite nanocrystal are formed, Na⁺ and OH⁻ in the reaction medium would be adhered on their surface and destroy the local equilibrium concentration giving gradient expense of shrinkage of smaller particles.⁴³¹ With a prolonged reaction time, these spindle like titania particles would weld together to reduce the surface energy and finally produce brookite flowers. However, anatase-rutile was observed with LiOH and KOH highlighting the importance of Na⁺ ions in brookite formation. The flower like brookite was thermally stable up to 900 °C without change in morphology and transformed to sphere like shaped rutile at 1000 °C. The high stability was closely related to flower shape facilitating the strong interactions among the fine particles for the assembly of brookite flowers.⁴³⁰ Compared to trivial titanium precursor, titanium amino-alcohol complexes exhibit improved hydrolysis-

condensation properties over the simple alkoxides, allowing for better control in the sol-gel reaction due to its “caged” structure.³⁹¹ The titantrane complex $[\text{N}(\text{CH}_2\text{CH}_2\text{O})_3\text{Ti}-\text{O}^i\text{Pr}]$ reacts with water and forms hydroxyl titanium chelate $[\text{N}(\text{CH}_2\text{CH}_2\text{O})_3\text{Ti}-\text{OH}]$, which is stable in water for extended period of time.^{432a} Since only -OH group is in the complex and no OH moiety in its dimer $[\text{N}(\text{CH}_2\text{CH}_2\text{O})_3\text{Ti}-\text{O}-\text{Ti N}(\text{CH}_2\text{CH}_2\text{O})_3]$, rutile nucleates without forming anatase. As the titanium is well protected by three arms of trialkoxide, formation of $[\text{TiO}_6]$ enhances the kinetic stability and hence condensation rate is very slow due to this steric effect.

As it is widely reported, anatase was the common phase from $\text{Ti}(\text{SO}_4)_2$ as the sulfate species inhibits the formation of rutile.^{432b-c} Several co-doped systems of titania in the anatase form as well as with reactive exposed {001} facets showing high photocatalytic activity is also prepared from this precursor.^{432d-g} The precipitated powders obtained from thermohydrolysis of $\text{Ti}(\text{SO}_4)_2$ in propanol-water was found to be amorphous and transformed to anatase-rutile after calcination at 600 °C for 2 h and pure rutile at 800 °C. It was interesting to note that the spherical morphology of the samples (as obtained) was retained during calcination.^{432h} The precipitate from $\text{Ti}(\text{SO}_4)_2$ and NaOH when dispersed in HNO_3 gave rutile after aging at room temperature without formation of anatase.⁴³²ⁱ The protons in the solution rearrange the amorphous aggregates to form rutile, while sulfate species retarded the crystalline growth. The active sulfate species (at 300 °C) gradually expelled out from TiO_2 network to form inactive sulfate species with increase in calcination temperature (800 °C). Peptizing with acid allowed sulfate species to homogeneously disperse throughout the bulk of the crystals, thus favouring its incorporation into TiO_2 network. In contrast, anatase, anatase-brookite and brookite was obtained via hydrothermal treatment (180 °C, 36 h) of $\text{Ti}(\text{SO}_4)_2$ and NaOH without any peptization at pH 5, 6 – 9 and 10 – 11 respectively.^{432j} The fluoride-free-self-templated synthesis of anatase-rutile hollow nanostructures was obtained via

hydrothermal treatment (473 K, 24 h) of $\text{Ti}(\text{SO}_4)_2$ with H_2O_2 at pH 1.^{432k} The lower amount of H_2O_2 (4 – 6 mM) resulted in agglomeration with a few hollow nanostructures, while larger amount (20 – 50 mM) leads to formation of NPs without any assembly of hierarchical nanostructures. The optimum (10 mM) H_2O_2 served as coordinating agent and stabilized the particle interface. The time dependent experiments revealed that solid particles (6 h) transformed to hollow structure (10 h) and hollowing process continued to obtain hollow particles with a uniform interconnected cavity (24 h). The $\text{Ti}(\text{SO}_4)_2$ reacts with H_2O_2 via ligand exchange reaction with O_2^{2-} ion under acidic conditions to form intermediate complex, which decomposes to titania phases. However, monodispersed NPs were obtained without H_2O_2 , suggesting that peroxide played a major role in the formation of hollow structures. It was found that inside-out Ostwald ripening was responsible for hollowing process, in which the evacuation of solid cores was driven by minimization of overall surface energy. Recently, Yu and co-workers^{432l} reported H_2O_2 assisted fluoride induced self transformation to obtain anatase hollow microspheres from $\text{Ti}(\text{SO}_4)_2\text{-NH}_4\text{F-H}_2\text{O}_2$ via hydrothermal method (180 °C, 3 h). This method is advantageous over Troung *et al.*,^{432k} as the reaction time is very low and pure anatase was obtained. Thus it can be concluded that presence of H_2O_2 favored rutile, while fluoride ion stabilized anatase. The formation mechanism involved three stages; (i) $\text{Ti}(\text{SO}_4)_2$ reacts with H_2O_2 to form urchin-like microspheres,^{432m} which are aggregated amorphous TiO_2 .



(ii) As the reaction proceeds further (up to 1 h), H_2O_2 decomposes and particle interface becomes vacant due to the presence of dangling bonds (unsaturated titanium species), which are prone to dissolve in the presence of fluoride ions. In addition, HF induces dissolution of particle interior and subsequent mass transfer to the external surface^{432m}; (iii) with further increase in reaction time (3 h), building blocks of TiO_2 solid are transformed to hollow

structure due to the decomposition of H_2O_2 complex at the interior. Therefore, redistribution of matter from interior to exterior of building blocks takes place spontaneously, forming hollow structures.

These results demonstrate that reactivity of precursor and process conditions need to be considered to produce well-defined nanostructured materials. Understanding the similarities between the fundamental structural unit (octahedral arrangement) and molecular structure of precursor provides insight into the nucleation and growth behavior with respect to reaction conditions. The screening new types of precursors for titania synthesis still has a great implications for materials syntheses and processing.

9.2 Crystallization of TiO_2 from layered titanates

The layered titanates are a group of solid TiO_2 hydrates intercalated by protonated water molecules. Each layer in the crystal structure consists of side-by-side aligned $[\text{TiO}_6]$ connected above and below by additionally shared apical edges of $[\text{TiO}_6]$ at different levels.⁴³³⁻⁴⁴¹ The layers within these titanate hydrates can either split into smaller fragments of $[\text{TiO}_6]$ for the assembly of more complex nanostructures or undergoes in situ dehydration to crystallize into specific titania polymorphs. Obviously, this is different from trivial titania formation via polymorphic growth units obtained from the hydrolysis of titanium precursor in the liquid medium.

The mixed or pure phase of titania was obtained after hydrothermal treatment ($180\text{ }^\circ\text{C}$, 12 h) of H/K titanate by varying the mineral acids and their relative concentration.⁴⁴² The rutile and anatase was observed at 4.0 M and 3 mM HCl respectively, while $\text{TiO}_2(\text{B})$ nucleated at 0.1 M HCl. The brookite-rutile and brookite-rutile- $\text{TiO}_2(\text{B})$ was observed in the concentration range of 0.2 – 2.0 M HCl, while anatase- $\text{TiO}_2(\text{B})$ was formed at 0.1 M – 3 mM HCl. The anatase content gradually increased with decrease in HCl concentration, while

content of TiO_2 (B) decreased and finally disappeared. Likewise, pure TiO_2 (B) and anatase was observed at 0.1 and 1 mM HNO_3 and above said mixed polymorphs was obtained at 4.0 – 0.5 M, 0.5 – 0.15 M and 0.1– 3.0 M HNO_3 respectively. In contrast, pure anatase and TiO_2 (B) along with anatase- TiO_2 (B) nucleated with H_2SO_4 depending on acid concentration (Fig. 21). Thus protons and anions played a dominant role in tuning the phase composition in the entire acidic range. Based on XRD analysis and time dependent morphological evolution of titanate to form different polymorphs of titania, it was concluded that change in solution pH during the hydrothermal treatment was the main factor in governing such phase transition. When $[\text{H}^+] < 0.1$ M, H/K titanate proceeds via topochemical reaction mechanism forming TiO_2 (B) nanowires, while dissolution-nucleation pathway prevails with increase in solution pH leading to anatase.⁴⁴³⁻⁴⁴⁴ When H^+ concentration is > 0.1 M, some of $\equiv\text{Ti-OH}$ protonates to form $\equiv\text{Ti-OH}_2^+$ and prefers corner sharing between octahedral as a result of repulsion to form rutile and brookite. The SO_4^{2-} favored anatase, while Cl^- facilitated rutile formation compared to NO_3^- at the same concentration.⁴⁴² The brookite content increased at the expense of anatase without affecting rutile fraction during hydrothermal treatment (100 – 200 °C, 5h) of TNT ($\text{H}_2\text{Ti}_n\text{O}_{2n+1}$ such as $\text{H}_2\text{Ti}_3\text{O}_7$ and $\text{H}_2\text{Ti}_4\text{O}_9$) with HClO_4 and HNO_3 .⁴⁴⁵ Although, similar trend was observed with HCl up to 150 °C, both BRT and ART dominated at 200 °C. This suggests that ABT is favoured over ART at the initial stages of hydrothermal treatment. The presence of inorganic salts in the reaction solution showed a complex behaviour; anatase and brookite was preferred with NaClO_4 (or NaCl) and HClO_4 respectively, while rutile dominated in NaCl-HClO_4 (Fig. 22). It was suggested that brookite nucleation from TNT precursor takes place only under high temperature, strong acidic conditions and appropriate anion like ClO_4^- that prevents BRT.⁴⁴⁵ The presence of anatase under weakly acidic or neutral solution with NaCl or NaClO_4 suggests that these anions do not work as a control reagent of crystal structure, presumably due to their weak co-ordination on the corner of $[\text{TiO}_6]$. The

reason for brookite formation with NO_3^- and ClO_4^- compared with Cl^- might be that former induces less formation of edge sharing assembly of $[\text{TiO}_6]$ compared to chloride ion. The large fraction of brookite from TNT compared to other research groups,^{86,367} is due to the arrangement of $[\text{TiO}_6]$ and related assembly without fragmentation to the minimum $[\text{TiO}_6]$ unit.

Wang *et al.*¹²⁸ for the first time reported unique phase transition sequence, anatase to rutile to anatase, according to dissolution-reassembling equilibrium via liquid phase solution-NaOH treatment of hydrolysate of titanium $\text{Ti}(\text{OBU})_4$ and subsequent acidic peptization of $\text{H}_2\text{Ti}_5\text{O}_{11}\cdot 3\text{H}_2\text{O}$ intermediate. At very early stage of peptization, anatase dominates owing to the similarity in crystal structure with intermediate H-titanate having four edge sharing zigzag ribbons.⁴⁴⁶⁻⁴⁴⁷ The lamellar H-titanate dehydrates after reaction with HNO_3 , while zigzag ribbons remains unchanged and anatase is formed via direct rearrangement of crystal lattice. Thus formed anatase nanosheets tend to split and forms crystal because of their structural assymetry, so as to release the strong stress and lower the total energy. After prolonging the acid peptization, rutile nucleates as a result of aggregation of anatase particles. The reconstruction of lattice is achieved by resolving zigzag ribbons of anatase into detached $[\text{TiO}_6]$ or their small clusters, which are later reconstructed as straight chains. With further increase in aging time, rutile fraction decreases followed by increase of anatase content, as rutile NRs dissolve in strong acidic medium and that dissolved crystals are smaller than critical size. Thus OR mechanism follows to form well defined anatase NRs. Therefore, phase transition in the acid peptization procedure may be regulated by the equilibrium between dissolution of rutile NRs and reassembling of smaller anatase grains. When the aging time lasted as long as 48 h, change in phase composition becomes indistinct, indicating that thermodynamic equilibrium might have been established between two phases (Fig. 23). The treatment of NaOH with Ti-O-Ti framework results in the formation of Ti-O-Na and Ti-

OH bonds in the structural units and that Na^+ located between the layers are replaced by H^+ in pH descending course of water washing, followed by the generation of protonated pentatitanate intermediate $\text{H}_2\text{Ti}_5\text{O}_{11}\cdot 3\text{H}_2\text{O}$ with lamellar structure. The steric hindrance caused by linkage of six water molecules in this intermediate, forces the large structural units (aggregation of octahedra) to arrange in the zigzag configuration rather than straight chain along c-axis.⁴⁴⁸⁻⁴⁴⁹ Finally, Ti-OH bonds are dehydrated in HNO_3 at final acid peptization stage and new Ti-O-Ti and Ti-O-H-O-Ti hydrogen bonds are generated to form TiO_2 crystals.¹²⁸

The $(\text{NH}_4)_2\text{Ti}_2\text{O}_5\cdot\text{H}_2\text{O}$ obtained by the reaction of TiCl_3 or $\text{Ti}(\text{OBU})_4$ with aqueous NH_3 (in alkaline media) transformed to anatase under hydrothermal conditions, due to the deintercalation of NH_4^+ ions from the layered titanate and combination of layers from ammonium dititanate.⁴⁵⁰⁻⁴⁵⁴ During the hydrothermal process, NH_4^+ gets hydrolyzed to NH_4OH and H^+ released induces hydroxyl condensation to form anatase. The presence of NaCl favoured the nucleation of brookite with TiCl_3 and pure brookite was observed only at high concentration of NaCl (4.2 M) and 68 mL of NH_4OH .⁴⁵² With the introduction of NaCl , both Na^+ and NH_4^+ exists in the interlayer to stabilize the structure and to balance the negative charge of titanate. During the hydrothermal treatment, deintercalation of NH_4^+ will induce the collapse of few layers, while some bonds will be restrained by Na^+ without breaking. Thus, structural transformation is delayed resulting in special lattice shear in the combination process of layer and leads to brookite like structure, which further expands to form brookite lattice. The introduction of water with NH_4OH reduced the concentration of Na^+ and retains NH_4^+ in the interlayer facilitating anatase (Fig. 24). At very high concentration of NaCl , layered architectures are overwhelmingly maintained by Na^+ ions forming $\text{Na}_2\text{Ti}_2\text{O}_5\cdot\text{H}_2\text{O}$, which transforms to $\text{H}_2\text{Ti}_2\text{O}_5\cdot\text{H}_2\text{O}$ after washing with acid.⁴⁵¹ Interestingly, anatase-brookite, brookite-hydrogen titanate along with pure brookite and

hydrogen titanate was obtained with varied concentration of NaCl (0.25 – 1.5 M) depending on hydrothermal temperature (180 °C).⁴⁵¹ Zhao *et al.*⁴⁵³ predicted that phase transition from hydrogen titanate to anatase follow OR rule,⁴⁵⁵ while Mao and Wong⁴⁵⁶ hypothesised that surface arrangements would be easier than complete solubilization and precipitation. As a result, primary anatase NPs that coalesced at specific points were altered to hydrogen titanate by reordering {101} plane in anatase to {110} plane in titanate with minimal lattice mismatch. This layered structure could be produced and maintained by NH_4^+ ions without the assistance of NaCl under hydrothermal conditions at 100 – 140 °C. The electrolyte NaCl facilitates the formation of hydrogen titanate at 80 °C and maintained up to 200 °C at high NaCl concentration. The Na^+ locally stop the direct closure of titanate layers at their adjacent position which induce the formation of brookite-like structure.⁴⁵⁷ Replacing NaCl with KCl or LiCl resulted in anatase and tetratitanate ($\text{H}_2\text{Ti}_4\text{O}_9 \cdot 1.9\text{H}_2\text{O}$) at lower and higher concentration respectively. Although, trace of brookite was observed with NH_4Cl , its content did not evidently increase with increase in the concentration of NH_4Cl . Thus, these cations seem to promote the condensation of $[\text{TiO}_6]$ and stabilize the titanate too much thereby suppressing the brookite formation. The NH_4^+ readily reacts with water to produce NH_3 and display similar results with those in electrolyte absence. The hydrated K^+ ion has similar radius compared to NH_4^+ and no internal stress arises from K^+ on intercalation. Consequently, phase transition with K^+ was similar to NH_4^+ at very low KCl concentration. However, K^+ assumes much stronger electrostatic interaction with the negative host titanate layer, which stabilizes the titanate and retard the transformation of titanate even at relatively low concentration. By prolonging hydrothermal treatment time (24 – 72 h), transition from titanate to anatase was observed with KCl (0.25 M) and LiCl (1 M). The presence NaNO_3 , $\text{Na}_2\text{B}_4\text{O}_7$ and CH_3COONa seems to favor pure brookite nucleation at 0.8 M (70 h), 0.06 M (84 h) and 0.3 M (60 h) respectively.⁴⁵⁰ Compared with chloride and nitrate, acetate and

borate are better chelators to Ti^{4+} ions. They would promote the phase transition of titanate by forming metal-ligand complex intermediate during the hydrothermal process. The ligands such as borate may even dope into titanate host layer (and TiO_2),⁴⁵⁸ promoting brookite formation at extremely low concentration of $\text{Na}_2\text{B}_4\text{O}_7$. Almost similar phase transition mechanism from titanate to anatase and brookite was observed with $\text{Ti}(\text{OBu})_4$ in ammoniacal medium and NaCl . The optimal hydrothermal reaction parameters for brookite formation were found to be $180\text{ }^\circ\text{C}$, 0.5 M NaCl and $\geq 72\text{ h}$.⁴⁵⁰ In another study, brookite nanoflowers aggregated from brookite NRs under hydrothermal conditions ($180\text{ }^\circ\text{C}$, 24 h) in ammoniacal medium and NaCl .⁴⁵⁴ However in the mixture of NaCl and NH_4Cl , brookite fraction is gradually reduced and this effect became pronounced with increase in the concentration of NH_4Cl .⁴⁵⁹ Thus, role of Na^+ to favour brookite formation was weakened by NH_4^+ ions. Owing to strong electrostatic attraction of Na^+ towards negatively charged host layers than NH_4^+ , it is difficult to expell Na^+ completely even at high concentration of NH_4Cl . In contrast, NH_4F stabilized the titanate and prevented the formation of anatase, as fluoride ion chemically interacts with $[\text{TiO}_6]$ and alters the phase transformation pathway. The fluoride ion catalyzes the condensation of Ti-OH to form Ti-O-Ti linkages,⁴⁶⁰⁻⁴⁶² which results in better crystallization of titanate. Interestingly, NaF promoted brookite formation and tendency was higher compared to NaCl . The high concentration of NaCl stabilized titanate, while NaF favoured brookite formation. The chloride ions interact weakly with $[\text{TiO}_6]$ of either titanate or titania. It was interesting to note that pure anatase was not observed with NaF or NH_4F independent of their concentration, but was achieved by the combination of 0.25 M NaF and $1.5\text{ M NH}_4\text{F}$ (Fig. 25). The fluoride ion can induce Na^+ ions to leave the interlayers of titanate more easily. Therefore, role of Na^+ ions is weakened and brookite formation is restrained with the addition of NH_4F . The large amount of fluoride ion enters the titanate, which ought to catalyse the condensation of Ti-OH by forming Ti-F group with

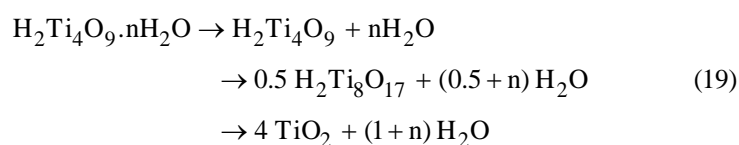
NH₄F. As induced condensation of Ti-OH enhances the crystallinity of titanate and results in the formation of residual titanate in the composite. At much higher concentration of fluoride ions, over condensation of Ti-OH occurs leading to the amalgamation of titanate layers and finally results in TiO₂. Thus preference of titanate to transform into anatase or brookite depends on the concentration of inorganic electrolytes in the reaction medium.

In a different synthesis route, anatase was stable up to 900 °C without any doping or modification synthesized from layered titanate. The K₂Ti₂O₅ exhibits a unique layered structure composed of edge sharing trigonal bipyramids with TiO₅ units comprising five oxygen anions coordinated to one titanium atom, which is different from all other layered titanates.^{463-464a} The water molecules entering the lattice changes the titanium co-ordination from five to six at an extensive rearrangement of original structure.⁴⁶⁵ It was postulated that water gradient develops between solid/liquid interface and core of K₂Ti₂O₅ fiber due to slow inward diffusion of H₃O⁺ ions. The original surface layers of (Ti₂O₅)²⁻ composed of trigonal bipyramidal TiO₅ units are now saturated and undergo structural rearrangement to (Ti₅O₁₁)²⁻ comprising [TiO₆], while unsaturated inner core K₂Ti₂O₅ remains unaffected. Consequently, HCl added and H₃O⁺ diffusion proceeds rapidly leading to the formation of H₂Ti₂O₅.H₂O and H₂Ti₅O₁₁.H₂O. During calcination, latter transforms to TiO₂(B) shell, while former crystallized to anatase core.^{43,466} The presence of TiO₂(B) stabilized anatase even at 900 °C and rutile formation was observed only at 1000 °C, despite the inhibition of crystal growth was not observed.⁴⁶⁷ This was attributed to the presence of protective TiO₂(B) shell which itself has thermal stability up to 800 °C. It was proposed that TiO₂(B) was converted to anatase either by the growth of steps on the lamellar margins that removed the shear component relating the interphase structure, or by a bulk mechanism when anatase nucleus was scarce or absent. This heterogeneous phase transformation is due to the unique and unstable structures of K₂Ti₂O₅, which is easily hydrated on exposure to moist air and partial

ion-exchanged even in distilled water.⁴⁶³ Thus, inner core anatase is surrounded by TiO₂ (B) outer shell which has specific crystallographic orientation with respect to anatase, i.e [010]_A // [010]_B and [100]_A // [001]_B. In another study, TiO₂ (B) was stable up to 650 °C and pure anatase was observed at 700 °C.^{464b}

The hydrothermal treatment (150 °C, 24 h) of H₂Ti₄O₉.1.2H₂O resulted in various titania polymorph depending on the concentration of mineral acids: pure rutile was observed at 0.1 – 0.4 M and 6 M of HCl; 0.1 – 0.2 M and > 7 M HNO₃; 0.1 – 0.8 M H₂SO₄.⁴⁶⁸ Likewise, anatase was obtained by using both HCl and HNO₃ at 0.9 M and broad concentration of 2 – 7 M H₂SO₄. The minority brookite was observed with 1 M HCl and 4 M HNO₃. A variety of nanostructures including aligned NRs, nanoporous, nanocubes, diamond shaped nanocrystals was obtained. The basic crystal structure units of H₂Ti₄O₉.1.2H₂O fibers are [Ti₄O₉]²⁻ sheets that are composed of four side-by-side aligned [TiO₆].^{435-438,469-470} The two central [TiO₆] connect with two adjacent [TiO₆] by sharing two opposite equatorial edges of octahedral at one level. The other two sides of [TiO₆] connect with four [TiO₆] units located at the same level by sharing the corners. The periodic repeating of such structure forms a single chain of [TiO₆]. In addition, four side-by-side aligned [TiO₆] at different levels are connected above and below by sharing additional apical edges of [TiO₆] forming zig zag strings extending in 'b' direction, as well as the axial direction of pristine fibers. The protons and H₃O⁺ ions are accommodated in the widely open interlayers of layered framework of [Ti₄O₉]²⁻ sheets. During the dehydration process, structural water content is totally removed and [Ti₄O₉]²⁻ sheets each involving four [TiO₆] units shift with respect to each other in the amount of $\bar{C}/4$ in the pristine structure. They share free corners of four [TiO₆] units and gradually condense with each other to form octatitanate with a tunnel like crystal structure from which nucleation of anatase and rutile proceeds by dehydration and condensation of [Ti₄O₉]²⁻ sheets. An anatase-rutile was observed for 0.5 – 0.8 M and 1 – 5 M HCl, 0.4 – 7 M

HNO₃ and 0.9 – 2 M H₂SO₄.⁴⁶⁸ The calcination (300 – 600 °C, 2 h) of titanates resulted in anatase-rutile at 700 °C and only rutile at 800 °C, indicating narrow temperature range for ART.⁴⁷¹ Bruce and co-workers reported that layered hydrogen titanates nanowires were converted to TiO₂(B) and layered hydrogen titanate nanotubes were transformed to anatase with the loss of tubular morphology.⁷¹ The rinsing of Na_{1.18}H_{0.82}Ti₃O₇ nanotubes with 0.1 M HCl followed by calcination (573 K) resulted in TiO₂ (B) and anatase co-existed at 673 – 773 K.⁴⁷² Feist and Davies⁴³ has reported heating layered hydrogen titanate at temperature < 623 K transforms to TiO₂ (B). The solvothermal treatment (400 – 450 °C, 1 h) of H₂Ti₄O₉.nH₂O in water showed anatase, while TiO₂ (B)-anatase was observed with methanol and ethanol. The transformation from monoclinic to anatase was slower in ethanol compared to methanol.⁴⁷³ This transformation results from crystallographic shear caused by heat treatment.^{469,474} The successive dehydration reaction are as follows;



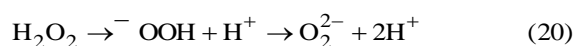
The dielectric constant of water is much larger than those of methanol and ethanol and thus H₂Ti₄O₉.nH₂O has high solubility in water compared to alcohol. Since solvothermal process continues to operate via dissolution-precipitation process, high solubility of H₂Ti₄O₉.nH₂O in water promotes faster anatase precipitation. The low solubility of titanate in alcohol facilitates the phase transformation to proceed much slowly and TiO₂(B) was obtained under these conditions. The sample prepared at 350 °C in water, methanol and ethanol showed pure anatase, monoclinic-anatase and pure monoclinic phase respectively. In this study, batch reactor made by heat resistant alloy was employed to extend the hydrothermal reaction temperature up to 450 °C.⁴⁷³ Zhu *et al.*⁴⁴⁷ concluded that phase transition between nanostructures of titanate and titania polymorphs takes place readily in simple wet chemical processes at temperature close to ambient temperature. The aging of monoclinic

$\text{H}_2\text{Ti}_3\text{O}_7 \cdot x\text{H}_2\text{O}$ transformed to anatase in very dilute HNO_3 (0.05 M) and to rutile for high concentration of 2 M HNO_3 at 30 °C. The hydrogen titanate prepared at low temperature (≤ 100 °C) transformed to anatase or rutile at 30 °C, while those synthesized at 100 – 200 °C transformed to anatase or rutile (0.05 and 2.65 M HNO_3) in the range of 60 – 200 °C (Fig. 26).⁴⁴⁷ In general, titanate fibers prepared at low temperature were thinner and possessed a high surface area, more defects (poorer crystallinity) and less rigid crystal structure so that phase change was easier. The aggregates of anatase nanocrystals inherit their morphology from the reactant titanate fibers, while rutile showed no morphology similar to the initial titanate fibers. The titanate and anatase have common structural features; both crystal lattice consist of octahedral sharing four edges and zigzag ribbons.^{59,475-476} In reaction with acid, H-titanate nanofibers dehydrate and large structural units of zigzag ribbon remains relatively unchanged, rearranging to form anatase lattice. The zigzag ribbons of $[\text{TiO}_6]$ with four shared edges in H-titanate nanofibers have to be resolved into detached $[\text{TiO}_6]$ or their small clusters there of to form straight chains. Thus, rutile lattice is reconstructed with the detached octahedral in acidic solution. These hydrogen titanates were stable against thermal treatment exhibiting mineral like behaviour; titanate prepared at low temperature (≤ 100 °C) transformed to anatase after calcination (400 – 500 °C), while those prepared at 200 °C was thermally stable up to 650 °C. The increase of power from 350 – 650 W in microwave-hydrothermal reaction of TiO_2 and NaOH showed evolution from titanate nanowires to anatase and later to brookite after calcination (450 °C, 2 – 5 h).⁴⁷⁷ Ribbens *et al.*⁴⁷⁸ found that hydrogen titanate partially transformed into anatase after calcination at 623 K.

The reversible phase transition between titanate and titania polymorphs under wet-chemical approaches are of significant interest owing to its flexibility to obtain TiO_2 (B) and brookite phase at low temperature. These studies indicated that titanates are potential precursor for the preparation of all the four polymorphs of titania.

9.3 Crystallization of TiO₂ from PTC

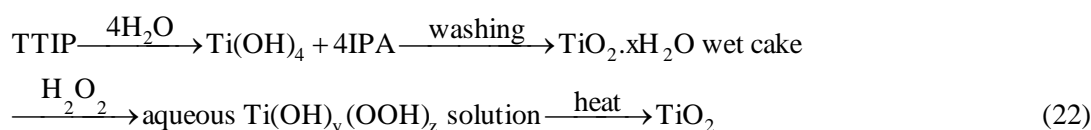
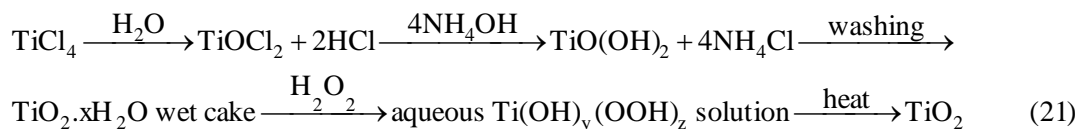
Although, several routes to prepare nanocrystalline titania with different phases is reported till date, alternative approaches that is simple and inexpensive, affording high purity are worth investigating. To this end, facile and low-cost water soluble PTC was found to be promising intermediate phase for the preparation of nanocrystalline titania.^{32-33,479-486} According to Salifoglou and co-workers⁴⁸⁷ PTC is a dinuclear of two Ti⁴⁺ ions coordinated by peroxide ligands, central core in the dimer being composed of Ti₂O₂ rhombic unit and is planar by the virtue of centre of inversion. The detailed structure of PTC dinuclear complex is Ti₂(OOH)₂(OH)_a(H₂O)_b, Ti₂(O₂)₂(OH)_a(H₂O)_b, Ti₂(O₂)(OOH)(OH)_a(H₂O)_b or [Ti₂O₅(OH)₂]_∞ which changes with the concentration of ligand. The H₂O₂ is added to the gel/amorphous titania to form PTC and dissociation of H₂O₂ in aqueous solution is;



Thus, the concentration of oxygen ligands varies depending on solution pH. The PTC is mononuclear Ti(O₂)OH⁺ at pH <1 and dimerises to [Ti₂O₅(OH₂)(H₂O)₂] at pH 1-3, which is capable of further deprotonation with base leading to the formation of dinuclear complexes like [Ti₂O₅(OH)₃(H₂O)]⁻, [Ti₂O₅(OH)₄]²⁻, [Ti₂O₅(OH)₅]³⁻ and [Ti₂O₅(OH)₆]⁴⁻.^{138,486,488} In all these dimeric species, Ti₂O₅ unit exist as two five membered rings with a common Ti-O-Ti linkage. The transformation to polynuclear complex [Ti₂O₅(OH)₂]_∞ at pH > 3 is also reported.⁴⁸⁶

The modification of titania precursor with H₂O₂ resulted in the formation of (interstitial oxygen) oxygen rich titania which stabilized anatase up to 900 °C.⁴⁸⁹ The stability increased with increase in H₂O₂ concentration. The in situ generation of oxygen due to thermal decomposition of PTC hinder the oxygen vacancy formation and strengthens Ti-O-Ti network rendering anatase stability and also prevents the grain growth. Contrarily, controlled titania samples becomes non-stoichiometric via oxygen vacancy formation during

calcination.^{130,490} The PTC derived from TiCl_4 showed only anatase, while anatase-rutile was observed with TTIP after aging (100 °C, 24 h) in a closed bottles.⁴⁹¹ The formation of TiO_2 via PTC from different titanium precursor is presented as follows:



The external addition of NH_4Cl to PTC derived from TTIP did not influence the resulting crystal structure confirming that neither NH_4^+ or Cl^- ions had no role in phase evolution. The addition of H_2O_2 to $\text{TiO}_2 \cdot x\text{H}_2\text{O}$ resulted in pH 1 for TTIP and pH 2 for TiCl_4 . However, pure anatase was obtained by increasing the pH to 2 and reducing to pH 1 respectively in the above precursors, suggesting that PTC derived from both the precursors had different chemical entities. At low pH, surface hydroxyl groups on hydrated $[\text{TiO}_6]$ units will be less and edge sharing condensation process become kinetically favourable leading to rutile, while the concentration of surface hydroxyl groups on hydrated $[\text{TiO}_6]$ increases with increase in pH facilitating the face-sharing condensation to form anatase. The hydrothermal treatment (200 °C, 2 h) of $[\text{Ti}(\text{OH})_3\text{O}_2]^-$ (obtained by aging metallic Ti and H_2O_2 at 100 °C followed by immersion in an ice bath) resulted in rutile at pH 0 and anatase in wide pH range of 2 – 12 followed by hydrogen titanate at pH 14 (Fig. 27).³² The orientation mechanism was predominantly observed in the growth of rutile nanorod and anatase nanoribbons at pH 0 and 8 respectively. At pH 14, total diffusion of previous structure resulted in the reprecipitation of lamellar hydrogen titanate. Riberio *et al.*^{32,492} suggested that role of pH in the phase transformation is not simply an attachment/detachment of ions induced by solution acidity/basicity. The situation is more complicated and OA mechanism of nanocrystals seems

to be rate determining step. Hydrothermal synthesis (220 °C, 24 h) of PTC with glycolic acid showed pure brookite, while anatase-brookite with citric acid.⁴⁹³ In contrast, only anatase was obtained with lactic and AcOH. Thus obtained brookite was directly transformed into rutile, after the thermal treatment at 1125 °C. The critical size for BRT was found to be 24 nm. Hydrothermal treatment of peroxotitanic acid (200 °C, 3 h) showed anatase-rutile in the pH regime 4 – 10, with dominant rutile and anatase at pH 4 and 10 respectively. The addition of polyvinyl alcohol stabilized only anatase phase with specific exposed facets {101} and {001} by adsorbing on TiO₂ during the crystallizing process and also prevented the particle agglomeration.⁴⁹⁴ The addition of AcOH to PTC followed by aging (100 °C, 24 h) resulted in similar content of anatase (57 %) and rutile (43 %), while addition of H₂O₂ to titanium acetate complex [Ti(OⁱPr)_{4-x}(OAc)_x] showed dominant anatase (92 %) with minor rutile (8 %).⁴⁸³ The absence of H₂O₂ showed only anatase. The PTC obtained by the addition of TTIP to 35 wt % H₂O₂ (pH 3.4 – 3.5) declines the pH to 1.1 and hence rutile nucleation begins.



The proton formed reduces the solution pH during the formation of peroxo complex. Thus, addition of AcOH will have little influence as PTC will be rapidly hydrolyzed. The rate of nucleation process of anatase and rutile will be approximately same yielding similar fraction for both the phases. The hydrolysis of TTIP/AcOH mixture in water results in pH 3.2 – 3.5 to favour anatase. The addition of H₂O₂ to Ti(OⁱPr)_{4-x}(OAc)₄ leads to peroxo complex of Ti(OⁱPr)_{4-x}(OAc)₄ which hydrolyzes very slowly due to the presence of acetate group and nucleation of anatase begins. The pH down fall was observed from 3.9 – 4.1 to 1.5 and nucleation of rutile thus begins. Due to slow rate of hydrolysis, rutile nucleation lags behind giving rise to anatase as major fraction. Thus, sequence of addition of complexing agents or modifiers also influences the final phase composition. The hydrothermal treatment (150 °C,

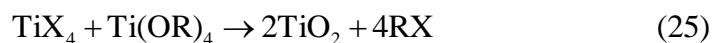
24 and 48 h) of PTC with CF_3COOH exhibited rice-like rutile, while only spherical anatase was observed under normal conditions.⁴⁹⁵ The PTC has tendency to form dinuclear Ti complexes like $[\text{Ti}_2\text{O}_5(\text{OH})_3]$, $[\text{Ti}_2\text{O}_5(\text{OH})_4]_2$, $[\text{Ti}_2\text{O}_5(\text{OH})_6]_3$ and $[\text{Ti}_2\text{O}_5(\text{OH})_6]_4$ followed by subsequent conversion to anatase via face sharing condensation.^{496,497} The rice like morphology was due to the anisotropic growth of TiO_2 along [001], which is perpendicular to [110] facet.⁴⁹⁸ The CF_3COOH played a dual role; adjusting the pH of reaction mixture and as growth regulator. In the initial stage of experiments, disintegration of PTC gel network takes place and that gel is converted into smaller TiO_2 nuclei which on further growth give TiO_2 with different morphology and phases. The nuclei first formed are grown into bigger particles at the expense of smaller ones through OR process. In the absence of CF_3COOH , solution pH was nearly neutral to promote anatase formation,⁴⁹⁹ while increase of fluoride anions in wet gel reduce the surface energy of {001} surfaces to a lower level than {110} surface in rutile. The refluxing (100 °C, 48 h) of PTC derived at pH 0 and 3 (6) resulted in rutile and anatase respectively.³³ However, brookite (63 %) co-existed with anatase at pH 1. These results suggest that phase transition can be achieved with PTC by simply varying the solution pH. By varying the $[\text{H}_2\text{O}_2]/\text{Ti}$ ratio from 5 to 20, anatase-brookite present at lower ratio completely and partially transformed to rutile at pH 0 and 1 respectively. In contrast, only anatase was observed irrespective of $[\text{H}_2\text{O}_2]/\text{Ti}$ ratio at pH 6. Thus, titania formation is associated with decomposition routes of different PTC structures, which leads to seeds for different phases at the same temperature. At pH 0, high acidity and $[\text{H}_2\text{O}_2]$ benefit the formation of OOH^- ligand and hence $\text{Ti}_2(\text{OOH})_2(\text{OH})_a(\text{H}_2\text{O})_b$ dominates in the solution. On the other hand, Ti atoms will bridge by two peroxy groups to form an octahedron. As a result, small rutile chain is favored by the decomposition of peroxo groups to yield free oxygen. Further condensation must proceed byolation and formation of bridging hydroxyl ligands between several small chains. Finally, linear linkage is arranged to form rutile. At high pH,

complexes like $Ti_2(O_2)_2(OH)_a(H_2O)_b$ or $[Ti_2O_5(OH)_2]_\infty$ are formed. The O^{2-} can form a Ti-O₂ triangle ring configuration.⁵⁰⁰ The peroxide group can laterally co-ordinate to Ti^{4+} and octahedral favours link together through shared edges only along the apical directions by decomposing peroxy groups and then olation proceeds resulting in anatase. At pH 1, $Ti_2(O_2)(OOH)(OH)_a(H_2O)_b$ will be available in the solution. Because of the concurrence of O_2^- and ^-OOH ligands, crystals could grow along the equatorial plane or apical directions. This linkage favors crystal structure between anatase and rutile and as a result, brookite was obtained.³³

10.0 Preparation of TiO₂ via non-aqueous route

The strong sensitivity of precursor in aqueous medium even towards slight changes in the synthesis conditions and simultaneous occurrence of hydrolysis-condensation makes it impossible to fully control the processing of metal oxides. The traditional hydrolysis is based mainly on the physical introduction of water as oxygen donor in the reaction system, which exert negative effects on the control of reaction rate and homogeneity of the resulting particles.^{182,501-503} The metal oxide obtained will be enriched with hydroxyl groups/adsorbed water, thus influencing surface properties of titania and hence their crystallization behaviour at the annealing stages. The non-aqueous routes do not rely on the hydrolysis for the creation of Ti-O bonds³⁶⁰ and high reactivity of titania precursor towards hydrolysis can be circumvented. The role of organic solvents used in these systems can be diverse providing not only size and shape control but also contributes to the particle formation and to the stabilization of the formed nanostructures enabling a very simple reaction set up.⁵⁰¹⁻⁵⁰³

The trivial route involves the reaction of $TiCl_4$ with titanium alkoxides or ethers accompanied by the elimination of alkyl halides.⁵⁰⁴⁻⁵⁰⁵



The 'X' function as electrophile attacking either oxygen-bound carbon or titanium center of alkoxide precursor, resulting in Ti-O bond without the incorporation of defects in the growing titania crystal. Trentler *et al.*⁵⁰⁶ suggested that this reaction follows S_N1 mechanism, as the reaction rate was enhanced with increase in the branching of R (primary to tertiary) and is independent of nature of halide. Although, average particle size remained unaffected irrespective of branching in R, smaller crystallite size and rutile formation was observed with increasing the nucleophilicity of halide in titanium precursor. In addition, high concentration of reactants gave off-white precipitates, while clear orange solution was observed at lower concentration.⁵⁰⁶ The mesoporous anatase-rutile was tuned by non-hydrolytic evaporation-induced self assembly method based on the effect of acid-base pairs using TiCl₄ and Ti(OBu)₄ along with Pluronic 123 template.⁵⁰⁷ The former acts as pH-adjustor and controls the hydrolysis-condensation pathways, while latter served as major titanium source and oxygen donor. The TiCl₄ reacts with ethanol to form Ti(Cl)_{4-x}(OEt)_x (x~2) species⁵⁰⁸ resulting in acidic mother solution (pH 1). The addition of Ti(OBu)₄ reduced the pH and was accompanied by the formation of oligomers TiX_x(OH)_yO_{2-(x+y)/2} (X=OR or Cl; x ~ 0.3 – 0.7; y = 0 – 0.2).⁵⁰⁹ The Ti-O-Ti bridge may partially result from condensation reaction between Ti-Cl or Ti-OR. It was suggested that mother solution pH leads to the respective formation of hydrophobic Ti-oxo-alkoxo and hydrophilic Ti-oxo-hydroxo species.^{509,510} The former will hinder the proper folding of polymers, “freezing” the disordered states, while latter promotes the ordered template folding, creating the conditions for an adequate phase segregation at the mesoscale. Moreover, rutile fraction increased gradually with increase in volume of TiCl₄. The gel obtained by solvothermal reaction (140 or 160 °C, 3 h) of TiCl₄ and TTIP in CCl₄ were anatase, which on calcination (750 °C, 3 h) transformed partially to rutile. The gel

obtained at low temperature (140 °C, 3 h) showed maximum rutile content (95 %) compared to the sample (60 %) obtained at high temperature (160 °C, 3 h). Thus, gel with smaller crystallite size (8.2 nm) inclined towards ART and that highly crystallized gel (8.5 nm) requires high temperature for ART.⁵¹¹ In another study, the very low crystallite size for anatase was observed with increasing gelation time. The IPA that was formed during gelation, might have confined the crystal growth.⁵¹²

The spontaneous in situ formation of water due to condensation of BA at Ti centres initiates nucleation and fast growth of titania NPs.⁵¹³ The particle formation occurs within a very limited time span in the course of synthesis, concurrently to a step-type pressure increase within the closed reaction system. The particle growth was parallel to the pressure rise, but when the pressure converges to a limiting level, the crystallite growth showed a small further increase. The investigations clearly revealed that increase of pressure, increased the formation of water and initiates the formation of NPs. In addition, Small Angle X-ray Scattering measurements proved the absence of any NPs before pressure surge, evidencing the crucial role of water on the particle formation kinetics.⁵¹³ The TiO₂ could not be generated with n-butanol, while diameter of TiO₂ NPs was low with BA compared to n-octanol. Thus, BA played a pivotal role in limiting size and controlling the morphology of NPs, which may be attributed to carbocation effect.⁵¹⁴ In the first step, carbocation and –OH was formed, with the latter serving as oxygen donor. The carbocation reacts with nucleophile, while –OH reacts with metal cation forming Ti-OH bonds. The reaction can be illustrated from the perspective of S_N1 mechanism attributed to the easy formation of benzyl carbocation and unique reactivity of benzyloxy group with nucleophilic agents. The carbocation served as capping agent to avoid the introduction of other surfactants for the simplification of reaction systems. The increase of metal chloride concentration, high reaction temperature and long reaction time are prone to polymerization of BA.⁵¹⁴ The non-aqueous reaction of TiCl₄ and

BA showed only anatase, while reaction medium seeded with ST21 (anatase) and P25 (anatase-rutile) showed anatase-rutile.⁵¹⁵ The rutile content initially increased with increase in ST21 content and later decreased, while low rutile fraction was observed in the titania obtained with P25 seeds. The presence of rutile regardless of the type of seeds was accounted as follows; hydrophilic P25 or ST21 contains high density of surface titanol groups. Thus, TiCl_4 would react with these titanol groups and adsorbed water molecules. The reaction thus produces new anatase on the seeds and HCl as by product. As the non-hydrolytic condensation proceeds, concentration gradient of HCl around the seed was then developed favoring the growth of rutile. The non-hydrolytic reaction of TiCl_4 in anhydrous BA (or *n*-butanol) with or without ultrasonication resulted in anatase.⁵¹⁶ The increase of calcination temperature enhanced the crystallization and rutile formation (700 °C, 3 h).

The solvothermal reaction (200 °C, 72 h) of TTIP with benzyl amine or *m*-xylylenediamine exhibited anatase nanoplatelets, that are arranged in lamellar, highly ordered fashion with thin organic layers in between them acting as ‘glue’.⁵¹⁷ The benzyl amine provides control over the growth and assembly of nanocrystals through selective binding of its amine groups to the (001) crystal surface. The phenyl groups of bound benzyl amine undergo π - π interactions, which therefore leads to assembly and stacking of the platelets into a highly ordered material. The elimination of isopropoxy ligands of TTIP must be underlying mechanism for the formation of Ti-OH groups. This further initiates the build up of oxygen bridges as the starting point of oxide formation. The crystalline anatase was obtained by reacting TTIP with ketones (acetone, 2-butanone, 3-pentanone, cyclohexanone, acetophenone and benzophenone) under solvothermal conditions (130 °C).⁵¹⁸ Based on ^1H and ^{13}C liquid state NMR, following mechanism were proposed considering acetone as model: (i) acetone is co-ordinated to titanium centre and deprotonation leads to the enolate complex under concurrent release of IPA; (ii) the enol ligand nucleophilically attacks a second ketone to

form C-C bond; (iii) ligand reacts with another titanium center to form Ti-O-Ti bond, which is the starting point of particle formation and crystallization followed by the release of IPA and mesityl oxide (Fig. 28). The non-aqueous reaction of TiCl_4 and TTIP lead to anatase and was stabilized up to $950\text{ }^\circ\text{C}$.⁵¹⁹ The gelation time for non aqueous reaction of TiCl_4 with various oxygen donor followed the sequence: di-isopropyl ether (2 h) > diethyl ether (17 h) > tetrahydro furan (60 h) > di-n propyl ether (70 h) > dimethoxyethane (85 h). The rutile fraction after calcination ($950\text{ }^\circ\text{C}$) followed the order: dimethoxyethane (100 %) > diethyl ether (58 %) > tetrahydro furan (43 %) > di-isopropyl ether (14 %) ~ di-propyl ether (11%). This suggests that there exists no correlation between gelation time and rutile formation. Alternatively, gelation time increased with increase in carbon chain length for primary alcohols and decreased from primary to tertiary alcohol. In fact, gelation time occurred after 50 h with ethylene glycol. The powder obtained after drying was rutile with ethanol and anatase with ethylene glycol, n-propanol, n-butanol and IPA. It was observed that rutile content decreased with increase in carbon chain length in primary alcohol. However, anatase-rutile and brookite-rutile was observed with secondary and tertiary butanol respectively. The BRT was observed at $900\text{ }^\circ\text{C}$ in the latter, while anatase was still stabilized in the former case. Thus, unique formation of hydroxyl groups in the reaction of tertiary butanol with TiCl_4 might be related to the crystallization of brookite. This formation may be accounted to the occurrence of tertiary butyl chloride instead of HCl, owing to increased cationic character on the tertiary-carbon, which favors the nucleophilic attack of chloride.⁵¹⁹

The water supplied via esterification reaction between AcOH and n-butanol in non-hydrolytic reaction using $\text{Ti}(\text{O}i\text{Bu})_4$ showed anatase ($320\text{ }^\circ\text{C}$, 2 h) and transformed completely to rutile at $700\text{ }^\circ\text{C}$.⁵²⁰ However, pure rutile was observed at $800\text{ }^\circ\text{C}$ with TTIP with ethanol (0.1 % water). The amorphous to anatase crystallization was same for both routes when calcined in air. Interestingly, ART was shifted to higher values upon calcination in helium

atmosphere and that titania obtained from $\text{Ti}(\text{OBU})_4$ occurred at high temperature compared to TTIP. The anatase nanoparticles was obtained by autoclaving treatment (150 °C, 12 h) of high molar ratio of $\text{TiCl}_4/\text{n-butanol}$, while rutile NRs was selectively synthesized at low molar ratio.⁵²¹ The evolved HCl was retained in the reaction solution in the latter to promote rutile, while HCl may escape from the reaction solution in the former. The TiCl_4 reacts with butanol producing $\text{TiCl}_{4-x}(\text{CH}_3\text{CH}_2\text{CH}_2\text{CH}_2\text{O})_x$, $\text{CH}_3(\text{CH}_2)_3\text{Cl}$ and HCl. Due to the steric hindrance of butanol, reaction is not vigorous and so the evolution of HCl. Thus, HCl dissolved in butanol through forming oxonium salts. The dissolved HCl promotes the etherification of butanol and water is produced as by product. The hydrolysis of TiCl_4 can produce $[\text{Ti}(\text{OH})_x\text{Cl}_{4-x}]$ species, because ligand field strength of hydroxyl anion is higher than that of chloride ions. Under hydrothermal conditions, polycondensation of $[\text{Ti}(\text{OH})_x\text{Cl}_{4-x}]$ species leads to the formation of Ti-O-Ti network and their crystallization. However, only anatase was observed both at high and low molar ratio of TiCl_4 to ethanol. The increase of TTIP concentration (2 – 200 mol%) in solvothermal reaction (250 °C, 20 h) with toluene increased the anatase crystallite size (10 to 23 nm).⁵²² The anatase with 11 nm underwent ART at a faster rate compared with 21 nm sample, attributed to faster coarsening rate of particles in the former case. The non-hydrolytic reaction between TiCl_4 and cellulosic natural materials followed by calcination (400 – 700 °C, 2 h) exhibited anatase.⁵²³ The cellulose constitutes D-glucose monomers linked by β -1,4 ether linkages and contains nearly 50 wt % of oxygen in alcohols and ether groups which makes it an excellent oxygen source for non-hydrolytic reaction with titanium halides. Thus, hydroxyl and ether groups in each cellulose unit react with TiCl_4 leading to titanium alkoxide groups, which condense with TiCl_4 to give titanium oxo bridges.

It is common that titania obtained via non-aqueous route often contains a certain amount of organic compounds or carbonaceous species that ligate to titania surface and

inhibits the grain growth.⁵²⁴ Also, post-thermal treatment is conducive for the complete removal of organic compounds. The organic solvents are highly interesting media for the formation of inorganic nano structures by non-aqueous process due to their versatile properties and their ability to selectively bind to specific facets of nanocrystals.⁵¹⁷ The absence of surface hydroxyls permits the evolution of new types of surface derivatization and the properties that are subject of current investigation. The study of organic solvents other than alcohol or ketone as oxygen suppliers to form Ti-O-Ti network is still an open avenue in this area.

11.0 Preparation of TiO₂ from Ball milling (Mechanochemical activation) method

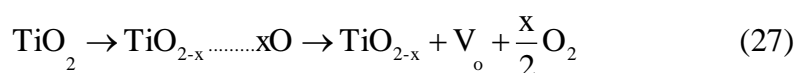
Mechanochemistry involves mechanical activation of solid-state reactions caused by collisions between particles and balls inside the mill.⁵²⁵⁻⁵²⁷ During milling, ball/reactant/ball or ball/reactant/wall collisions impart mechanical energy to the reactant and raise the temperature through which activation energy of the solid transformation is achieved.⁵²⁸⁻⁵³¹ The local temperature of powder particles at the collision sites will be 180 – 500 °C higher than average environmental temperature, depending on the milling conditions and powder characteristics.⁵³²⁻⁵³⁴ In this process, cold-welding, fracturing and annealing of powder grains simultaneously takes place. The ball milling apart from the particle fracture may induce lattice strain in the form of lattice distortion. The development of strain is constant with time, but the residual strain is additive. Therefore, cumulative strain which is locked up in the material increases with increasing time. By this process, many stable structures existing at high pressure or high temperature can even form at laboratory conditions.

Anatase with small crystallite size (22 nm) transformed to srilankite and rutile upon ball milling (220 rpm, 10 h) at a faster rate, compared to large crystallites (96 nm).⁵³³ Since both powders were milled at the same conditions, impact pressure (8.08 GPa) and local

temperature rise (425 °C) experienced are roughly estimated to be the same. However, defects such as vacancies, triple junctions and grain boundaries in small crystallites raise the free energy of anatase and accelerate the phase transformations,⁵³⁵ while the rate of grain refinement is faster in titania with larger grain size. Colin *et al.*⁵³⁶ proposed a generalised phase transformation pathway as “anatase to brookite to rutile” irrespective of milling conditions. The ball milling of anatase resulted in anatase-brookite for 400 rpm, while ABT at 500 rpm followed by ART and BRT at high milling speed (600 rpm).¹⁰⁹ The increased milling speed above a critical value provides sufficient energy required for volume contraction.⁵³⁷ The pressure experienced by anatase particles during the collision of two colliding balls is estimated to be above 1 GPa and increase in defect density may further reduce the lower pressure limit (1.5-10 GPa) required for ABT. After annealing (850 °C, 2 h) brookite disappeared and rutile content increased from 18.85 – 79.71 %.¹⁰⁹ The high pressure polymorph of titania (orthorhombic, α -PbO₂; Pbcn) were obtained by high energy impact vibrational ball milling of anatase powder.⁵³⁸ It was concluded that prolonged milling creates sufficient impact shock in a localized point, similar to the shock waves generated by dynamic loading, forcing the transformation of anatase to orthorhombic phase. If the milling time is short, small amount of strain will be generated and much of it was dissipated by particle fracture which fails to initiate any transformation. The shock waves are responsible for high pressure formation and intergrowth of other crystalline phases with a short range order that takes place inside the anatase lattice in a compressive stress field. The ball milling of anatase (450 rpm, 5 min) resulted in partial transformation to anatase-rutile-srilankite and only rutile-srilankite was observed thereafter (3 – 15 h).⁵³⁹ The fraction of rutile gradually increased from 3 – 62 % with increase in milling time from 5 min to 15 h (Fig. 29), while srilankite increased (24 – 68%) in the initial stages (0 – 1h) and decreased thereafter (3 – 15 h). The anatase preferred to srilankite transformation rather than to rutile at the initial stages (0-1 h).

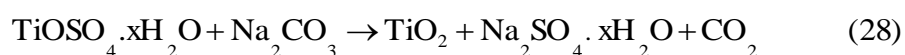
Thus, rutile growth was prevented due to anatase at the initial stages and rapid growth was observed due to instability of srilankite. The transformation from srilankite to rutile was slower compared with anatase to srilankite indicating mutual interference of each phase on transitions pathways. The local temperature rise and impact pressure at the collision sites of powder and the balls, as well as an additional energy due to the grain refinement, defects and the lattice distortion contributes to the milling induced transformations.⁵⁴⁰ The ball milling (600 rpm) of anatase-rutile with graphite transformed to srilankite-rutile, with increase in milling time (6-12 h). The decrease of anatase was followed by increase of srilankite up to milling time of 12 h, with both anatase and srilankite transformed to rutile or amorphous at later stages (Fig. 30).⁵⁴¹ The graphite suppressed the transformation of anatase to other crystalline/amorphous phase together with suppressing crystalline confinement. The presence of graphite was to provide lubrication and reduce the average pressure in collision. The average environmental milling temperature for water cooled conditions was constant (20 °C) throughout the milling process, while it increased at the beginning of milling and stabilized at 120 °C after milling for 0.5 h in the case of air cooling. The increase of local temperature enhances the diffusivity of atoms to favour the transformation of anatase to srilankite and rutile. The formation of rutile is from anatase at initial stages and from amorphous at later stages. The graphite was made amorphous during the course of milling.

The transformation rate of anatase to srilankite and rutile increased with decrease in oxygen partial pressure of milling atmosphere (220 rpm, 40 h), although local temperature and impact pressure experienced by powders were same.⁵⁴² During ball milling, partial Ti-O bonds on surface layer may be broken due to mechanical activation and oxygen is released from the TiO₂ lattice leading to oxygen vacancies;

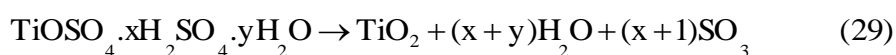


The milling atmosphere with low oxygen partial pressure favors the formation of oxygen vacancies and accelerates the milling induced transformation. Since oxygen atmosphere do not favour the production of oxygen vacancies, transformation rate in oxygen milled powder is distinctly slowed down, while more oxygen vacancies are produced under nitrogen atmosphere to favor such transformation. Irrespective of powder to ball weight ratio (1:50 or 1:10), phase transition from anatase to TiO₂ II to rutile prevailed after ball milling (500 rpm) during the entire course.⁵⁴³ Interestingly, this transition was faster for high powder to ball weight ratio and completed in 1 h, while it took longer time (10 h) for other. The ART started from the centre of particle due to local heating as a result of ball milling effect, while anatase to TiO₂ II commenced on the particle surface. The high pressure being dominant at the particle surface during collisions, favored the formation of high pressure TiO₂ II. Rezaee *et al.*,⁵⁴⁴ concluded that increasing the milling time has no significant effect on phase transformation, while milling speed and ball to powder ratio is most effective factor in tuning the phase transition. For a given collision time, increase in ball to powder ratio leads to higher energy release for each particle. The collision frequencies of both ball to ball and ball to wall impact enhances with increasing speed, leading to significant kinetic energy transfer to the particles. This results in excess microstructural defects such as dislocations and vacancies.^{537,544-545} Alternatively, it is very likely that the microstructural changes in milling speed reduce the microstructural diffusion path lengths which accelerate phase transformation kinetics.

The complete rutile was observed after ball milling (880 rpm, 60 min) of TiOSO₄.xH₂O and anhydrous Na₂CO₃, while anatase was obtained after calcining (300 °C, 1 h) the ball milled sample (5 min).⁵²⁹



After 2 min of ball milling, peaks of TiOSO_4 was not visible and Na_2SO_4 were observed, indicating the formation of amorphous phase. This short duration was attributed to the strong solid state acidobasic interaction and presence of water during the milling process. The TiOSO_4 by itself contains 18 mass % of water, which acts as solvent and facilitates the hydrolytic reaction between TiOSO_4 and Na_2CO_3 to enhance the reaction rates. The rutile fraction was declined with increase in diluents phase (NaCl) content in $\text{NaCl}:\text{TiOSO}_4$ mixture from 2:1 to 9:1 after ball milling (400 rpm, 4 h) followed by calcination (700 °C, 30 min).⁵⁴⁶ The anatase crystallite size increased, while rutile showed decrease up to 5:1 followed by sudden increase at high NaCl content. The increase of diluent phase reduces the volume of reactant and that TiOSO_4 particles will be surrounded by more number of diluent phase particles. This lowers the collision between balls and reactant particles inside the mill and hence reactant particles are shielded from mechanical activation. In addition, they avoid the rise of local temperature inside the mill by absorbing heat and kinetic energy from the reactant particles. The ball milling of NaCl and $\text{TiOSO}_4 \cdot x\text{H}_2\text{SO}_4 \cdot y\text{H}_2\text{O}$ (400 rpm, 4h) showed anatase after calcination (600 °C, 0.5 h) and complete rutile at 900 °C.⁵⁴⁷



The anatase transformed to brookite-rutile after mechanical activation (6 h) and transformation to pure rutile after calcination (1050 °C, 1 h).⁵³⁰ The BRT activation energy was found to be 28 kJ/mol based on first order Avrami-Erofeev kinetic model which indicates the random nucleation of rutile followed by the instantaneous growth of nuclei accompanied by the decrease of microstrain with increased annealing temperature. The TiO_2 obtained with sol-gel and ball milling showed anatase (350 °C, 2 h) and transformed to rutile with increase in annealing temperature (900 °C).⁵⁴⁸

The ball milling is a complex process depending on many factors like type of mill, dynamic conditions of milling, local temperature and atmosphere, chemical composition of

powder and properties of grinding media. During milling, equilibrium between breakage and rewelding of powders may be reached and particle size remains almost unaltered on further milling due to agglomeration of smaller particles into grains.⁵⁴⁹⁻⁵⁵¹ In a rare instances, contamination from the milling media in the course of excess milling creates additional crisis. Above the critical milling speed, balls are pinned onto the inner walls of the jar and do not fall down to exert any impact force. A partial surface amorphization and occurrence of oxygen vacancies are also responsible during milling, although these effects were not noticed by experimental methods. The accurate effects of its parameters on the transformation have not been completely understood because of limitations for in situ analysis during the course of ball milling.

12.0 Conclusion and future prospects

The critical understanding of nucleation, particle growth, crystallization mechanism and thermodynamic behaviour at various particle size regimes among the titania polymorph remains as a central goal, inspiring for designing nanostructures with fascinating properties for many green energy applications. The fact that a large number of reports are published and are still being extensively investigated is a reflection of interest in its material properties. Each crystal phase of titania; anatase, rutile, brookite and $\text{TiO}_2(\text{B})$ along with mixed crystal framework finds excellent scope in a broad spectrum of applications. This has triggered the need to employ low-processing temperature methods for activating the phase transformation in order to prevent rapid grain growth that occurs at high temperature. This focused review underpins and sheds light on nature of chemistry associated with titania synthesis, phase transition/stabilization and growth mechanism under variety of experimental conditions to deepen our knowledge for industrialization (Table 1 & Fig. 31). The easy reproducibility and versatility of wet chemical approaches offers strategy to produce delicate nanostructure of

phase pure or mixed crystal framework with great control and examination of their size-shape-morphology dependent properties.

In spite of extensive research, ability to control the TiO₂ polymorphs is still difficult in identifying suitable preparation process. A complicating factor in understanding the nanoparticle formation is the multitude of experimental conditions used for the synthesis making it difficult to understand the reaction mechanisms. For instance, effect of synthetic variables on brookite content and their influence on materials properties is not entirely understood till date. On the other hand, role of solvents and complexing agents in the crystallization depending on solution pH reveals widespread disagreement in the literature. There is no thumb rule for phase transition to occur, since nucleation sites formed varies with preparative methods and chemical reactions occurring at the molecular level cannot be fully controlled. The nature of such defects in phase transition is largely unknown at this stage. The uncovering of these processes occur in solution is challenging as hydrolysis of precursors and nucleation of particles are so fast and that experimental techniques to characterize the reaction intermediates are lacking and these processes are highly sensitive to small variations in reaction conditions. The factors that control phase stability and crystal shape for this intensively studied system are not completely understood at the nanoscale. The establishment of relation between performance and properties of obtained material, their processing conditions and production costs necessitates a delicate continuous effort. The realization of solution based approaches is expected to enhance our capacity to tailor the composition and morphology and thus their properties. The simplicity of the method suggests that it is amenable to commercial scale-up in near future.

Acknowledgements

The author S. Girish Kumar acknowledges financial support from Dr. Daulat Singh Kothari Post Doctoral Fellowship (University Grants Commission, New Delhi, INDIA) and the Department of Physics, IISc, Bangalore for providing the research facilities.

References

- (1) (a) X. Lang, X. Chen and J. Zhao, *Chem. Soc. Rev.*, 2014, **43**, 473-486; (b) J. B. Joo, M. Dahl, N. Li, F. Zaera and Y. D. Yin, *Energy Environ. Sci.*, 2013, **6**, 2082-2092; (c) L. Jing, W. Zhou, G. Tian and H. Fu, *Chem. Soc. Rev.*, 2013, **42**, 9509-9549; (d) Y. Wang, Q. Wang, X. Zhan, F. Wang, M. Safdar and J. He, *Nanoscale*, 2013, **5**, 8326-8339; (e) A. G. Dylla, G. Henkelman and K. J. Stevenson, *Acc. Chem. Res.*, 2013, **46**, 1104-1112.
- (2) (a) C. Aprile, A. Corma and H. Garcia, *Phys. Chem. Chem. Phys.*, 2008, **10**, 769-783; (b) M. A. Lazar and W. A. Daoud, *RSC Adv.*, 2013, **3**, 4130-4140; (c) S. Liu, J. Yu and M. Jaroniec, *Chem. Mater.*, 2011, **23**, 4085-4093; (d) Q. Xiang and J. Yu, *J. Phys. Chem. Lett.*, 2013, **4**, 753-759; (e) S. Liu, J. Yu, B. Cheng and M. Jaroniec, *Adv. Colloid Interface Sci.*, 2012, **173**, 35-53.
- (3) (a) Z. Yin, L. Wu, H. G. Yang and Y. H. Su, *Phys. Chem. Chem. Phys.*, 2013, **15**, 4844-4858; (b) K. Lv, B. Cheng, J. Yu and G. Liu, *Phys. Chem. Chem. Phys.*, 2012, **14**, 5349-5362; (c) X. Pan, M. Q. Yang, X. Fu, N. Zhang and Y. J. Xu, *Nanoscale*, 2013, **5**, 3601-3614; (d) G. Liu, L. Wang, H. G. Yang, H. M. Cheng, G. Q. Lu, *J. Mater. Chem.*, 2010, **20**, 831-843; (e) X. Zhou, G. Liu, J. Yu and W. Fan, *J. Mater. Chem.*, 2012, **22**, 21337-21354;
- (4) (a) G. Kim, C. Jo, W. Kim, J. Chun, S. Yoon, J. Lee and W. Choi, *Energy Environ. Sci.*, 2013, **6**, 2932-2938; (b) M. Auffan, M. Pedoutour, J. Rose, A. Masion, F. Ziarelli, D. Borschneck, C. Chaneac, C. Botta, P. Chaurand, J. Labille and J. Y. Bottero, *Environ. Sci. Technol.*, 2010, **44**, 2689-2694; (c) A. Al-Kattan, A. Wichser, R. Vonbank, S. Brunner, A. Ulrich, S. Zuin and B. Nowack, *Environ. Sci.: Processes Impacts*, 2013, **15**, 2186-2193; (d)

- H. J. Kwon, Y. W. Lee, H. S. Kim, C. K. Zhoh and K. W. Park, *Mater. Lett.*, 2013, **93**, 175-178; (e) M. Radetic, *J. Photochem. Photobiol. C: Photochem. Rev.*, 2013, **16**, 62-76.
- (5) (a) K. Fukushima, I. Yamada, *J. Appl. Phys.*, 1989, **65**, 619-623; (b) A. J. Bard, *Science*, 1980, **207**, 139-144; (c) U. Bach, D. Lupo, P. Comte, J. E. Moser, F. Weissortel, J. Salbeck, H. Spreitzer and M. Gratzel, *Nature*, 1998, **395**, 583-585; (d) J. Fan, S. Liu and J. Yu, *J. Mater. Chem.*, 2012, **22**, 17027-17036.
- (6) A. Hamberg, S. Konstantinidis, P. Viville, F. Renaux, J. P. Dauchot, E. Llobet and R. Snyders, *Sensors Actuat. B: Chem.*, 2012, **171-172**, 18-24.
- (7) (a) S. G. Kumar and L. G. Devi, *J. Phys. Chem. A*, 2011, **115**, 13211-13241; (b) L. G. Devi and S. G. Kumar, *Cent. Eur. J. Chem.*, 2011, **9**, 959-961; (c) G. Liu, J. C. Yu, G. Q. Lu and H. M. Cheng, *Chem. Commun.*, 2011, **47**, 6763-6783; (d) L. G. Devi and R. Kavitha, *Appl. Catal. B: Environ.*, 2013, **140-141**, 559-587.
- (8) (a) Z. Zhang, J. T. Yates, *Chem. Rev.*, 2012, **112**, 5520-5551; (b) M. A. Henderson, *Surf. Sci. Rep.*, 2011, **66**, 185-297; (c) S. Nishimoto and B. Bhushan, *RSC Adv.*, 2013, **3**, 671-690.
- (9) (a) A. S. Weber, A. M. Grady and R. T. Koodali, *Catal. Sci. Technol.*, 2012, **2**, 683-693; (b) A. Kubacka, M. F. Garcia, and G. Colon, *Chem. Rev.*, 2012, **112**, 1555-1614.
- (10) (a) X. Hu, G. Li and J. C. Yu, *Langmuir*, 2010, **26**, 3031-3039; (b) A. A. Ismail and D. W. Bahnemann, *J. Mater. Chem.*, 2011, **21**, 11686-11707; (c) C. Z. Wen, H. B. Jiang, S. Z. Qiao, H. G. Yang and G. Q. Lu, *J. Mater. Chem.*, 2011, **21**, 7052-7061; (d) S. Bingham and W. A. Daoud, *J. Mater. Chem.*, 2011, **21**, 2041-2050.
- (11) (a) D. Beydoun, R. Amal, G. Low and S. McEvoy, *J. Nanoparticles Res.*, 1999, **1**, 439-458; (b) A. L. Stroyuk, A. I. Kryukov, S. Y. Kuchmii, and V. D. Pokhodenko, *Theoretical Exp. Chem.*, 2005, **41**, 67-91.
- (12) Q. Gao, X. Wu, Y. Fan and X. Zhou, *Dyes Pigments*, 2012, **95**, 534-539.

- (13) M. N. Tahir, P. Theato, P. Oberle, G. Melnyk, S. Faiss, U. Kolb, A. Janshoff, M. Stepputat and W. Tremel, *Langmuir*, 2006, **22**, 5209-5212.
- (14) S. Liu, H. Jia, L. Han, J. Wang, P. Gao, D. Xu, J. Yang and S. Che, *Adv. Mater.*, 2012, **24**, 3201-3204.
- (15) Y. Dong, K. Pan, G. Tian, W. Zhou, Q. Pan, T. Xie, D. Wang and H. Fu, *Dalton Trans.*, 2011, **40**, 3808-3814; (b) G. Xiang, T. Li, J. Zhuang and X. Wang, *Chem. Commun.*, 2010, **46**, 6801-6803.
- (16) T. Beuvier, M. R. Plouet and L. Brohan, *J. Phys. Chem. C*, 2009, **113**, 13703-13706.
- (17) (a) G. Zhu, T. Lin, X. Lu, W. Zhao, C. Yang, Z. Wang, H. Yin, Z. Liu, F. Huang and J. Lin, *J. Mater. Chem. A*, 2013, **1**, 9650-9653; (b) K. Li, J. Xu, W. Shi, Y. Wang and T. Peng, *J. Mater. Chem. A*, 2014, **2**, 1886-1896.
- (18) (a) K. Nagaveni, M. S. Hegde and Giridhar Madras, *J. Phys. Chem. B*, 2004, **108**, 20204-20212; (b) K. Nagaveni, G. Sivalingam, M. S. Hegde and Giridhar Madras, *Appl. Catal. B: Environ.*, 2004, **48**, 83-93; (c) G. Sivalingam, K. Nagaveni, M. S. Hegde and Giridhar Madras, *Appl. Catal. B: Environ.*, 2003, **45**, 23-28.
- (19) J. Yu, J. Fan and K. Lv, *Nanoscale*, 2010, **2**, 2144-2149.
- (20) (a) G. Li, C. P. Richter, R. L. Milot, L. Cai, C. A. Schmuttenmaer, R. H. Crabtree, G. W. Brudvig and V. S. Batista, *Dalton Trans.*, 2009, **38**, 10078-10085; (b) W. Zhou, L. Gai, P. Hu, J. Cui, X. Liu, D. Wang, G. Li, H. Jiang, D. Liu and H. Liu, J. Wang, *CrystEngComm.*, 2011, **13**, 6643-6649.
- (21) (a) S. Song, Z. Liu, Z. He, A. Zhang, J. Chen, Y. Yang and X. Xu, *Environ. Sci. Technol.*, 2010, **44**, 3913-3918; (b) Y. Bai, W. Li, C. Liu, Z. Yang, X. Feng, X. Lu and K. Y. Chan, *J. Mater. Chem.*, 2009, **19**, 7055-7061.

- (22) (a) D. Tsukamoto, Y. Shiraishi, Y. Sugano, S. Ichikawa, S. Tanaka and T. Hirai, *T. J. Am. Chem. Soc.*, 2012, **134**, 6309-6315; (b) S. Li, J. Chen, F. Zheng, Y. Li and F. Huang, *Nanoscale*, 2013, **5**, 12150-12155.
- (23) (a) F. Shi, Y. Li, Q. Zhang and H. Wang, *J. Am. Ceram. Soc.*, 2012, **95**, 1927-1932; (b) Q. Xiang, J. Yu, P. K. Wong, *J. Colloid Interface Sci.*, 2011, **357**, 163-167. (c) G. Liu, X. Wang, L. Wang, Z. Chen, F. Li, G. Q. Lu and H. M. Cheng, *J. Colloid Interface Sci.*, 2009, **334**, 171-175; (d) G. Liu, X. Wang, Z. Chen, H. M. Cheng and G. Q. Lu, *J. Colloid Interface Sci.*, 2009, **329**, 331-338.
- (24) (a) J. Yu, M. Zhou, B. Cheng, H. Yu and X. Zhao, *J. Mol. Catal. A: Chem.*, 2005, **227**, 75-80; (b) D. O. Scanlon, C. W. Dunnill, J. Buckeridge, S. A. Shevlin, A. J. Logsdail, S. M. Woodley, C. R. A. Catlow, M. J. Powell, R. G. Palgrave, I. P. Parkin, G. W. Watson, T. W. Keal, P. Sherwood, A. Walsh and A. A. Sokol, *Nat. Mater.*, 2013, **12**, 798-801; (c) J. Yu, J. Xiong, B. Cheng and S. Liu, *Appl. Catal. B: Environ.*, 2005, **60**, 211-221.
- (25) (a) X. M. Song, J. M. Wu, M. Z. Tang, B. Qi and M. Yan, *J. Phys. Chem. C*, 2008, **112**, 19484-19492; (b) G. Li and K. A. Gray, *Chem. Phys.*, 2007, **339**, 173-187; (c) S. G. Kumar and K. S. R. K. Rao, *Energy Environ. Sci.*, 2014, **7**, 45-102.
- (26) (a) J. Zhang, F. Huang and Z. Lin, *Nanoscale*, 2010, **2**, 18-34; (b) D. R. Hummer, J. D. Kubicki, P. R. C. Kent, J. E. Post and P. J. Heaney, *J. Phys. Chem. C*, 2009, **113**, 4240-4245; (c) M. Raju, A. C. T. Van Duin and K. A. Fichthorn, *Nano Lett.*, 2014, **14**, 1836-1842;
- (27) K. R. Zhu, M. S. Zhang, J. M. Hong and Z. Yin, *Mater. Sci. Eng. A*, 2005, **403**, 87-93.
- (28) (a) D. J. Reidy, J. D. Holmes and M. A. Morris, *J. Eur. Ceram. Soc.*, 2006, **26**, 1527-1534; (b) A. Testino, I. R. Bellobono, V. Buscaglia, C. Canevali, M. D'Arienzo, S. Polizzi, R. Scotti and F. Morazzoni, *J. Am. Chem. Soc.*, 2007, **129**, 3564-3575.

- (29) (a) J. Li, Y. Ye, L. Shen, J. Chen and H. Zhou, *Mater. Sci. Eng. A*, 2005, **390**, 265-270; (b) H. I. Hsiang and S. C. Lin, *Mater. Chem. Phys.*, 2006, **95**, 275-279; (c) D. Chandra and A. Bhaumik, *Microporous Mesoporous Mater.*, 2008, **112**, 533-541.
- (30) J. Yang, S. Mei and J. M. F. Ferreira, *J. Am. Ceram. Soc.*, 2000, **83**, 1361-1368.
- (31) H. I. Hsiang and S. C. Lin, *Ceram. Int.*, 2008, **34**, 557-561.
- (32) C. Ribeiro, C. M. Barrado, E. R. D. Camargo, E. Longo and E. R. Leite, *Chem. Eur. J.*, 2009, **15**, 2217-2222.
- (33) Y. Zhang, L. Wu, Q. Zeng and J. Zhi, *J. Phys. Chem. C*, 2008, **112**, 16457-16462.
- (34) (a) S. M. Gupta and M. Tripathi, *Cent. Eur. J. Chem.*, 2012, **10**, 279-294; (b) T. H. Wang, A. M. N. Lopez, S. Li, D. A. Dixon and J. L. Gole, *J. Phys. Chem. A*, 2010, **114**, 7561-7570; (c) M. Kakihana, M. Kobayashi, K. Tomita and V. Petrykin, *Bull. Chem. Soc. Jpn.*, 2010, **83**, 1285-1308; (d) D. Chen and R. A. Caruso, *Adv. Funct. Mater.*, 2013, **23**, 1356-1374; (e) M. Gateshki, S. Yin, Y. Ren and V. Petkov, *Chem. Mater.*, 2007, **19**, 2512-2518.
- (35) (a) X. B. Chen, *Chin. J. Catal.*, 2009, **30**, 839-851; (b) N. Liu, X. Chen, J. Zhang and J. W. Schwank, *Catal. Today*, 2014, **225**, 34-51; (c) P. Roy, S. Berger and P. Schmuki, *Angew. Chem. Int. Ed.*, 2011, **50**, 2904-2939; (d) D. P. Macwan, P. N. Dave and S. Chaturvedi, *J. Mater. Sci.*, 2011, **46**, 3669-3686.
- (36) U. Schubert, *J. Mater. Chem.*, 2005, **15**, 3701-3715.
- (37) T. Froschl, U. Hormann, P. Kubiak, G. Kucerova, M. Pfanzelt, C. K. Weiss, R. J. Behm, N. Husing, U. Kaiser, K. Landfester and M. W. Mehrens, *Chem. Soc. Rev.*, 2012, **41**, 5313-5360.
- (38) D. T. Cromer and K. Herrington, *J. Am. Chem. Soc.*, 1955, **77**, 4708-4709.
- (39) G. A. Tompsett, G. A. Bowmaker, R. P. Conney, J. B. Metson, K. A. Rodgers and J. M. Seakins, *J. Raman Spectrosc.*, 1995, **26**, 57-62.

- (40) R. Marchand, L. Brohan and M. Tournoux, *Mater. Res. Bull.*, 1980, **15**, 1129-1133.
- (41) M. Lacroche, L. Brohan, R. Marchand and M. Tournoux, *J. Solid State Chem.*, 1989, **81**, 78-82.
- (42) J. Akimoto, Y. Gotoh, Y. Oosawa, N. Nonose, T. Kumagai, K. Aoki and H. Takei, *J. Solid State Chem.*, 1994, **113**, 27-36.
- (43) T. P. Feist and P. K. Davies, *J. Solid State Chem.*, 1992, **101**, 275-295.
- (44) P. Y. Simons and F. Dachille, *Acta Crystallogr.*, 1967, **23**, 334-336.
- (45) Y. Takahashi, N. Kijima and J. Akimoto, *Chem. Mater.*, 2006, **18**, 748-752.
- (46) S. Bakardjieva, V. Stengl, Szatmary, J. Subrt, J. Lukac, N. Murafa, D. Nizansky, K. Cizek, J. Jirkovsky and N. Petrova, *J. Mater. Chem.*, 2006, **16**, 1709-1716.
- (47) R. L. Penn and J. F. Banfield, *Am. Mineral.*, 1999, **84**, 871-876.
- (48) R. L. Penn and J. F. Banfield, *Am. Mineral.*, 1998, **83**, 1077-1082.
- (49) Y. Liao, W. Que, Q. Jia, Y. He, J. Zhang and P. Zhong, *J. Mater. Chem.*, 2012, **22**, 7937-7944.
- (50) M. Gopal, W. J. M. Chan and L. C. D. Jonghe, *J. Mater. Sci.*, 1997, **32**, 6001-6008.
- (51) U. Diebold, *Surf. Sci. Rep.*, 2003, **48**, 53-229.
- (52) X. Chen and S. S. Mao, *Chem. Rev.*, 2007, **107**, 2891-2959.
- (53) H. Kaper, F. Endres, I. Djerdj, M. Antonietti, B. M. Smarsly, J. Maier and Y. S. Hu, *Small*, 2007, **3**, 1753-1763.
- (54) H. Cheng, J. Ma, Z. Zhao and L. Qi, *Chem. Mater.*, 1995, **7**, 663-671.
- (55) M. Lazzeri, A. Vittadini and A. Selloni, *Phys. Rev. B*, 2001, **63**, 155409.
- (56) A. Vittadini, A. Selloni, F. P. Rotzinger and M. Grätzel, *Phys. Rev. Lett.*, 1998, **81**, 2954-2957.
- (57) A. G. Dylla, G. Henkelman and K. J. Stevenson, *Acc. Chem. Res.*, 2013, **46**, 1104-1112.
- (58) S. D. Mo and W. Y. Ching, *Phys. Rev. B*, 1995, **51**, 13023-13032.

- (59) J. K. Burdett, T. Hughbanks, G. J. Miller, J. W. Richardson and J. V. Smith, *J. Am. Chem. Soc.*, 1987, **109**, 3639-3646.
- (60) X. Bokhimi, A. Morales, M. Aguilar, J. A. T. Antonio and F. Pedraza, *Int. J. Hydrogen Energy*, 2001, **26**, 1279-1287.
- (61) Y. Li, T. J. White and S. H. Lim, *J. Solid State Chem.*, 2004, **177**, 1372-1381.
- (62) J. Huberty, and H. Xu, *J. Solid State Chem.*, 2008, **181**, 508-514.
- (63) S. J. Kim, K. Lee, J. H. Kim, N. H. Lee and S. J. Kim, *Mater. Lett.*, 2006, **60**, 364-367.
- (64) R. Zallen and M. P. Moret, *Solid State Commun.*, 2006, **137**, 154-157.
- (65) M. Koelsch, S. Cassaignon, J. F. Guillemoles and J. P. Jolivet, *Thin Solid Films*, 2002, **403-404**, 312-319.
- (66) B. I. Lee, X. Wang, R. Bhave and M. Hu, *Mater. Lett.*, 2006, **60**, 1179-1183.
- (67) J. G. Li, T. Ishigaki and X. Sun, *J. Phys. Chem. C*, 2007, **111**, 4969-4976.
- (68) D. Yang, H. Liu, Z. Zheng, Y. Yuan, J. Zhao, E. R. Waclawik, X. Ke and H. Zhu, *J. Am. Chem. Soc.*, 2009, **131**, 17885-17893.
- (69) A. Vittadini, M. Casarin and A. Selloni, *J. Phys. Chem. C*, 2009, **113**, 18973-18977.
- (70) W. Li, Y. Bai, W. Zhuang, K. Y. Chan, C. Liu, Z. Yang, X. Feng and X. Lu, *J. Phys. Chem. C*, 2014, **118**, 3049-3055.
- (71) A. R. Armstrong, G. Armstrong, J. Calales and P. G. Bruce, *Angew. Chem. Int. Ed.*, 2004, **43**, 2286-2288.
- (72) A. K. Chakraborty, Z. Qi, S. Y. Chai, C. Lee, S. Y. Park, D. J. Jang and W. I. Lee, *Appl. Catal. B: Environ.*, 2010, **93**, 368-375.
- (73) J. F. Banfield and D. R. Veblen, *Am. Mineral.*, 1992, **77**, 545-557.
- (74) H. Sato, S. Endo, M. Sugiyama, T. Kikegawa, O. Shimomura and K. Kusaba, *Science*, 1991, **251**, 786-788.

- (75) M. Mattesini, J. S. D. Almedia, L. Dubrovinsky, N. Dubrovinskaia, B. Johansson, and R. Ahuja, *Phys. Rev. B*, 2004, **70**, 212101.
- (76) P. Xiaoyan, C. Yi, M. Xueming and Z. Lihui, *J. Am. Ceram. Soc.*, 2004, **87**, 1164-1166.
- (77) J. K. Dewhurst and J. E. Lowther, *Phys. Rev. B*, 1996, **54**, R3673-R3675.
- (78) J. F. Mammone and M. Nicol, *J. Phys. Chem. Solids*, 1981, **42**, 379-384.
- (79) Z. Yanqing, S. Erwei, C. Zhizhan, L. Wenjun and H. Xingfang, *J. Mater. Chem.*, 2001, **11**, 1547-1551.
- (80) X. Ye, J. Sha, Z. Jiao and L. Zhang, *Nanostruct. Mater.*, 1997, **8**, 919-927.
- (81) X. Kang and S. Chen, *J. Mater. Sci.*, 2010, **45**, 2696-2702.
- (82) J. G. Li, C. Tang, D. Li, H. Haneda and T. Ishigaki, *J. Am. Ceram. Soc.*, 2004, **87**, 1358-1361.
- (83) M. H. Yang, P. C. Chen, M. C. Tsai, T. T. Chen, I. C. Chang, H. T. Chiu and C. Y. Lee, *CrystEngComm.*, 2014, **16**, 441-447.
- (84) J. G. Li and T. Ishigaki, *Acta Mater.*, 2004, **52**, 5143-5150.
- (85) X. L. Nie, S. P. Zhuo, G. Maeng and K. Sohlberg, *Int. J. Photoenergy*, 2009, 294042.
- (86) A. Pottier, C. Chaneac, E. Tronc, L. Mazerolles and J. P. Jolivet, *J. Mater. Chem.*, 2001, **11**, 1116-1121.
- (87) Y. Zheng, *J. Am. Ceram. Soc.*, 2000, **83**, 2634-2636.
- (88) (a) H. Kominami, M. Kohno and Y. Kera, *J. Mater. Chem.*, 2000, **10**, 1151-1156; (b) B. Ohtani, J. Handa, S. Nishimoto and T. Kagiya, *Chem. Phys. Lett.*, 1985, **120**, 292-294.
- (89) S. Yin, H. Yamaki, M. Komatsu, Q. Zhang, J. Wang, Q. Tang, F. Saito and T. Sato, *J. Mater. Chem.*, 2003, **13**, 2996-3001.
- (90) B. L. Bischoff and M. A. Anderson, *Chem. Mater.*, 1995, **7**, 1772-1778.
- (91) A. S. Hall, A. Kondo, K. Maeda and T. E. Mallouk, *J. Am. Chem. Soc.*, 2013, **135**, 16276-16279.

- (92) S. Music, M. Gotic, M. Ivanda, S. Popovic, A. Turkovic, R. Trojko, A. Sekulic and K. Furic, *Mater. Sci. Eng. B*, 1997, **47**, 33-40.
- (93) X. Bokhimi, A. Morales, O. Novaro, T. Lopez, E. Sanchez and R. Gomez, *R. J. Mater. Res.*, 1995, **10**, 2788-2796.
- (94) J. P. Jalava, L. Heikkila, O. Hovi, R. Laiho, E. Hiltunen, A. Hakanen and H. Harma, *Ind. Eng. Chem. Res.*, 1998, **37**, 1317-1323.
- (95) J. L. Mi, C. Clausen, M. Bremholm, N. Lock, K. M. O. Jensen, M. Christensen and B. B. Iversen, *Cryst. Growth Des.*, 2012, **12**, 6092-6097.
- (96) Y. Hu, H. T. Tsai, C. L. Huang, *Mater. Sci. Eng. A*, 2003, **344**, 209-214.
- (97) K. T. Ranjit, I. Willner, S. H. Bossmann and A. M. Braun, *Environ. Sci. Technol.*, 2001, **35**, 1544-1549.
- (98) K. T. Ranjit, I. Willner, S. H. Bossmann and A. M. Braun, *J. Catal.*, 2001, **204**, 305-313.
- (99) R. D. Shannon and J. A. Pask, *J. Am. Ceram. Soc.*, 1965, **48**, 391-398.
- (100) K. N. P. Kumar, K. Keizer, A. J. Burggraaf, T. Okubo and H. Nagamoto, *J. Mater. Chem.*, 1993, **3**, 1151-1159.
- (101) K. J. D. MacKenzie, *Trans. J. Brit. Ceram. Soc.*, 1975, **74**, 77-84.
- (102) H. Zhang, and J. F. Banfield, *Am. Mineral.* 1999, **84**, 528-535.
- (103) H. Mehranpour, M. Askari, M. S. Ghamsari and H. Farzalibeik, *J. Nanomater.*, 2010, 626978.
- (104) K. N. P. Kumar, K. Keizer and A. J. Burggraaf, *J. Mater. Chem.*, 1993, **3**, 1141-1149.
- (105) A. A. Gribb and J. F. Banfield, *Am. Mineral.*, 1997, **82**, 717-728.
- (106) T. Mitsuhashi and O. J. Kleppa, *J. Am. Ceram. Soc.*, 1979, **62**, 356-357.
- (107) D. A. Hanaor and C. C. Sorrell, *J. Mater. Sci.*, 2011, **46**, 855-874.
- (108) H. Zhang and J. F. Banfield, *J. Phys. Chem. B*, 2000, **104**, 3481-3487.

- (109) M. Rezaee, S. Mohammad, M. Khoie and K. H. Liu, *CrystEngComm.*, 2011, **13**, 5055-5061.
- (110) Y. Zhou and K. A. Fichthorn, *J. Phys. Chem. C*, 2012, **116**, 8314-8321.
- (111) H. Zhang and J. F. Banfield, *J. Mater. Chem.*, 1998, **8**, 2073-2076.
- (112) A. S. Barnard and L. A. Curtiss, *Nano Lett.*, 2005, **5**, 1261-1266.
- (113) A. S. Barnard, P. Zapol and L. A. Curtiss, *Surf. Sci.*, 2005, **582**, 173-178.
- (114) H. Zhang and J. F. Banfield, *J. Mater. Res.*, 2000, **15**, 437-448.
- (115) B. Gilbert, H. Zhang, F. Huang, M. P. Finnegan, G. A. Waychunas and J. F. Banfield, *Geochem. Trans.*, 2003, **4**, 20-27.
- (116) M. P. Finnegan, H. Zhang and J. F. Banfield, *J. Phys. Chem. C*, 2007, **111**, 1962-1968.
- (117) M. P. Finnegan, H. Zhang and J. F. Banfield, *Chem. Mater.*, 2008, **20**, 3443-3449.
- (118) R. L. Penn and J. F. Banfield, *Science*, 1998, **281**, 969-971.
- (119) R. L. Penn and J. F. Banfield, *Geochim. Cosmochim. Acta*, 1999, **63**, 1549-1557.
- (120) C. C. Wang and J. Y. Ying, *Chem. Mater.* **1999**, *11*, 3113-3120.
- (121) A. Navrotsky, *Geochem. Trans.*, 2003, **4**, 34-37.
- (122) A. S. Barnard, P. Zapol and L. A. Curtiss, *J. Chem. Theory Comput.*, 2005, **1**, 107-116.
- (123) (a) V. N. Koparde and P. T. Cummings, *ACS Nano*, 2008, **2**, 1620-1624; (b) V. N. Koparde and P. T. Cummings, *J. Phys. Chem. C*, 2007, **111**, 6920-6926.
- (124) B. Chen, H. Zhang, B. Gilbert and J. F. Banfield, *Phys. Rev. Lett.*, 2007, **98**, 4-8.
- (125) M. R. Mohammadi, D. J. Fray and A. Mohammadi, *Microporous Mesoporous Mater.*, 2008, **112**, 392-402.
- (126) H. Zhang M. P. Finnegan and J. F. Banfield, *Nanoscale*, 2013, **5**, 6742-6746.
- (127) X. Z. Ding and X. H. Liu, *J. Mater. Res.*, 1998, **13**, 2556-2559.
- (128) J. Wang, X. Han, C. Liu, W. Zhang, R. Cai and Z. Liu, *Cryst. Growth Des.*, 2010, **10**, 2185-2191.

- (129) P. I. Gouma and M. J. Mills, *J. Am. Ceram. Soc.*, 2001, **84**, 619-622.
- (130) (a) R. D. Shannon and J. A. Pask, *Am. Mineral.*, 1964, **49**, 1707-1717; (b) R. D. Shannon, *Chem. Abstr.*, 1964, **63**, 2468.
- (131) (a) Y. Iida and S. Ozaki, *J. Am. Ceram. Soc.*, 1961, **44**, 120-127; (b) J. G. Serrano, E. G. Hernandez, M. O. Fernandez and U. Pal, *Curr. Appl. Phys.*, 2009, **9**, 1097-1105; (c) P. W. Chou, Y. S. Wang, C. C. Lin, Y. J. Chen, C. L. Cheng and M. S. Wong, *Surf. Coat. Technol.*, 2009, **204**, 834-839.
- (132) J. Livage, M. Henry and C. Sanchez, *Prog. Solid State Chem.*, 1988, **18**, 259-341.
- (133) J. P. Jolivet, *Metal oxide chemistry and synthesis; From solution to solid state*; Wiley: New York, 2000.
- (134) S. T. Aruna, S. Tirosh and A. Zaban, *J. Mater. Chem.*, 2000, **10**, 2388-2391.
- (135) D. Zhang, L. Qi, J. Ma and H. Cheng, *J. Mater. Chem.*, 2002, **12**, 3677-3680.
- (136) J. Sun and L. Gao, *J. Am. Ceram. Soc.*, 2002, **85**, 2382-2384.
- (137) S. Yin, H. Hasegawa, D. Maeda, M. Ishitsuka and T. Sato, *J. Photochem. Photobiol. A: Chem.*, 2004, **163**, 1-8.
- (138) M. Henry, J. P. Jolivet and J. Livage, *J. Struct. Bond.*, 1992, **77**, 155-206.
- (139) B. Tian, F. Chen, J. Zhang and M. Anpo, *J. Colloid Interface Sci.*, 2006, **303**, 142-148.
- (140) M. Henry, J. P. Jolivet and J. Livage, In *Aqueous Chemistry of Metal Cations, Hydrolysis, Condensation, and Complexation*; Reisfeld, R.; Jorgensen, C. K.; Eds.; Springer-Verlag: Berlin, 1992.
- (141) H. Yin, Y. Wada, T. Kitamura, S. Kambe, S. Murasawa, H. Mori, T. Sakata, and S. Yanagida, *J. Mater. Chem.*, 2001, **11**, 1694-1703.
- (142) C. J. Barbe, F. Arendse, P. Comte, M. Jirousek, F. Lenzmann, V. Shklover and M. Gratzel, *J. Am. Ceram. Soc.*, 1997, **80**, 3157-3171.
- (143) H. Zhang and J. F. Banfield, *Chem. Mater.*, 2005, **17**, 3421-3425.

- (144) G. Oskam, Z. Hu, R. L. Penn, N. Pesika and P. C. Searson, *Phys. Rev. E*, 2002, **66**, 011403.
- (145) E. A. Barringer and H. K. Bowen, *Langmuir*, 1985, **1**, 414-420.
- (146) E. A. Barringer and H. K. Bowen, *Langmuir*, 1985, **1**, 420-428.
- (147) J. H. Jean and T. A. Ring, *Langmuir*, 1986, **2**, 251-255.
- (148) J. L. Look and C. F. Zukoski, *J. Am. Ceram. Soc.*, 1992, **75**, 1587-1595.
- (149) J. L. Look and C. F. Zukoski, *J. Am. Ceram. Soc.*, 1995, **78**, 21-32.
- (150) D. Vorkapic and T. Matsoukas, *J. Am. Ceram. Soc.*, 1998, **81**, 2815-2820.
- (151) D. Vorkapic and T. Matsoukas, *J. Colloid Interface Sci.*, 1999, **214**, 283-291.
- (152) J. Park, V. Privman and E. J. Matijevic, *J. Phys. Chem. B*, 2001, **105**, 11630-11635.
- (153) K. N. P. Kumar, K. Keizer, A. J. Burggraaf, T. Okubo, H. Nagamoto and S. Morooka, *Nature* (London), 1992, **358**, 48-51.
- (154) K. N. P. Kumar, J. Kumar and K. Keizer, *J. Am. Ceram. Soc.*, 1994, **77**, 1396-1400.
- (155) J. Nair, P. Nair, J. G. V. Ommen, J. R. H. Ross, A. J. Burggraaf and F. Mizukami, *J. Am. Ceram. Soc.*, 1998, **81**, 2709-2712.
- (156) J. Yang, S. Mei and J. M. F. Ferreira, *J. Am. Ceram. Soc.*, 2001, **84**, 1696-1702.
- (157) R. R. Bacsa and M. Gratzel, *J. Am. Ceram. Soc.*, 1996, **79**, 2185-2188.
- (158) (a) M. T. Colomer, J. Guzman and R. Moreno, *J. Am. Ceram. Soc.*, 2010, **93**, 59-64; (b) H. S. Chen, C. Su, J. L. Chen, T. Y. Yang, N. M. Hsu and W. R. Li, *J. Nanomater.*, 2011, 869618.
- (159) A. Chemseddine and T. Moritz, *Eur. J. Inorg. Chem.* 1999, 235-245.
- (160) M. S. Whittingham, J. Li, J. D. Guo and P. Zavalij, *Mater. Sci. Forum*, 1994, **152-153**, 99-108.
- (161) I. M. Lifshitz and V. V. Slyozov, *J. Phys. Chem. Solids*, 1961, **19**, 35-50.
- (162) M. Kahlweit, *Adv. Colloid Interface Sci.*, 1975, **5**, 1-35.

- (163) (a) N. V. Mantzaris, *Chem. Eng. Sci.*, 2005, **60**, 4749-4770; (b) F. Wang, V. N. Richards, S. P. Shields and W. E. Buhro, *Chem. Mater.*, 2014, **26**, 5-21.
- (164) (a) X. Xue, R. L. Penn, E. R. Leite, F. Huang and Z. Lin, *CrystEngComm.*, 2014, **16**, 1419-1429; (b) J. Polleux, N. Pinna, M. Antonietti and M. Niederberger, *Adv. Mater.*, 2004, **16**, 436-439.
- (165) E. J. H. Lee, C. Ribeiro, E. Longo and E. R. Leite, *J. Phys. Chem. B*, 2005, **109**, 20842-20846.
- (166) J. Zhang, F. Huang and Z. Lin, *Nanoscale*, 2010, **2**, 18-34.
- (167) V. M. Yuwono, N. D. Burrows, J. A. Soltis and R. L. Penn, *J. Am. Chem. Soc.*, 2010, **132**, 2163-2165.
- (168) M. Niederberger and H. Colfen, *Phys. Chem. Chem. Phys.*, 2006, **8**, 3271-3287.
- (169) S. Hirano, K. Masuya and M. Kuwabara, *J. Phys. Chem. B*, 2004, **108**, 4576-4578.
- (170) B. Ma, G. K. L. Goh, J. Ma and T. J. White, *J. Electrochem. Soc.*, 2007, **154**, D557-D561.
- (171) G. Oskam, A. Nellore, N. R. Penn and P. C. Searson, *J. Phys. Chem. B*, 2003, **107**, 1734-1738.
- (172) R. L. Penn, G. Oskam, T. J. Strathmann, P. C. Searson, A. T. Stone and D. R. Veblen, *J. Phys. Chem. B*, 2001, **105**, 2177-2182.
- (173) A. P. Alivisatos, *Science*, 2000, **289**, 736-737.
- (174) W. Huang, X. Tang, Y. Wang, Y. Kolytyn and A. Gedanken, *Chem. Commun.*, 2000, 1415-1416.
- (175) D. Nichollos, *Complexes and First-row transition elements*, The Macmillan Press Ltd, New York, 1974 (chapter 11).
- (176) V. D. Hildenbrand, H. Fuess, G. Pfaff and P. Reynders, *Z. Phys. Chem. (Munich)* 1996, **194**, 139-150.

- (177) P. Comba and A. Merbach, *Inorg. Chem.*, 1987, **26**, 1315-1323.
- (178) J. D. Ellis, G. A. K. Tompson and A. G. Sykes, *Inorg. Chem.*, 1976, **15**, 3172-3174.
- (179) M. Henry, J. P. Jolivet and J. Livage, *Structure and bonding*, Vol. 77, eds. R. Reisfeld and C. K. Jorgensen, Springer-Verlag, Berlin, 1992, p. 155.
- (180) Q. Zhang and L. Gao *Langmuir*, 2003, **19**, 967-971.
- (181) P. M. Oliver, G. W. Watson, E. T. Kelsey and S. C. Parker, *J. Mater. Chem.*, 1997, **7**, 563-568.
- (182) C. Wang, Z. X. Deng and Y. Li, *Inorg. Chem.*, 2001, **40**, 5210-5214.
- (183) S. Yoon, E. S. Lee and A. Manthiram, *Inorg. Chem.*, 2012, **51**, 3505-3512.
- (184) J. P. Jolivet, S. Cassaignon, C. Chaneac, D. Chiche and E. Tronc, *J. Sol-Gel Sci. Technol.*, 2008, **46**, 299-305.
- (185) L. Shi and D. Weng, *D. J. Environ. Sci.*, 2008, **20**, 1263-1267.
- (186) S. Y. Kim, T. Lim, T. Chang and C. Shin, *Catal. Lett.*, 2007, **117**, 112-118.
- (187) K. Yanagisawa and J. Ovenstone, *J. Phys. Chem. B*, 1999, **103**, 7781-7787.
- (188) Y. Wu, H. Liu and B. Xu, *Appl. Organometal. Chem.*, 2007, **21**, 146-149.
- (189) M. Paulis, M. Martin, D. B. Soria, A. Diaz, J. A. Odriozola and M. Montes, *Appl. Catal. A: Gen.*, 1999, **180**, 411-420.
- (190) C. J. Brinker, G. W. Scherer, in *Sol-Gel Science: The physics and chemistry of Sol-Gel Processing: Academic Press*, New York, 1990, p.240.
- (191) T. Jesty and M. L. P. Reddy, *Int. J. Nanotechnol.* 2011, **8**, 841-854.
- (192) X. Shen, J. Zhang, B. Tian and M. Anpo, *J. Mater. Sci.*, 2012, **47**, 5743-5751.
- (193) Y. Li, N. H. Lee, D. S. Hwang, J. S. Song, E. G. Lee and S. J. Kim, *Langmuir*, 2004, **20**, 10838-10844.
- (194) H. T. Ren, S. Y. Jia, S. H. Wu, Y. Liu and X. Han, *Mater. Lett.*, 2013, **101**, 69-71.
- (195) J. Ovenstone, and K. Yanagisawa, *Chem. Mater.*, 1999, **11**, 2770-2774.

- (196) L. G. Devi, N. Kottam and B. N. Murthy, *J. Mol. Catal. A: Chem.*, 2010, **328**, 44-52.
- (197) L. G. Devi, S. G. Kumar, B. N. Murthy and N. Kottam, *Catal. Commun.*, 2009, **10**, 794-798.
- (198) L. G. Devi, N. Kottam and S. G. Kumar, *Chin. J. Chem.*, 2010, **28**, 2151-2161.
- (199) L. G. Devi, N. Kottam, S. G. Kumar and K. S. A. Raju, *Catal. Lett.*, 2009, **131**, 612-617.
- (200) L. G. Devi, N. Kottam and S. G. Kumar, *J. Phys. Chem. C*, 2009, **113**, 15593-15601.
- (201) L. G. Devi and S. G. Kumar, *Appl. Surf. Sci.*, 2011, **257**, 2779-2790.
- (202) H. Xu and L. Zhang *J. Phys. Chem. C*, 2009, **113**, 1785-1790.
- (203) J. Wei, J. Yao, X. Zhang, W. Zhu, H. Wang and M. J. Rhodes, *Mater. Lett.*, 2007, **61**, 4610-4613.
- (204) H. Wang, B.A. Holmberg and Y. Yan, *J. Am. Chem. Soc.*, 2003, **125**, 9928-9929.
- (205) Y. Xu and L. Li, *Polymer*, 2005, **46**, 7410-7417.
- (206) X. Bokhimi and F. Pedraza, *J. Phys. Chem. Solids*, 2004, **177**, 2456-2463.
- (207) (a) Y. Li, X. Sun, H. Li, S. Wang and Y. Wei, *Powder Technol.*, 2009, **194**, 149-152;
(b) D. S. Kim and S. Y. Kwak, *Appl. Catal. A: Gen.*, 2007, **323**, 110-118.
- (208) M. Wu, G. Lin, D. Chen, G. Wang, D. He, S. Feng and R. Xu, *Chem. Mater.*, 2002, **14**, 1974-1980.
- (209) S. S. Mali, C. A. Betty, P. N. Bhosale and P. S. Patil, *CrystEngComm.*, 2011, **13**, 6349-6351.
- (210) H. Kominami, S. Murakami, M. Kohno, Y. Kera, K. Okada and B. Ohtani, *Phys. Chem. Chem. Phys.*, 2001, **3**, 4102-4106.
- (211) M. Rehan, X. Lai and G. M. Kale, *CrystEngComm.*, 2011, **13**, 3725-3732.
- (212) G. Li and K. A. Gray *Chem. Mater.*, 2007, **19**, 1143-1146.

- (213) D. R. Coronado, G. R. Gattorno, M. E. E. Pesqueira, C. Cab, R. D. Coss and G. Oskam, *Nanotechnology*, 2008, **19**, 145605.
- (214) K. Sabyrov, N. D. Burrows and R. L Penn, *Chem. Mater.*, 2013, **25**, 1408-1415.
- (215) T. Sugimoto, X. Zhou and A. Muramatsu, *J. Colloid Interface Sci.*, 2002, **252**, 339-346.
- (216) A. Liberti, V. Chiantella and F. Corigliano, *J. Inorg. Nucl. Chem.*, 1963, **25**, 415-427.
- (217) S. L. Isley and R. L. Penn, *J. Phys. Chem. B*, 2006, **110**, 15134-15139.
- (218) (a) M. Koelsch, S. Cassaignon and J. P. Jolivet, *Mater. Res. Soc. Symp. Proc.*, 2004, **822**, S5.3; (b) J. H. Lee and Y. S. Yang, *J. Mater. Sci.*, 2005, **40**, 2843-2847.
- (219) G. H. Lee and J. M. Zuo, *J. Am. Ceram. Soc.*, 2004, **87**, 473-479.
- (220) S. L. Isley and R. L. Penn, *J. Phys. Chem. C*, 2008, **112**, 4469-4474.
- (221) S. L. Isley, D. S. Jordan and R. L. Penn, *Mater. Res. Bull.*, 2009, **44**, 119-125.
- (222) G. Tian, H. Fu, L. Jing, B. Xin and K. Pan, *J. Phys. Chem. C*, 2008, **112**, 3083-3089.
- (223) E. Beyers, P. Cool and E. F. Vansant, *J. Phys. Chem. B*, 2005, **109**, 10081-10086.
- (224) G. J. S. Illia, A. Louis and C. Sanchez, *Chem. Mater.*, 2002, **14**, 750-759.
- (225) T. Y. Peng, D. Zhao, K. Dai, W. Shi and K. Hirao, *J. Phys. Chem. B*, 2005, **109**, 4947-4952.
- (226) K. Cassiers, T. Linssen, M. Mathieu, Y. Q. Bai, H. Y. Zhu, P. Cool and E. F. Vansant, *J. Phys. Chem. B*, 2004, **108**, 3713-3721.
- (227) (a) C. Sanchez and F. Ribot, *New J. Chem.*, 1994, **18**, 1007-1047; (b) M. Kakihana, *J. Sol-Gel Sci. Technol.*, 1996, **6**, 7-55; (c) L. L. Hench and J. K. West, *Chem. Rev.*, 1990, **90**, 33-72; (d) R. Sui and P. Charpentier, *Chem. Rev.*, 2012, **112**, 3057-3082.
- (228) C. Su, B. Y. Hong and C. M. Tseng, *Catal. Today*, 2004, **96**, 119-126.
- (229) (a) M. T. Harris and C. H. Byers, *J. Non-Cryst. Solids*, 1988, **103**, 49-64; (b) U. G. Akpan and B. H. Hameed, *Appl. Catal. A: Gen.*, 2010, **375**, 1-11.

- (230) T. Ogihara, M. Iizuka, T. Yanagawa, N. Ogata and K. Yoshida, *J. Mater. Sci.*, 1992, **27**, 55-62.
- (231) B. E. Yoldas, *J. Mater. Sci.*, 1986, **21**, 1087-1092.
- (232) (a) C. Sanchez, J. Livage, M. Henry and F. Babonneau, *J. Non-Cryst. Solids*, 1988, **100**, 65-76; (b) M. Guglielmi and G. Carturan, *J. Non-Cryst. Solids*, 1988, **100**, 16-30; (c) R. C. Mehrotra, *J. Non-Cryst. Solids*, 1988, **100**, 1-15.
- (233) B. E. Yoldas, *J. Non-Cryst. Solids*, 1984, **63**, 145-154.
- (234) C. Sanchez and J. Livage, *New J. Chem.*, 1990, **14**, 513-521.
- (235) (a) T. Sugimoto, X. Zhou and A. Muramatsu, *J. Colloid Interface Sci.*, 2003, **259**, 53-61; (b) T. Sugimoto and X. Zhou, *J. Colloid Interface Sci.*, 2002, **252**, 347-353; (c) T. Sugimoto, X. Zhou and A. Muramatsu, *J. Colloid Interface Sci.*, 2003, **259**, 43-52; (d) T. Sugimoto, X. Zhou and A. Muramatsu, *J. Colloid Interface Sci.*, 2002, **252**, 339-346.
- (236) H. J. Youn, P. S. Ha, H. S. Jung, K. S. Hong, Y. H. Park and K. H. Ko, *J. Colloid Interface Sci.*, 1999, **211**, 321-325.
- (237) P. S. Ha, H. J. Youn, H. S. Jung, K. S. Hong, Y. H. Park and K. H. Ko, *J. Colloid Interface Sci.*, 2000, **223**, 16-20.
- (238) M. H. Lee and B. C. Choi, *J. Am. Ceram. Soc.*, 1991, **74**, 2309-2311.
- (239) M. Ocana, J. V. G. Ramos and C. J. Serna, *J. Am. Ceram. Soc.*, 1992, **75**, 2010-2012.
- (240) K. J. D. MacKenzie, *Trans. J. Br. Ceram. Soc.*, 1975, **74**, 121-125.
- (241) R. D. Shannon, *J. Appl. Phys.*, 1964, **35**, 3414-3416.
- (242) (a) Y. Hu, H. L. Tsai and C. L. Huang, *J. Eur. Ceram. Soc.*, 2003, **23**, 691-696; (b) T. A. Kandiel, L. Robben, A. Alkaim and W. Bahnemann, *Photochem. Photobiol. Sci.*, 2013, **12**, 602-609.
- (243) M. Addamo, M. Bellardita, A. D. Paola and L. Palmisano, *Chem. Commun.*, 2006, 4943-4945.

- (244) C. Rath, P. Mohanty, A. C. Pandey, N. C. Mishra, *J. Phys. D: Appl. Phys.*, 2009, **42**, 205101.
- (245) V. Loryuenyong, K. Angamnuaysiri, J. Sukcharoenpong and A. Suwannasri, *Ceram. Int.*, 2012, **38**, 2233-2237.
- (246) M. E. Simonsen and E. G. Sogaard, *J. Sol-Gel Sci. Technol.*, 2010, **53**, 485-497.
- (247) M. Kallala, C. Sanchez and B. Cabane, *J. Non-Cryst. Solids*, 1992, **147-148**, 189-193.
- (248) K. C. Song and S. E. Pratsinis, *J. Am. Ceram. Soc.*, 2001, **84**, 92-98.
- (249) X. Z. Ding, X. H. Liu and Y. Z. He, *J. Mater. Sci. Lett.*, 1996, **15**, 1789-1791.
- (250) K. Terabe, K. Kato, H. Miyazaki, S. Yamaguchi, A. Imai and Y. Iguchi, *J. Mater. Sci.*, 1994, **29**, 1617-1622.
- (251) W. W. So, S. B. Park, and S. J. Moon, *J. Mater. Sci. Lett.*, 1998, **17**, 1219-1222.
- (252) Y. Chen, A. Lin and F. Gan, *Powder Technol.*, 2006, **167**, 109-116.
- (253) T. Lopez, R. Gomez, E. Sanchez, F. Tzompantzi and L. Vera, *J. Sol-Gel Sci. Technol.*, 2001, **22**, 99-107.
- (254) S. Yan, Q. Sheng, J. Zhang, F. Chen and M. Anpo, *Mater. Lett.*, 2004, **58**, 2757-2760.
- (255) E. L. Crepaldi, G. J. A. A. S. Illia, D. Grosso, F. Cagnol, F. Ribot and C. Sanchez, *J. Am. Chem. Soc.*, 2003, **125**, 9770-9786.
- (256) R. Bleta, P. Alphonse and L. Lorenzato, *J. Phys. Chem. C*, 2010, **114**, 2039-2048.
- (257) N. Wetchakun and S. Phanichphant, *Curr. Appl. Phys.*, 2008, **8**, 343-346.
- (258) S. C. Lee, H. U. Lee, S. M. Lee, G. Lee, W. G. Hong, J. Lee and H. J. Kim, *Mater. Lett.*, 2012, **79**, 191-194.
- (259) R. Scotti, I. R. Bellobono, C. Canevali, C. Cannas, M. Catti, M. D. Arienzo, A. Musinu, S. Polizzi, M. Sommariva, A. Testino and F. Morazzoni, *Chem. Mater.*, 2008, **20**, 4051-4061.
- (260) Y. Ou, J. Lin, S. Fang and D. Liao, *Catal. Commun.*, 2007, **8**, 936-940.

- (261) J. C. Hu, Y. Cao, P. Yang, J. Deng and K. Fan, *J. Mol. Catal. A: Chem.*, 2002, **185**, 1-9.
- (262) T. Sreethawong, Y. Suzuki and S. Yoshikawa, *Catal. Commun.*, 2005, **6**, 119-124.
- (263) Y. M. Sung, J. K. Lee and W. S. Chae, *Cryst. Growth Des.*, **2006**, **6**, 805-808.
- (264) Y. Yue and Z. Gao, *Chem. Commun.*, 2000, 1755-1756.
- (265) D. Chen, L. Cao, F. Huang, P. Imperia, Y. B. Cheng and R. A. Caruso, *J. Am. Chem. Soc.*, 2010, **132**, 4438-4444.
- (266) P. Kluson, P. Kacer, Cajthaml and M. Kalaji, *J. Mater. Chem.*, 2001, **11**, 644-651.
- (267) G. Calleja, D. P. Serrano, R. Sanz, P. Pizarro and A. Garcia, *Ind. Eng. Chem. Res.*, 2004, **43**, 2485-2492.
- (268) T. Z. Ren, Z. Y. Yuan and B. I. Su, *Chem. Phys. Lett.*, 2003, **374**, 170-175.
- (269) S. Sahni, S. B. Reddy and B. S. Murty, *Mater. Sci. Eng. A*, 2007, **452-453**, 758-762.
- (270) A. Ponton, S. B. Doeuff and C. Sanchez, *Colloids Surf. A: Physicochem. Eng. Aspects*, 2000, **162**, 177-192.
- (271) J. Kim, K. C. Song and S. E. Pratsinis, *J. Nanopart. Res.*, 2000, **2**, 419-424.
- (272) X. Z. Ding, Z. Z. Qi, and Y. Z. He, *J. Mater. Sci. Lett.*, 1995, **14**, 21-22.
- (273) N. Mahdjoub, N. Allen, P. Kelly and V. Vishnyakov, *J. Photochem. Photobiol. A: Chem.*, 2010, **210**, 125-129.
- (274) C. Suresh, V. Baiju, P. Mukundan and K. G. K. Warriar, *Polyhedron*, 1998, **17**, 3131-3135.
- (275) H. H. Kung and E. I. Kuo, *Chem. Eng. J.*, 1996, **64**, 203-214.
- (276) S. C. Padmanabhan, S. C. Pillai, J. Colreavy, S. Balakrishnan, D. C. McCormack, T. S. Perova, Y. Gunko, S. J. Hinder and J. M. Kelly, *Chem. Mater.*, 2007, **19**, 4474-4481.
- (277) N. T. Nolan, M. K. Serry and S. C. Pillai, *J. Phys. Chem. C*, 2009, **113**, 16151-16157.
- (278) P. A. Venz, R. L. Frost, J. R. Barlett, J. L. Woolfrey and J. T. Klopogge, *Thermochimica Acta*, 2000, **346**, 73-82.

- (279) Y. Djaoued, S. Badilescu, P. V. Ashrit, D. Bersani, P. P. Lottici and J. Robichaud, *J. Sol-Gel. Sci. Technol.*, 2002, **24**, 255-264.
- (280) J. Zhu, J. Zhang, F. Chen and M. Anpo, *Mater. Lett.*, 2005, **59**, 3378-3381.
- (281) M. Pal, J. G. Serrano, P. Santiago, U. Pal, *J. Phys. Chem. C*, 2007, **111**, 96-102.
- (282) X. Jiang, T. Herricks and Y. Xia, *Adv. Mater.*, 2003, **15**, 1205-1209.
- (283) S. Manickam, *Theoretical and experimental sonochemistry involving inorganic systems*, Springer, Heidelberg, 2011.
- (284) K. S. Suslick, *Science*, 1990, **247**, 1439-1445.
- (285) K. S. Suslick, S. B. Choe, A. A. Cichowlas and M. W. Grinstaff, *Nature*, 1991, **353**, 414-416.
- (286) T. Hyeon, M. Fang and K. S. Suslick, *J. Am. Chem. Soc.*, 1996, **118**, 5492-5493.
- (287) S. Koda, K. Tanaka, H. Sakamoto, T. Matsuoka and H. Nomura, *J. Phys. Chem. A*, 2004, **108**, 11609-11612.
- (288) K. S. Suslick and G. J. Price, *Ann. Rev. Mater. Sci.*, 1999, **29**, 295-326.
- (289) A. Gedanken, *Ultrason. Sonochem.*, 2004, **11**, 47-55.
- (290) S. J. Doktycz and K. S. Suslick, *Science*, 1990, **247**, 1067-1069.
- (291) S. Ramesh, Y. Koltypin and A. Gedanken, *J. Mater. Res.*, 1997, **12**, 3271-3277.
- (292) K. Yang, J. Zhu, J. Zhu, S. Huang, X. Zhu and G. Ma, *Mater. Lett.*, 2003, **57**, 4639-4642.
- (293) Y. Q. Wang, S. G. Chen, X. H. Tang, O. Palchik, A. Zaban, Y. Koltypin and A. Gedanken, *J. Mater. Chem.*, 2001, **11**, 521-526.
- (294) P. Jeevanandam, Y. Kotylin, Y. Mastai and A. Gedanken, *J. Mater. Chem.*, 2000, **10**, 2143-2146.
- (295) W. Guo, Z. Lin, X. Wang and G. Song, *Microelectron. Eng.*, 2003, **66**, 95-101.
- (296) S. Y. Kim, T. S. Chang and C. H. Shin, *Catal. Lett.*, 2007, **118**, 224-230.

- (297) O. C. Duvarci and M. Ciftcioglu, *Powder Technol.*, 2012, **228**, 231-240.
- (298) Y. Wang, X. Tang, L. Yin, W. Huang, Y. R. Hacoheh and A. Gedanken, *Adv. Mater.*, 2000, **12**, 1183-1186.
- (299) J. C. Yu, L. Zhang and J. Yu, *New J. Chem.*, 2002, **26**, 416-420.
- (300) J. C. Yu, L. Zhang and J. Yu, *Chem. Mater.*, 2002, **14**, 4647-4653.
- (301) T. Nagase, T. Ebina, T. Iwasaki, H. Hayashi, Y. Onodera and M. Chatterjee, *Chem. Lett.*, 1999, 911-912.
- (302) J. C. Yu, J. Yu, L. Zhang and W. Ho, *J. Photochem. Photobiol. A: Chem.*, 2002, **148**, 263-271.
- (303) P. S. Awati, S.V. Awate, P. P. Shah and V. Ramaswamy, *Catal. Commun.*, 2003, **4**, 393-400.
- (304) B. Neppolian, Q. Wang, H. Jung and H. Choi, *Ultrason. Sonochem.*, 2008, **15**, 649-658.
- (305) K. Prasad, D. V. Pinjari, A. B. Pandit and S. T. Mhaske, *Ultrason. Sonochem.*, 2010, **17**, 697-703.
- (306) H. Liu, W. Yang, Y. Ma, Y. Cao and J. Yao, *New J. Chem.*, 2002, **26**, 975-977.
- (307) H. Liu, W. Yang, Y. Ma, X. Ye and J. Yao, *New J. Chem.*, 2003, **27**, 529-532.
- (308) N. Sakai, R. Wang, A. Fujishima, T. Watanabe and K. Hashimoto, *Langmuir*, **1998**, **14**, 5918-5920.
- (309) R. Wang, K. Hashimoto, A. Fujishima, M. Chikuni, E. Kojima, A. Kitamura, M. Shimohigoshi and T. Watanabe, *Adv. Mater.*, **1998**, **10**, 135-138.
- (310) A. N. Shultz, W. Jang, W. M. Hetherington, D. R. Baer, L. Q. Wang and M. H. Engelhard, *Surf. Sci.*, 1995, **339**, 114-124.
- (311) H. Liu, W. Yang, Y. Ma, Y. Cao, J. Yao, J. Zhang and T. Hu, *Langmuir*, 2003, **19**, 3001-3005.

- (312) S. B. Atla, C. C. Chen, C. Y. Chen, P. Y. Lin, W. Pan, K. C. Cheng, Y. M. Huang, Y. F. Chang and J. S. Jean, *J. Photochem. Photobiol. A: Chem.*, 2012, **236**, 1-8.
- (313) H. Liu, W. Yang, Y. Ma and J. Yao, *Appl. Catal. A: Gen.*, 2006, **299**, 218-223.
- (314) B. Gao, Y. Ma, Y. Cao, J. Zhao and J. Yao, *J. Solid State Chem.*, 2006, **179**, 41-48.
- (315) H. Imai, M. Yasumori, H. Hirashima, K. Awazu and H. Onuki, *J. Appl. Phys.*, 1996, **79**, 8304-8309.
- (316) T. Nagase, T. Ooie and J. Sakakibara, *Thin Solid Films*, 1999, **357**, 151-158.
- (317) Z. S. Guan, X. T. Zhang, Y. Ma, Y. A. Cao and J. N. Yao, *J. Mater. Res.*, 2001, **16**, 907-909.
- (318) H. S. Jung, H. Shin, J. R. Kim, J. Y. Kim, K. S. Hong and J. K. Lee, *Langmuir*, 2004, **20**, 11732-11737.
- (319) Z. Tang, J. Zhang, Z. Cheng and Z. Zhang, *Mater. Chem. Phys.*, 2003, **77**, 314-317.
- (320) S. Yang, Y. Liu, Y. Guo, J. Zhao, H. Xu and Z. Wang, *Mater. Chem. Phys.*, 2003, **77**, 501-506.
- (321) J. Blanchard, M. In, B. Schaudel and C. Sanchez, *Eur. J. Inorg. Chem.*, 1998, 1115-1127.
- (322) M. J. Velasco, F. Rubio, J. Rubio and J. L. Oteo, *Thermochim. Acta*, 1999, **326**, 91-97.
- (323) J. Zhu, Z. Bian, J. Ren, Y. Liu, Y. Cao, H. Li, W. Dai, H. He and K. Fan, *Catal. Commun.*, 2007, **8**, 971-976.
- (324) (a) T. Welton, *Chem. Rev.*, 1999, **99**, 2071-2084; (b) Z. Ma, J. Yu and S. Dai, *Adv. Mater.*, 2010, **22**, 261-285; (c) J. P. Hallett and T. Welton, *Chem. Rev.*, 2011, **111**, 3508-3576.
- (325) J. Dupont, R. F. Swozsa and P. A. Z. Suarez, *Chem. Rev.*, 2002, **102**, 3667-3692.
- (326) V. I. Parvulescu and C. Hardacre, *C. Chem. Rev.*, 2007, **107**, 2615-2665.

- (327) M. Antonietti, D. Kuang, B. Smarsly and Y. Zhou, *Angew. Chem., Int. Ed.*, 2004, **43**, 4988-4992.
- (328) L. Wang, S. Tomura, M. Maeda, F. Ohashi, K. Inukai and M. Suzuki, *Chem. Lett.*, 2000, 1414-1415.
- (329) O. Aschenbrenner, S. Supasitmongkol, M. Taylor and P. Styring, *Green Chem.*, 2009, **11**, 1217-1221.
- (330) Y. Liu, J. Li, M. Wang, Z. Li, H. Liu, P. He, X. Yang and J. Li, *Cryst. Growth Des.*, 2005, **5**, 1643-1649.
- (331) S. S. Mali, C. A. Betty, P. N. Bhosale, R. S. Devan, Y. R. Ma, S. S. Kolekar and P. S. Patil, *CrystEngComm.*, 2012, **14**, 1920-1924.
- (332) W. Wang, B. Gu, L. Liang, W. A. Hamilton and D. J. Wesolowski, *J. Phys. Chem. B*, 2004, **108**, 14789-14792.
- (333) W. Zheng, X. Liu, Z. Yan and L. Zhu, *ACS Nano*, 2009, **3**, 115-122.
- (334) B. L. Bullock, L. Patthey, S. G. Steinemann and S. G. Clean, *Surf. Sci.*, 1996, **352-354**, 504-510.
- (335) O. M. Yaghi, G. M. Li and H. L. Li *Nature*, 1995, **378**, 703-706.
- (336) J. Jin, T. Iyoda, C. Cao, Y. Song, L. Jiang, T. Li and D. Zhu, *Angew. Chem., Int. Ed.*, 2001, **40**, 2135-2138.
- (337) K. Ding, Z. Miao, B. Hu, G. An, Z. Sun, B. Han and Z. Liu, *Langmuir*, 2010, **26**, 5129-5134.
- (338) K. Ding, Z. Miao, B. Hu, G. An, Z. Sun, B. Han and Z. Liu, *Langmuir*, 2010, **26**, 10294-10302.
- (339) H. Liu, Y. Liang, H. Hu and M. Wang, *Solid State Sci.*, 2009, **11**, 1655-1660.
- (340) M. Yan, F. Chen, J. Zhang and M. Anpo, *J. Phys. Chem. B*, 2005, **109**, 8673-8678.

- (341) Y. H. Liu, M. C. Chang, H. Shao, M. S. Huang and A. C. M. Yang, *J. Mater. Sci.*, 2010, **45**, 369-376.
- (342) X. Zhu, Y. Wang and H. Li, *AIChE J.*, 2009, **55**, 198-205.
- (343) W. Liu, T. Zhao, Y. Zhang, H. Wang and M. Yu, *J. Solution Chem.*, 2006, **35**, 1337-1346.
- (344) K. S. Yoo, T. G. Lee and J. Kim, *Microporous Mesoporous Mater.*, 2005, **84**, 211-217.
- (345) K. S. Yoo, H. Choi and D. D. Dionysiou, *Catal. Commun.*, 2006, **6**, 259-262.
- (346) K. S. Yoo, H. Choi and D. D. Dionysiou, *Chem. Commun.*, 2004, 2000-2001.
- (347) Y. Zhou and M. Antonietti, *J. Am. Chem. Soc.*, 2003, **125**, 14960-14961.
- (348) L. Cammarata, S. G. Kazarian, P. A. Salter and T. Welton, *Phys. Chem. Chem. Phys.*, 2001, **3**, 5192-5200.
- (349) Y. Zhou, J. H. Schattka, M. Antonietti, *Nano Lett.*, 2004, **4**, 477-481.
- (350) I. Mukhopadhyay and W. Freyland, *Langmuir*, 2003, **19**, 1951-1953.
- (351) A. Elaiwi, P. B. Hitchcock, K. R. Seddon, N. Srinivasan, Y. M. Tan, T. Welton and J. A. Zora, *J. Chem. Soc. Dalton Trans.*, 1995, 3467-3472.
- (352) H. Choi, Y. J. Kim, R. S. Varma and D. D. Dionysiou, *Chem. Mater.*, 2006, **18**, 5377-5384.
- (353) G. Law and P. R. Watson, *Langmuir*, 2001, **17**, 6138-6141.
- (354) T. Alammar, H. Noei, Y. Wang and A. V. Mudring, *Nanoscale*, 2013, **5**, 8045-8055.
- (355) H. Kaper, S. Sallard, I. Djerdj, M. Antonietti and B. M. Smarsly, *Chem. Mater.*, 2010, **22**, 3502-3510.
- (356) M. Addamo, V. Augugliaro, A. D. Paola, E. G. Lopez, V. Loddo, G. Marci and L. Palmisano, *Colloids Surfaces A: Physicochem. Eng. Aspects*, 2005, **265**, 23-31.
- (357) A. D. Paola, M. Bellardita, R. Ceccato, L. Palmisano and F. Parrino, *J. Phys. Chem. C*, 2009, **113**, 15166-15174.

- (358) Y. Li, N. H. Lee, E. G. Lee, J. S. Song and S. J. Kim, *Chem. Phys. Lett.*, 2004, **389**, 124-128.
- (359) Y. Wang, L. Zhang, K. Deng, X. Chen and Z. Zhou, *J. Phys. Chem. C*, 2007, **111**, 2709–2714.
- (360) G. Li, L. Li, B. Goates and B. F. Woodfield, *J. Am. Chem. Soc.*, 2005, **127**, 8659-8666.
- (361) Y. Zhu, L. Zhang, C. Gao and L. Cao, *J. Mater. Sci.*, 2000, **35**, 4049-4054.
- (362) C. A. Nolph, D. E. Sievers, S. Kaewgun, C. J. Kucera, D. H. McKinney, J. P. Rientjes, J. L. White, R. Bhave and B. I. Lee, *Catal. Lett.*, 2007, **117**, 102-106.
- (363) R. Boppella, P. Basak and S. V. Manorama, *Appl. Mater. Interfaces*, 2012, **4**, 1239-1246.
- (364) R. Chen, L. Zhang, Y. Wei and D. Hou, *J. Mater. Sci.*, 2007, **42**, 7141-7146.
- (365) Q. Yang, C. Xie, Z. Xu, Z. Gao and Y. Du, *J. Phys. Chem. B*, 2005, **109**, 5554-5560.
- (366) J. Beukenkamp and K. D. Herrington, *J. Am. Chem. Soc.*, 1960, **82**, 3025-3031.
- (367) S. Cassaignon, M. Koelsch and J. P. Jolivet, *J. Mater. Sci.*, 2007, **42**, 6689-6695.
- (368) A. H. Sun, P. J. Guo, Z. X. Li, Y. Li and P. Cui, *J. Alloys Compd.*, 2009, **481**, 605-609.
- (369) S. Cassaignon, M. Koelsch and J. P. Jolivet, *J. Phys. Chem. Solids*, 2007, **68**, 695-700.
- (370) M. Kanna and S. Wongnawa, *Mater. Chem. Phys.*, 2008, **110**, 166-175.
- (371) H. I. Hsiang and S. C. Lin, *Mater. Sci. Eng. A*, 2004, **380**, 67-72.
- (372) C. J. Brinker and G. W. Scherer, *Sol-Gel Science: The physics and Chemistry of Sol-Gel Processing*, Academic Press, San Diego, 1990, pp. 357-405.
- (373) Y. Li, N. H. Lee, J. S. Song, E. G. Lee and S. J. Kim, *Res. Chem. Intermed.*, 2005, **31**, 309-318.
- (374) X. Z. Ding and Y. Z. He, *J. Mater. Sci. Lett.*, 1996, **15**, 320-322.
- (375) F. Bosc, A. Ayral, P. A. Albouy and C. Guizard, *Chem. Mater.*, 2003, **15**, 2463-2468.

- (376) J. Sanz, J. Soria, I. Sobrados, S. Yurdakal and V. Augugliaro, *J. Phys. Chem. C*, 2012, **116**, 5110-5115.
- (377) W. Z. Ostwald, *Z. Phys. Chem.*, 1897, **22**, 289-330.
- (378) G. Palmisano, S. Yurdakal, V. Augugliaro, V. Loddo and L. Palmisano, *Adv. Synth. Catal.*, 2007, **349**, 964-970.
- (379) V. Augugliaro, H. Kisch, V. Loddo, M. M. Loez, C. M. Alvarez, G. Palmisano, L. Palmisano, F. Parrino and S. Yurdakal, *S. Appl. Catal. A: Gen.*, 2008, **349**, 182-188.
- (380) T. A. Kandiel, A. Feldhoff, L. Robben, R. Dillert and D. W. Bahnemann, *Chem. Mater.*, 2010, **22**, 2050-2060.
- (381) M. Kobayashi, K. Tomita, V. Petrykin, M. Yoshimura and M. Kakihana, *J. Mater. Sci.*, 2008, **43**, 2158-2162.
- (382) A. Hanprasopwattana, T. Rieker, A. G. Sault and A. K. Datye, *Catal. Lett.*, 1997, **45**, 165-175.
- (383) L. Liu, Y. Zhao, H. Liu, H. Kou and Y. Wang, *Nanotechnology*, 2006, **17**, 5046-5050.
- (384) D. Dambournet, I. Belharouak and K. Amine, *Chem. Mater.*, 2010, **22**, 1173-1179.
- (385) W. F. Sullivan and S. S. Cole, *J. Am. Ceram. Soc.*, 1959, **42**, 127-133.
- (386) G. Colon, M. C. Hidalgo, J. A. Navio, A. Kubacka and M. F. Garcia, *Appl. Catal. B: Environ.*, 2009, **90**, 633-641.
- (387) J. P. Jolivet, *Metal oxide chemistry and synthesis: From solution to solid state*; Wiley: New York, 2000.
- (388) C. Boudaren, C. Bataille, J. P. Auffredic and D. Louer, *Solid State Sci.*, 2003, **5**, 175-182.
- (389) S. Perera and E. G. Gillan, *Solid State Sci.*, 2008, **10**, 864-872.
- (390) D. S. Hwang, N. H. Lee, D. Y. Lee, J. S. Song, S. H. Shin and S. J. Kim, *Smart Mater. Struct.*, 2006, **15**, S74-S80.

- (391) L. Kong, I. Karatchevtseva, M. Blackford, I. Chironi and G. Triani, *J. Am. Ceram. Soc.*, 2012, **95**, 816-822.
- (392) S. Yin, R. Li, Q. He and T. Sato, *Mater. Chem. Phys.*, 2002, **75**, 76-80.
- (393) T. Kawahara, T. Ozawa, M. Iwasaki, H. Tada and S. Ito, *J. Colloid Interface Sci.*, 2003, **267**, 377-381.
- (394) S. Nad, P. Sharma, I. Roy and A. Maitra, *J. Colloid Interface Sci.*, 2003, **264**, 89-94.
- (395) K. Haouemi, F. Touati and N. Gharbi, *Chem. Papers*, 2012, **66**, 202-210.
- (396) Q. Chen, X. Shen and H. Gao, *J. Colloid Interface Sci.*, 2007, **312**, 272-278.
- (397) M. Andersson, L. Osterlund, S. Ljungstrom and A. Palmqvist, *J. Phys. Chem. B*, 2002, **106**, 10674-10679.
- (398) M. Wu, R. Xu, S. H. Feng, L. Li, D. Chen and Y. Luo, *J. Mater. Sci.*, 1996, **31**, 6201-6205.
- (399) M. P. Pileni, *J. Phys. Chem.*, 1993, **97**, 6961-6973.
- (400) A. G. Ganguli, A. Ganguly and S. Vaidya, *Chem. Soc. Rev.*, 2010, **32**, 474-485.
- (401) V. Pillai, D. O. Shah, in: C. Soalns, H. Kunieda (Ed.s), *Industrial Application of Microemulsion*, Marcel Dekker, New York, 1997, p. 227.
- (402) N. Munshi, T.K. De and A.N. Maitra, *J. Colloid Interface Sci.*, 1997, **190**, 387-391.
- (403) S. Zhang, Q. Yu, Z. Chen, Y. Li and Y. You, *Mater. Lett.*, 2007, **61**, 4839-4842.
- (404) X. Li, T. Li, C. Wu and Z. Zhang, *J. Nanopart. Res.*, 2007, **9**, 1081-1086.
- (405) M. S. Lee, S. S. Park, G. D. Lee, C. S. Ju and S. S. Hong, *Catal. Today*, 2005, **101**, 283-290.
- (406) V. Chhabra, V. Pillai, B. K. Mishra, A. Morrone and D. O. Shah, *Langmuir*, 1995, **11**, 3307-3311.
- (407) X. Shen, J. Zhang and B. Tian, *J. Hazard. Mater.*, 2011, **192**, 651-657.

- (408) L. Kavan, O. Regan, A. Kay and M. Gratzel, *J. Electroanal. Chem.*, 1993, **346**, 291-307.
- (409) F. P. Rotzinger and M. Gratzel, *Inorg. Chem.*, 1987, **26**, 3704-3708.
- (410) M. Wu, J. Long, A. Huang and Y. Luo, *Langmuir*, 1999, **15**, 8822-8825.
- (411) (a) Y. Wang, A. Zhou and Z. Yang, *Mater. Lett.*, 2008, **62**, 1930-1932; (b) J. Yu and J. Zhang, *Dalton Trans.*, 2010, **39**, 5860-5867; (c) J. Yu and X. Yu, *Environ. Sci. Technol.*, 2008, **42**, 4902-4907; (d) J. Yu and G. Wang, *J. Phys. Chem. Solids*, 2008, **69**, 1147-1151; (e) J. Yu, X. Yu, B. Huang, X. Zhang and Y. Dai, *Cryst. Growth Des.*, 2009, **9**, 1474-1480.
- (412) Q. Zhong, D. A. Steinhurst, E. E. Carpenter and J. C. Owrutsky, *Langmuir*, 2002, **18**, 7401-7408.
- (413) V. Uskoković and M. Drogenik, *Adv. Colloid Interface Sci.*, 2007, **133**, 23-34.
- (414) S. Yamabi and H. Imai, *Chem. Mater.*, 2002, **14**, 609-614.
- (415) K. Tomita, M. Kobayashi, V. Petrykin, S. Yin, T. Sato, M. Yoshimura and M. Kakihana, *J. Mater. Sci.*, 2008, **43**, 2217-2221.
- (416) G. Liu, H. G. Yang, C. Sun, L. Cheng, L. Wang, G. Q. Lu and H. M. Cheng, *CrystEngComm.*, 2009, **11**, 2677-2682.
- (417) H. G. Yang and H. C. Zeng, *J. Phys. Chem. B*, 2004, **108**, 3492-3495.
- (418) K. Lv, J. Yu, L. Cui, S. Shen and M. Li, *J. Alloys Compd.*, 2011, **509**, 4557-4562.
- (419) Y. Lv, L. Yu, H. Huang, H. Liu and Y. Feng, *Appl. Surf. Sci.*, 2009, **255**, 9548-9552.
- (420) (a) H. G. Yang, C. H. Sun, S. Z. Qiao, J. Zou, G. Liu, S. C. Smith, H. M. Cheng and G. Q. Lu, *Nature*, 2008, **453**, 638-641; (b) M. V. Sofianou, V. Psycharis, N. Boukos, T. Vaimakis, J. Yu, R. Dillert, D. Bahnemann and C. Trapalis, *Appl. Catal. B: Environ.*, 2013, **142-143**, 761-768; (c) K. Lv, Q. Xiang and J. Yu, *Appl. Catal. B: Environ.*, 2011, **104**, 275-281.
- (421) H. F. Yu and S. T. Yang, *J. Alloys Compd.*, 2010, **492**, 695-700.

- (422) S. Komarneni, R. Roy and Q. H. Li, *Mater. Res. Bull.*, 1992, **27**, 1393-1405.
- (423) A. B. Corradi, F. Bondioli, B. Focher, A. M. Ferrari, C. Grippo, E. Mariani and C. Villa, *J. Am. Ceram. Soc.*, 2005, **88**, 2639-2641.
- (424) N. M. Kinsinger, A. Wong, D. Li, F. Villalobos and D. Kisailus, *Cryst. Growth Des.*, 2010, **10**, 5254-5261.
- (425) W. H. Casey, B. L. Phillips, J. P. Nordin and D. J. Sullivan, *Geochim. Cosmochim. Acta*, 1998, **62**, 2789-2797.
- (426) H. Mockel, M. Giersig and F. Willig, *J. Mater. Chem.*, 1999, **9**, 3051-3056.
- (427) H. Colfen and M. Antonjeiti, *Mesocrystals and Nonclassical Crystallization*; CPI Antony Rowe: Chippenham, Wiltshire, 2008.
- (428) G. Liu, X. Yan, Z. Chen, X. Wang, L. Wang, G. Q. Lu and H. M. Cheng, *J. Mater. Chem.*, 2009, **19**, 6590-6596.
- (429) Q. Tay, X. Liu, Y. Tang, Z. Jiang, T. C. Sum and Z. Chen, *J. Phys. Chem. C*, 2013, **117**, 14973-14982.
- (430) W. Hu, L. Li, G. Li, C. Tang and L. Sun, *Cryst. Growth Des.*, 2009, **9**, 3676-3682.
- (431) E. M. Wong, J. E. Bonevich and P. C. Searson, *J. Phys. Chem. B*, 1998, **102**, 7770-7775.
- (432) (a) N. Menon, F. D. Blum, and L. R. Dharani, *J. Appl. Polym. Sci.*, 1994, **54**, 113-123. (b) M. Xing, J. Zhang and F. Chen, *J. Phys. Chem. C*, 2009, **113**, 12848-12853. (c) Y. D. Tu, Z. Zhou, R. J. Yan, Y. P. Gan, W. Z. Huang, X. X. Weng and H. Huang, W. K. Zhang and X. Y. Tao, *CrystEngComm.*, 2012, **2**, 10585-10591. (d) J. Yu, M. Zhou, B. Cheng and X. Zhao, *J. Mol. Catal. A: Chem.*, 2006, **246**, 176-184. (e) M. Nasir, J. Zhang, F. Chen and B. Tian, *Res. Chem. Intermed.*, DOI 10.1007/s11164-013-1297-7. (f) M. Y. Xing, D. Y. Qi, J. Zhang and F. Chen, *Chem. Eur. J.*, 2011, **17**, 11432-11436. (g) B. Qiu, M. Xing and J. Zhang, *J. Am. Chem. Soc.*, 2014, **136**, 5852-5855. (h) H. K. Park, Y. T. Moon, D. K. Kim and C. H. Kim, *J.*

- Am. Ceram. Soc.*, 1996, **79**, 2727-2732. (i) Q. Yang, C. Xie, Z. Xu, Z. Gao and Y. Du, *J. Phys. Chem. B*, 2005, **109**, 5554-5560. (j) X. Lu, D. Mao, X. Wei, H. Zhang, J. Xie and W. Wei, *J. Mater. Res.*, 2013, **28**, 400-404. (k) Q. D. Truong, T. S. Le and H. T. Hoa, *CrystEngComm.*, 2012, **14**, 4274-4278. (l) J. Cai, Z. Wang, K. Lv, Y. Zheng, J. Yu and M. Li, *RSC Adv.*, 2013, **3**, 15273-15281. (m) K. Lv, J. Yu, J. Fan and M. Jaroniec, *CrystEngComm.*, 2011, **13**, 7044-7048.
- (433) N. Bao, L. Shen, X. Feng and X. Lu, *J. Am. Ceram. Soc.*, 2004, **87**, 326-330.
- (434) N. Bao, X. Feng, X. Lu, L. Shen and K. Yanagisawa, *AIChE, J.*, 2004, **50**, 1568-1577.
- (435) T. Sasaki, M. Watanabe, Y. Fujiki and Y. Kitami, *Chem. Mater.*, 1994, **6**, 1749-1756.
- (436) S. Yin and T. Sato, *Ind. Eng. Chem. Res.*, 2000, **39**, 4526-4530.
- (437) N. Bao, L. Shen and K. Yanagisawa, *J. Phys. Chem. B*, 2004, **108**, 16739-16745.
- (438) N. Bao, X. Feng, Z. Yang, L. Shen and X. Lu, *Environ. Sci. Technol.*, 2004, **38**, 2729-2736.
- (439) Q. Feng, M. Hirasawa and K. Yanagisawa, *Chem. Mater.*, 2001, **13**, 290-296.
- (440) Y. Ohara, K. Koumoto and H. Yanagida, *J. Am. Ceram. Soc.*, 1994, **77**, 2327-2331.
- (441) Q. Feng, M. Hirasawa, K. Kajiyoshi and K. Yanagisawa, *J. Am. Ceram. Soc.*, 2005, **88**, 1415-1420.
- (442) J. Li, H. Yang, Q. Li and D. Xu, *CrystEngComm.*, 2012, **14**, 3019-3026.
- (443) J. Li, Y. Yu, Q. Chen, J. Li and D. Xu, *Cryst. Growth Des.*, 2010, **10**, 2111-2115.
- (444) J. Li, W. Wan, H. Zhou, J. Li and D. Xu, *Chem. Commun.*, 2011, **47**, 3439-3441.
- (445) N. Murakami, T. Kamai, T. Tsubota and T. Ohno, *CrystEngComm.*, 2010, **12**, 532-537.
- (446) C. C. Tsai and H. Teng, *Chem. Mater.*, 2006, **18**, 367-373.
- (447) H. Y. Zhu, Y. Lan, X. P. Gao, S. P. Ringer, Z. F. Zheng, D. Y. Song and J. C. Zhao, *J. Am. Chem. Soc.*, 2005, **127**, 6730-6736.

- (448) Y. Yang, G. Wang, Q. Deng, S. Kang, D. H. L. Ng and H. Zhao, *CrystEngComm.*, 2014, **16**, 3091-3096.
- (449) T. Sasaki, Y. Komatsu and Y. Fujiki, *Chem. Mater.*, 1992, **4**, 894-899.
- (450) Y. Jiao, B. Zhao, F. Chen and J. Zhang, *CrystEngComm.*, 2011, **13**, 4167-4173.
- (451) B. Zhao, F. Chen, Y. Jiao and J. Zhang, *J. Mater. Chem.*, 2010, **20**, 7990-7997.
- (452) X. Shen, B. Tian and J. Zhang, *Catal. Today*, 2013, **201**, 151-158.
- (453) B. Zhao, F. Chen, X. Gu and J. Zhang, *Chem. Asian J.*, 2010, **5**, 1546-1549.
- (454) B. Zhao, F. Chen, Q. Huang and J. Zhang, *Chem. Commun.*, 2009, 5115-5117.
- (455) R. A. V. Santen, *J. Phys. Chem.*, 1984, **88**, 5768-5769.
- (456) Y. Mao and S. S. Wong, *J. Am. Chem. Soc.*, 2006, **128**, 8217-8226.
- (457) R. Buonsanti, V. Grillo, E. Carlino, C. Giannini, T. Kipp, R. Cingolani and P. D. Cozzoli, *J. Am. Chem. Soc.*, 2008, **130**, 11223-11233.
- (458) Y. Wu, M. Xing, J. Zhang and F. Chen, *Appl. Catal. B: Environ.*, 2010, **97**, 182-189.
- (459) H. Yang, F. Chen, Y. Jiao and J. Zhang, *Chem. Eng. J.*, 2013, **214**, 229-236.
- (460) M. Dishon, O. Zohar and U. Sivan, *Langmuir*, 2009, **25**, 2831-2836.
- (461) C. Minero, G. Mariella, V. Maurino and E. Pelizzetti, *Langmuir*, 2000, **16**, 2632-2641.
- (462) C. Minero, G. Mariella, V. Maurino, D. Vione and E. Pelizzetti, *Langmuir*, 2000, **16**, 8964-8972.
- (463) S. Andersson and A. D. Wadsley, *Nature*, 1960, **187**, 499-500.
- (464) (a) Q. Wang, Z. Guo and J. S. Chung, *Chem. Commun.*, 2009, 5284-5286; (b) Z. Zheng, H. Liu, J. Ye, J. Zhao, E. R. Waclawik and H. Zhu, *J. Mol. Catal. Chem. A: Chem.*, 2010, **316**, 75-82.
- (465) S. Andersson and A. D. Wadsley, *Acta Chem. Scand.*, 1961, **15**, 664-669.

- (466) (a) J. N. Nian and H. S. Teng, *J. Phys. Chem. B*, 2006, **110**, 4193-4198; (b) W. Li, C. Liu, Y. Zhou, Y. Bai, X. Feng, Z. Yang, L. Lu, X. Lu and K. Y. Chan, *J. Phys. Chem. C*, 2008, **112**, 20539-20545.
- (467) W. Li, Y. Bai, C. Liu, Z. Yang, X. Feng, X. Lu, N. K. V. Laak and K. Chan, *Environ. Sci. Technol.*, 2009, **43**, 5423-5428.
- (468) L. Shen, N. Bao, Y. Zheng, A. Gupta, T. An and K. Yanagisawa, *J. Phys. Chem. C*, 2008, **112**, 8809-8818.
- (469) H. Izawa, S. Kikkawa and M. Koizumi, *J. Phys. Chem.*, 1982, **86**, 5023-5026.
- (470) T. Sasaki, M. Watanabe, Y. Komatsu and Y. Fujiki, *Inorg. Chem.*, 1985, **24**, 2265-2271.
- (471) J. Yu, H. Yu, B. Cheng and C. Trapalis, *J. Mol. Catal. A: Chem.*, 2006, **249**, 135-142.
- (472) H. L. Kuo, C. Y. Kuo, C. H. Liu, J. H. Chao and C. H. Lin, *Catal. Lett.*, 2007, **113**, 7-12.
- (473) P. Zhang, S. Yin, V. Petrykin, M. Kakihana and T. Sato, *J. Mol. Catal. A: Chem.*, 2009, **309**, 50-56.
- (474) M. Tournoux, R. Marchand and L. Brohan, *Prog. Solid State Chem.*, 1986, **17**, 33-52.
- (475) S. Andersson and A. D. Wadsley, *Acta Crystallogr.*, 1962, **15**, 194-201.
- (476) Y. Zheng, E. Shi, W. Li, Z. Chen, W. Zhong and X. Hu, *Sci. China Ser. E*, 2002, **45**, 120-129.
- (477) C. C. Chung, T. W. Chung and T. C. K. Yang, *Ind. Eng. Chem. Res.*, 2008, **47**, 2301-2307.
- (478) S. Ribbens, I. Caretti, E. Beyers, S. Zamani, E. Vinck, S. V. Doorslaer and P. Cool, P. *J. Phys. Chem. C*, 2011, **115**, 2302-2313.
- (479) Y. Gao, Y. Masuda, Z. Peng, T. Yonezawa and K. Koumoto, *K. J. Mater. Chem.*, 2003, **13**, 608-613.

- (480) Y. F. Gao, M. Nagai, W. S. Seo and K. Koumoto, *Langmuir*, 2007, **23**, 4712-4714.
- (481) Y. Gao, H. Luo, S. Mizusugi and M. Nagai, *Cryst. Growth Des.*, 2008, **8**, 1804-1807.
- (482) S. I. Seok, B. Y. Ahn, N. C. Pramanik, H. Kim and S. I. Hong, *J. Am. Ceram. Soc.*, 2006, **89**, 1147-1149.
- (483) J. A. Chang, M. Vithal, I. C. Baek and S. I. Seok, *J. Solid State Chem.*, 2009, **182**, 749-756.
- (484) I. C. Baek, M. Vithal, J. A. Chang, J. H. Yum, M. Nazeeruddin, M. Gratzel, Y. C. Chung and S. I. Seok, *Electrochem. Commun.*, 2009, **11**, 909-912.
- (485) Y. J. Liu, M. Aizawa, Z. M. Wang, H. Hatori, N. Uekawa and H. Kanoh, *J. Colloid Interface Sci.*, 2008, **322**, 497-504.
- (486) G. Schwarzenbach, J. Muehlebach and K. Mueller, *Inorg. Chem.*, 1970, **9**, 2381-2390.
- (487) M. Dakanali, E. T. Kefalas, C. P. Raptopoulou, A. Terzis, G. Voyiatzis, I. Kyrikou, T. Mavromoustakos and A. Salifoglou, *Inorg. Chem.*, 2003, **42**, 4632-4639.
- (488) D. W. Bahnemann, A. Henglein and L. Spanhel, *Faraday Discuss. Chem. Soc.*, 1984, **78**, 151-163.
- (489) V. Etacheri, M. K. Serry, S. J. Hinder and S. C. Pillai, *Adv. Funct. Mater.*, 2011, **21**, 3744-3752.
- (490) P. M. Kumar, S. Badrinarayanan and M. Sastry, *Thin Solid Films*, 2000, **358**, 122-130.
- (491) S. I. Seok, M. Vithal and J. A. Chang, *J. Colloid Interface Sci.*, 2010, **346**, 66-71.
- (492) C. Ribeiro, C. Vila, J. M. E. D. Matos, J. Bettini, E. Longo and E. R. Leite, *Chem. Eur. J.*, 2007, **13**, 5798-5803.
- (493) V. Stengl and D. Kralova, *Mater. Chem. Phys.*, 2011, **129**, 794-801.
- (494) N. Murakami, Y. Kurihara, T. Tsubota and T. Ohno, *J. Phys. Chem. C*, 2009, **113**, 3062-3069.
- (495) R. S. Sonawane and S. Ramakrishna, *Mater. Sci. Eng. B*, 2012, **177**, 652-660.

- (496) C. Pacholski, A. Kornowski and H. Weller, *Angew. Chem., Int. Ed.*, 2002, **41**, 1188-1191.
- (497) J. F. Banfield, S. A. Welch, H. Zhang, T. T. Ebert and R. L. Penn, *Science*, 2000, **89**, 751-754.
- (498) E. Hosono, S. Fujihara, I. Honma and H. Zhou, *Adv. Mater.*, 2005, **17**, 2091-2094.
- (499) Y. Li, J. Liu and Z. Jia, *Mater. Lett.*, 2006, **60**, 1753-1757.
- (500) D. Schwarzenbach, *Inorg. Chem.*, 1970, **9**, 2391-2397.
- (501) (a) I. Djerdj, D. Arcon, Z. Jaglicic and M. Niederberger, *J. Solid State Chem.*, 2008, **181**, 1571-1581; (b) C. Wang, Z. X. Deng, G. Zhang, S. Fan and Y. D. Li, *Powder Technol.*, 2002, **125**, 39-44; (c) G. V. Jensen, M. Breholm, N. Lock, G. R. Deen, T. R. Jensen, B. B. Iversen, M. Niederberger, J. S. Pedersen and H. Birkedal, *Chem. Mater.*, 2010, **22**, 6044-6055; (d) G. Garnweitner and M. Niederberger, *J. Mater. Chem.*, 2008, **18**, 1171-1182.
- (502) M. Niederberger, M. H. Bartl and G. D. Stucky, *Chem. Mater.*, 2002, **14**, 4364-4370.
- (503) A. M. Collins, C. Spickermann and S. Mann, *J. Mater. Chem.*, 2003, **13**, 1112-1114.
- (504) G. Guo, J. K. Whitesell and M. A. Fox, *J. Phys. Chem. B*, 2005, **109**, 18781-18785.
- (505) P. Arnal, R. J. P. Corriu, D. Leclercq, P. H. Mutin and A. Vioux, *Chem. Mater.*, 1997, **9**, 694-698.
- (506) T. J. Trentler, T. E. Denler, J. F. Bertone, A. Agrawal and V. L. Colvin, *J. Am. Chem. Soc.*, 1999, **121**, 1613-1614.
- (507) L. Chen, B. Yao, Y. Cao and K. Fan, *J. Phys. Chem. C*, 2007, **111**, 11849-11853.
- (508) P. A. Vioux, *Chem. Mater.*, 1997, **9**, 2292-2299.
- (509) J. Blanchard, F. Ribot, C. Sanchez, P. V. Bellot and A. Trokiner, *J. Non-Cryst. Solids*, 2000, **265**, 83-97.
- (510) G. A. A. S. Illa and C. Sanchez, *New J. Chem.*, 2000, **24**, 493-499.

- (511) R. Petrovic, N. Tanaskovic, V. Djokic, Z. Radovanovic, I. J. Castvan, I. Stamenkovic and D. Janackovic, *Powder Technol.*, 2012, **219**, 239-243.
- (512) N. Tanaskovic, Z. Radovanovic, V. Dokic, J. Krstic, S. Drmanic, Dj. Janackovic and R. Petrovic, *Superlatt. Microstruct.* 2009, **46**, 217-222.
- (513) M. Zimmermann and G. Garnweitner, *CrystEngComm.*, 2012, **14**, 8562-8568.
- (514) M. Hu, J. Xu, J. Gao, S. Yang, J. S. P. Wong and R. K. Y. Li, *Dalton Trans.*, 2013, **42**, 9777-9784.
- (515) Y. C. Hsu, H. C. Lin, C. H. Chen, Y. T. Liao and C. M. Yang, *J. Solid State Chem.*, 2010, **183**, 1917-1924.
- (516) (a) J. Zhu, J. Yang, Z. F. Bian, J. Ren, Y. M. Liu, Y. Cao, H. X. Li, H. Y. He and K. N. Fan, *Appl. Catal. B Environ.* 2007, **76**, 82-91; (b) N. D. Abazovic, M. I. Comor, M. D. Dramicanin, D. J. Jovanovic, S. P. Ahrenkiel and J. M. Nedeljkovic, *J. Phys. Chem. B*, 2006, **110**, 25366-25370.
- (517) G. Garnweitner, N. Tsedev, H. Dierke and M. Niederberger, *Eur. J. Inorg. Chem.*, 2008, 890-895.
- (518) G. Garnweitner, M. Antonietti and M. Niederberger, *Chem. Commun.*, 2005, 397-399.
- (519) P. Arnal, R. J. P. Corriu, D. Leclercq, P. H. Mutin and A. Vioux, *J. Mater. Chem.*, 1996, **6**, 1925-1932.
- (520) N. Avci, P. F. Smet, H. Poelman, N. V. D. Velde, K. D. Buysser, I. V. Driessche and D. Poelman, *J. Sol-Gel Sci. Technol.*, 2009, **52**, 424-431.
- (521) T. Cao, Y. Li, C. Wang, C. Shao and Y. Liu, *J. Nanomater.*, 2011, 267415.
- (522) C. S. Kim, I. M. Kwon, B. K. Moon, J. H. Jeong, B. C. Choi, J. H. Kim, H. Choi, S. S. Yi, D. H. Yoo, K. S. Hong, J. H. Park and H. S. Lee, *Mater. Sci. Eng. C*, 2007, **27**, 1343-1346.

- (523) B. Boury, R. G. Nair, S. K. Samdarshi, T. Makiabadi and P. H. Mutin, *New J. Chem.*, 2012, **36**, 2196-2200.
- (524) J. Joo, S. G. Kwon, T. Yu, M. Cho, J. Lee, J. Yoon and T. Hyeon, *J. Phys. Chem. B*, 2005, **109**, 15297-15302.
- (525) (a) S. L. James, C. J. Adams, C. Bolm, D. Braga, P. Collier, T. Firscic, F. Grepioni, K. D. M. Harris, G. Hyett, W. Jones, A. Krebs, J. Mack, L. Maini, A. G. Orpen, I. P. Parkin, W. C. Shearouse, J. W. Steed and D. C. Waddell, *Chem. Soc. Rev.*, 2012, **41**, 413-447; (b) V. Sepelak, A. Duvel, M. Wilkening, K. D. Becker and P. Heitjans, *Chem. Soc. Rev.*, 2013, **42**, 7507-7520.
- (526) W. Ao, J. Li, H. Yang, X. Zeng and X. Ma, *Powder Technol.*, 2006, **168**, 148-151.
- (527) (a) V. Brezova, Z. Vreckova, P. Billik, M. Caplovicova and G. Plesch, *J. Photochem. Photobiol. A: Chem.*, 2009, **206**, 177-187; (b) V. Brezova, P. Billik, Z. Vreckova and G. Plesch, *J. Mol. Catal. A: Chem.*, 2010, **327**, 101-109; (c) M. U. Bujnova, D. Dimitrov, D. Radev, A. Bonjinov and D. Todorovsky, *Mater. Chem. Phys.*, 2008, **110**, 291-298.
- (528) P. Billik, G. Plesch, V. Brezova, L. Kuchta, M. Valko and M. Mazur, *J. Phys. Chem. Solids*, 2007, **68**, 1112-1116.
- (529) P. Billik and G. Plesch, *Mater. Lett.*, 2007, **61**, 1183-1186.
- (530) M. Rezaee and S. M. M. Khoie, *J. Alloys Compd.*, 2010, **507**, 484-488.
- (531) F. Delogu, *J. Alloys Compd.*, 2009, **468**, 22-27.
- (532) C. Suryanarayana, *Prog. Mater. Sci.*, 2001, **46**, 1-184.
- (533) X. Pan and X. Ma, *Mater. Lett.*, 2004, **58**, 513-515.
- (534) R. Schulz, M. Trudeau, J. Y. Huot and A. V. Neste, *Phys. Rev. Lett.*, 1989, **62**, 2849-2852.
- (535) (a) G. Palumbo, S. J. Thorpe and K. T. Aust, *Scr. Metall. Mater.*, 1990, **24**, 1347-1350.
(b) J. C. Parker and R. W. Siegel, *J. Mater. Res.*, 1990, **5**, 1246-1252.

- (536) S. B. Colin, T. Girot, G. L. Caer and A. Mocellin, *J. Solid State Chem.*, 2000, **149**, 41-48.
- (537) Kh. Gheisari, S. Javadpour, J. T. Oh and M. Ghaffari, *J. Alloys Compd.*, 2009, **472**, 416-420.
- (538) J. Chaudhuri, M. L. Ram and B. K. Sarkar, *J. Mater. Sci.*, 1994, **29**, 3484-3488.
- (539) H. Dutta, P. Sahu, S. K. Pradhan and M. De, *Mater. Chem. Phys.*, 2002, **77**, 153-164.
- (540) X. Y. Pan, Y. Chen, X. M. Ma and L. H. Zhu, *Trans. Nonferrous Metals Soc.*, 2003, **13**, 271-275.
- (541) R. Ren, Z. Yang and L. L. Shaw, *J. Mater. Sci.*, 2000, **35**, 6015-6026.
- (542) X. Pan and X. Ma, *J. Solid State Chem.*, 2004, **177**, 4098-4103.
- (543) A. Gajovic, K. Furic, N. Tomasic, S. Popovic, Z. Skoko and S. Music, *J. Alloys Compd.*, 2005, **398**, 188-199.
- (544) M. Rezaee, S. M. M. Khoie, D. H. Fatmehsari and H. K. Liu, *J. Alloys Compd.*, 2011, **509**, 8912-8916.
- (545) K. Ralphs, C. Hardacre and S. L. James, *Chem. Soc. Rev.*, 2013, **42**, 7701-7718.
- (546) M. Salari, M. Rezaee, S. P. H. Marashi and S. H. Aboutalebi, *Powder Technol.*, 2009, **192**, 54-57.
- (547) M. Salari, S. M. M. Khoie, P. Marashi and M. Rezaee, *J. Alloys Compd.*, 2009, **469**, 386-390.
- (548) M. Farbod and M. Khademalrasool, *Powder Technol.*, 2011, **214**, 344-348.
- (549) N. J. Welham, *Mater. Sci. Eng. A*, 1998, **255**, 81-89.
- (550) N. J. Welham, *J. Mater. Res.*, 1999, **14**, 619-627.
- (551) N. J. Welham and D. J. Llewellyn, *Miner. Eng.*, 1998, **11**, 827-841.

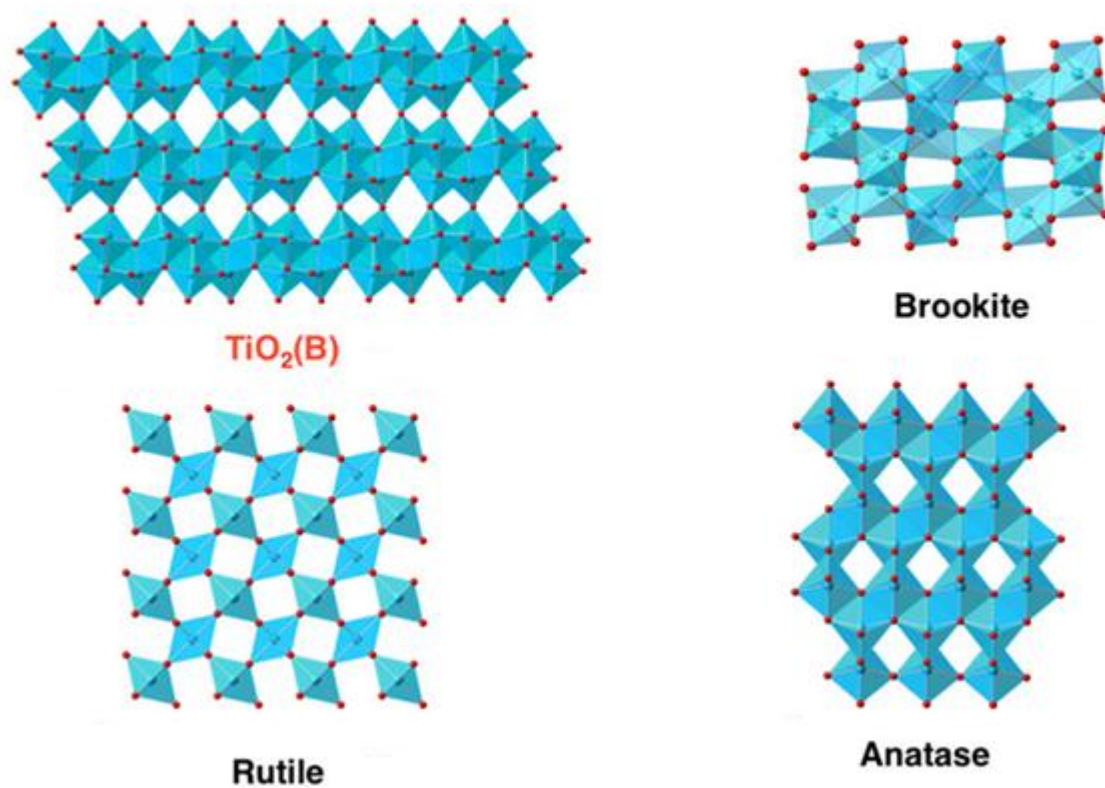


Fig. 1 Arrangement of [TiO₆] in titania polymorphs (reprinted with permission from ref. 1e; Copyright © 2013 American Chemical Society).

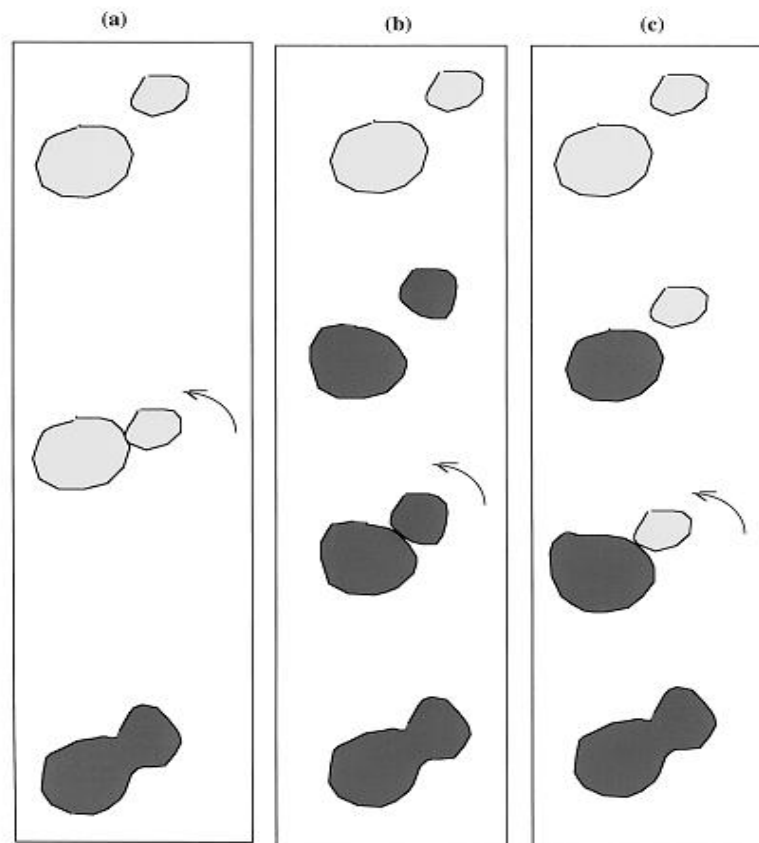


Fig. 2 Growth of rutile particle during sintering (reprinted with permission from ref. 129; Copyright © 2001 John Wiley and Sons).

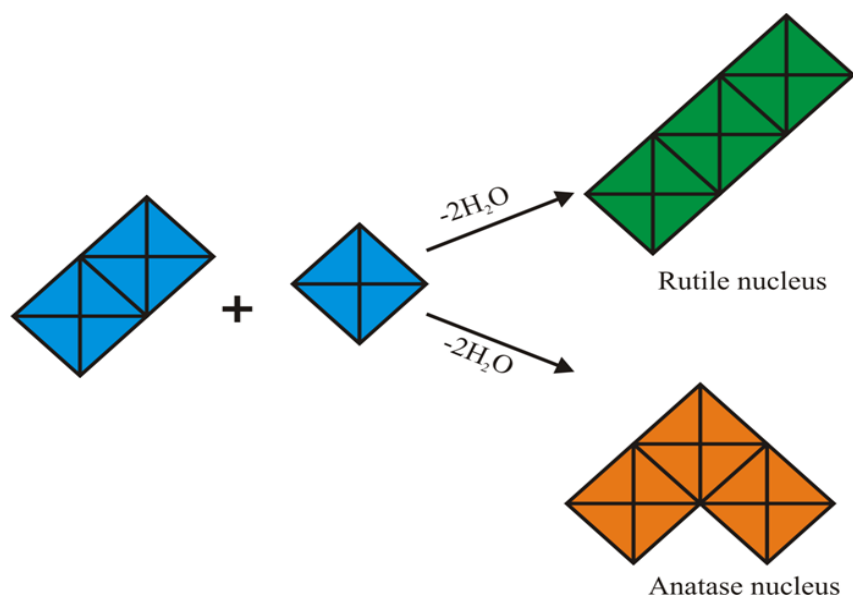


Fig. 3 Orientation of third $[\text{TiO}_6]$ in linear and zig-zag fashion.

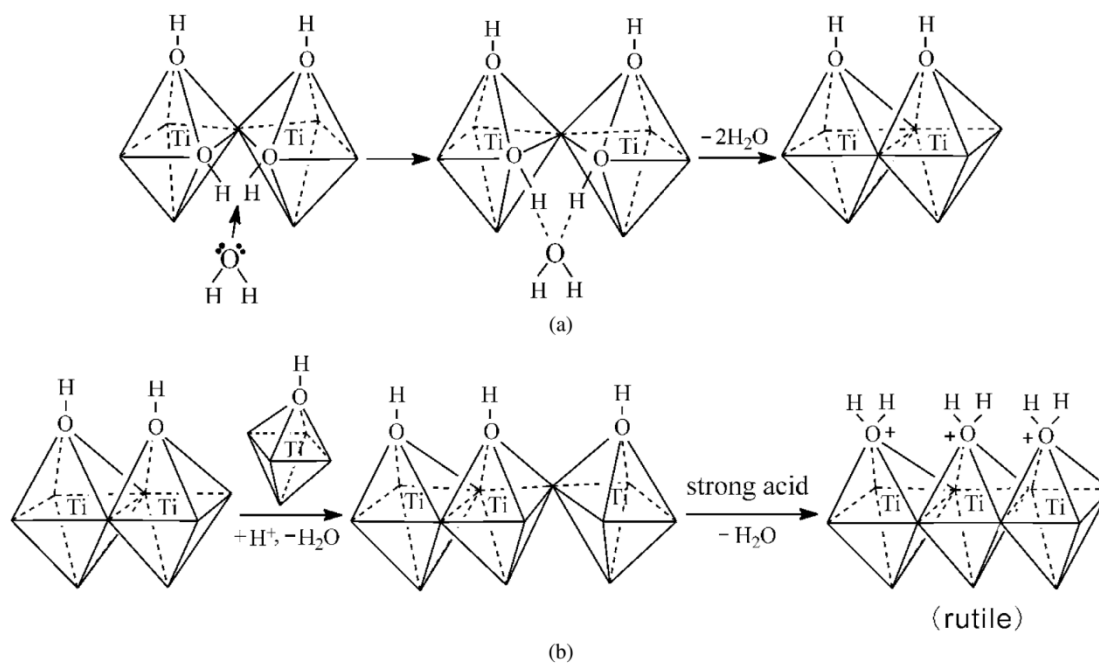


Fig. 4 The formation of rutile at acidic condition (reprinted with permission from ref. 139; Copyright © 2006 Elsevier).

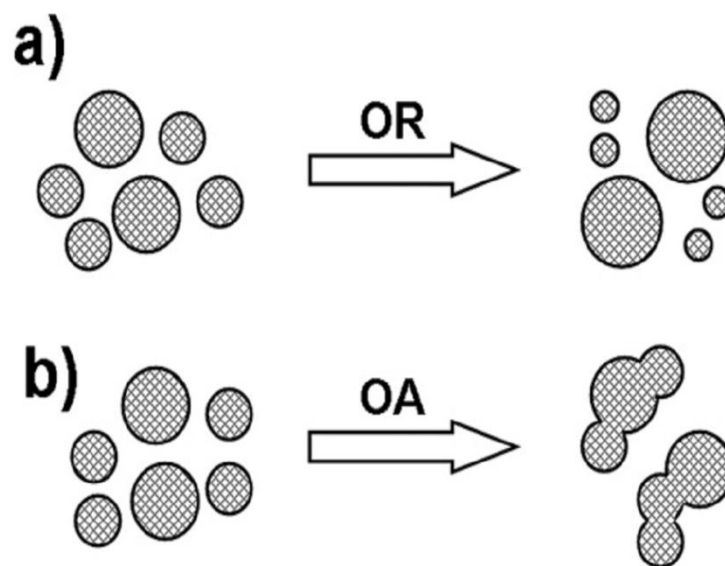


Fig. 5 Growth of nanoparticles by OR and OA mechanisms (reprinted with permission from ref. 166; Copyright @ 2010 Royal Society of Chemistry).

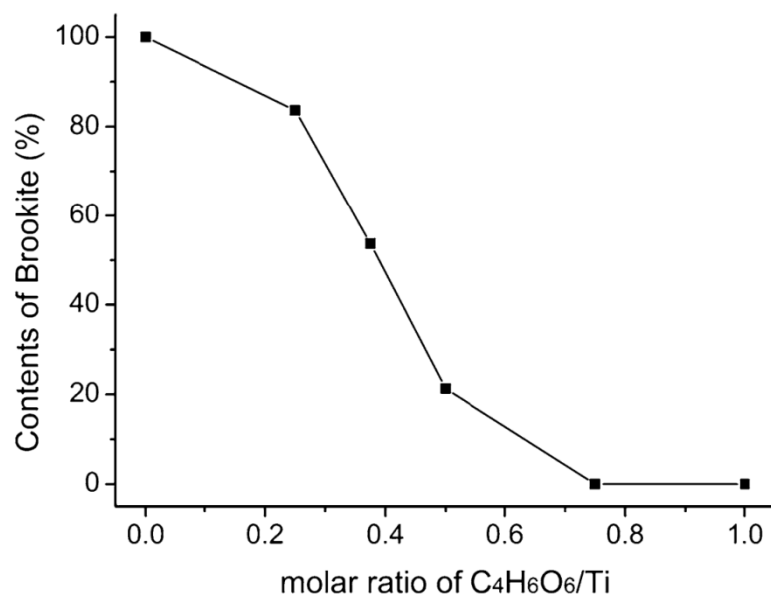


Fig. 6 Influence of tartaric acid on brookite content (reprinted with permission from ref. 192;

Copyright © 2012 Springer).

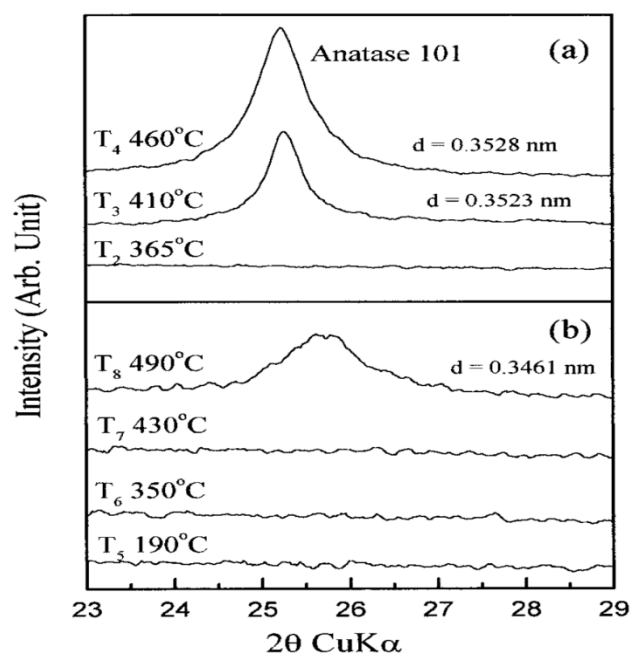


Fig. 7 XRD profile for (a) water washed sample; (b) alcohol washed sample calcined at various temperature (reprinted with permission from ref. 236; Copyright @ 1999 Elsevier).

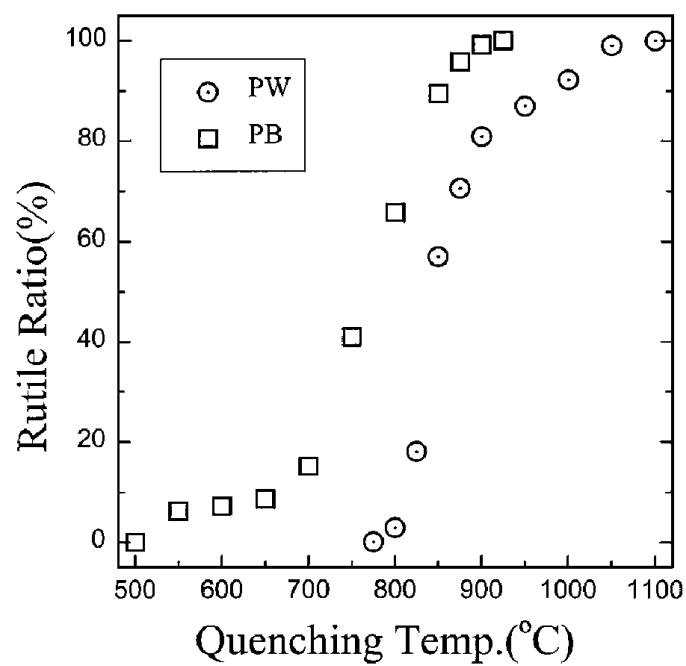


Fig. 8 Fraction of rutile for the powder washed with water (PW) and butanol (PB) after thermal treatment (reprinted with permission from ref. 237; Copyright @ 2000 Elsevier).

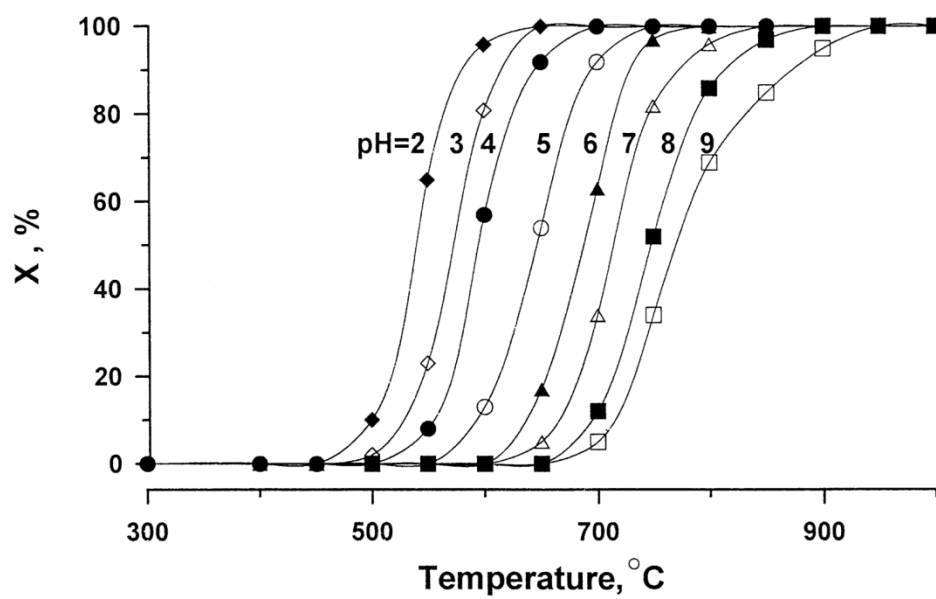


Fig. 9 Kinetics of ART for the powders precipitated at different pH conditions (reprinted with permission from ref. 242a; Copyright @ 2003 Elsevier).

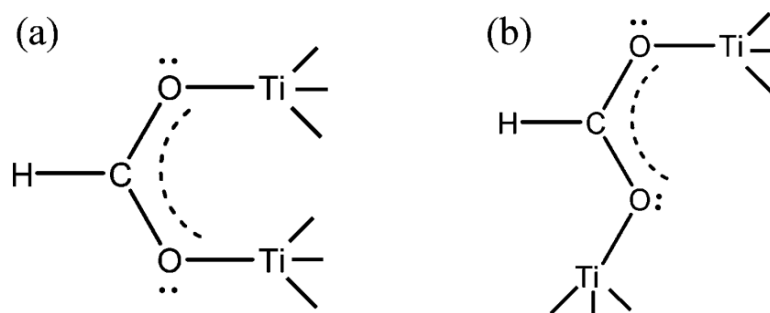


Fig. 10 Chelation of formate ion to Ti^{4+} via (a) syn-syn mode; (b) syn-anti mode (reprinted with permission from ref. 277; Copyright @ 2009 American Chemical Society).

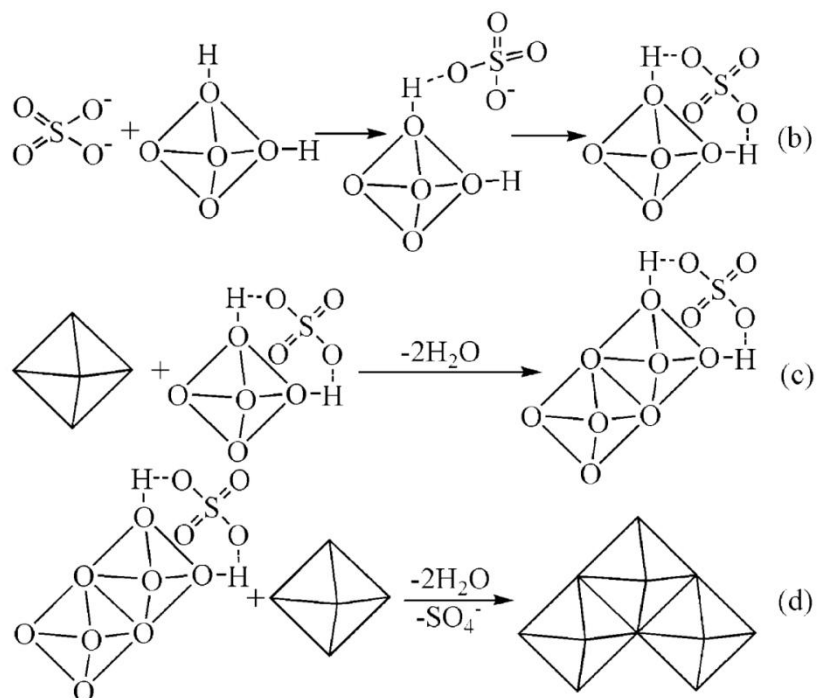


Fig. 11 Ligation of sulfate anion on [TiO₆] to facilitate anatase formation (reprinted with permission from ref. 340; Copyright @ 2005 American Chemical Society).

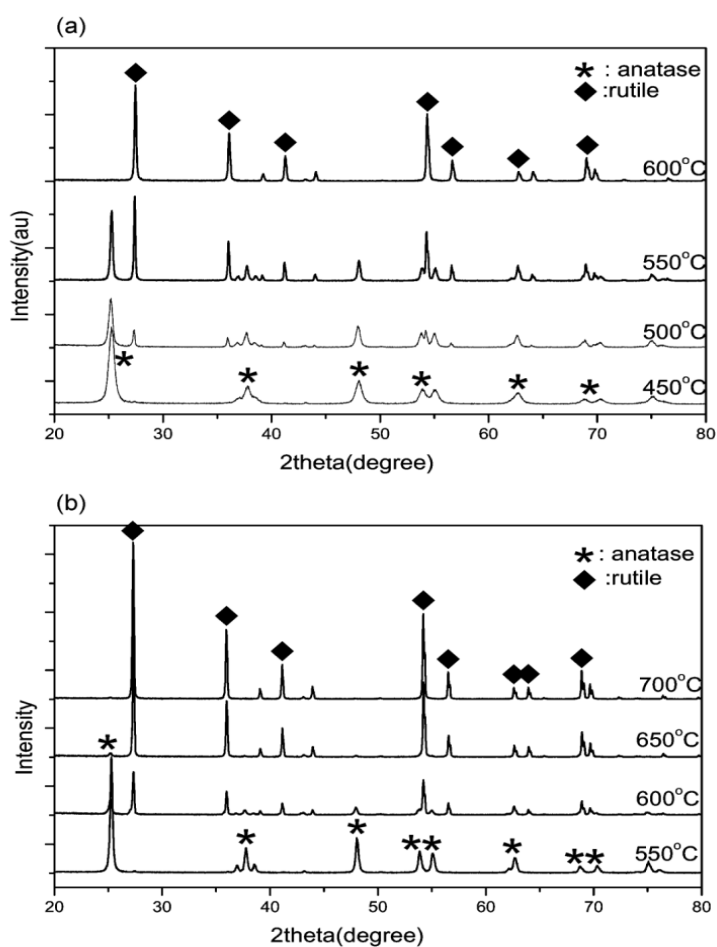


Fig. 12 XRD profile of powder with (a) and without (b) UV illumination followed by calcination at various temperature (reprinted with permission from ref. 307; Copyright @ 2003 Royal Society of Chemistry).

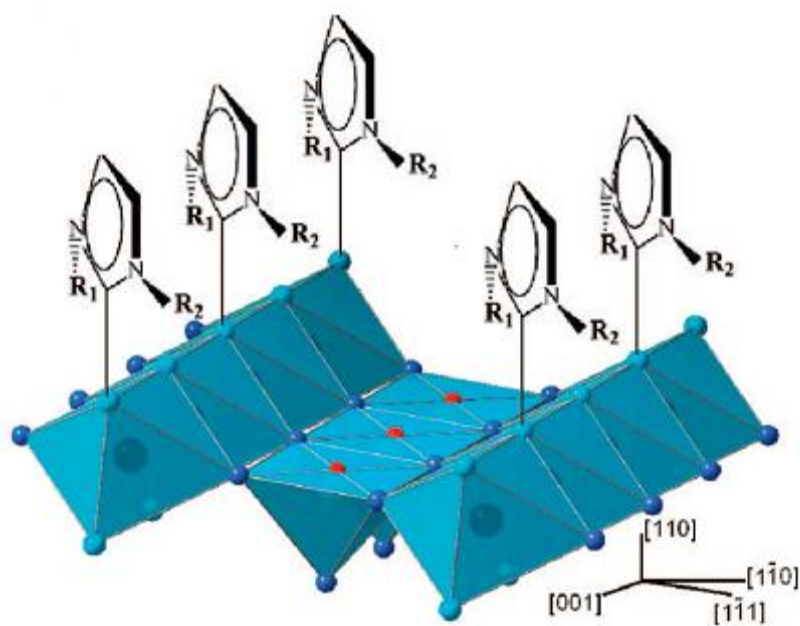


Fig. 13 Anchoring of [emim]⁺ on rutile {110} crystal planes (reprinted with permission from ref. 333; Copyright @ 2009 American Chemical Society).

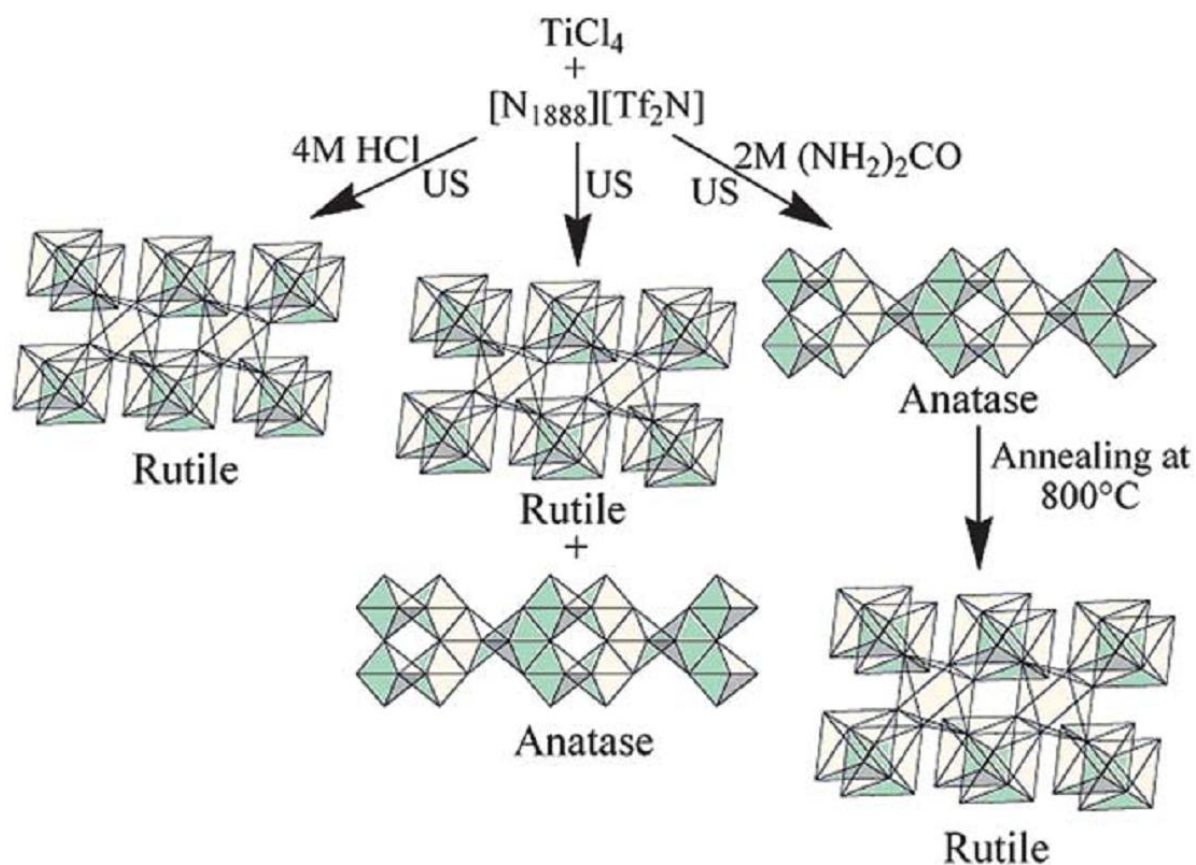


Fig. 14 Tuning of crystal phase with IL by varying the reaction parameters under ultrasonication (US). (reprinted with permission from ref. 354; Copyright @ 2013 Royal Society of Chemistry).

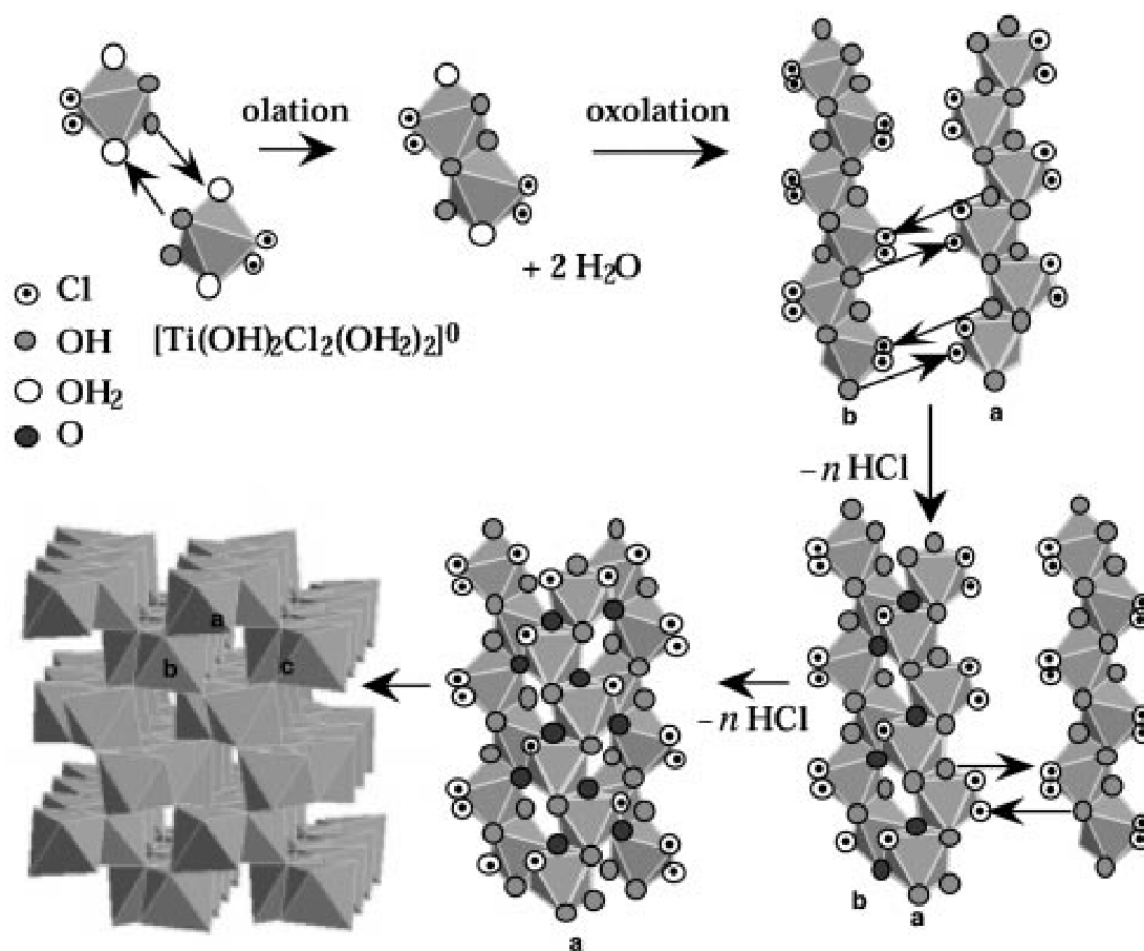


Fig. 15 Formation of brookite from $[\text{Ti}(\text{OH})_2\text{Cl}_2(\text{OH}_2)_2]^0$ precursor (reprinted with permission from ref. 86; Copyright @ 2001 Royal Society of Chemistry).

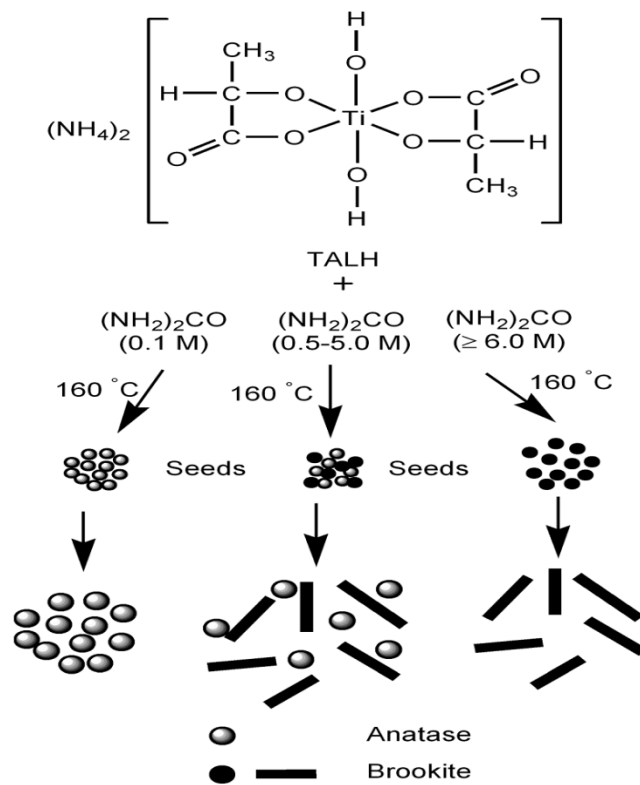


Fig. 16 Nucleation mechanism for brookite NRs and anatase nanoparticles from TiALBDH precursor (reprinted with permission from ref. 380; Copyright @ 2010 American Chemical Society).

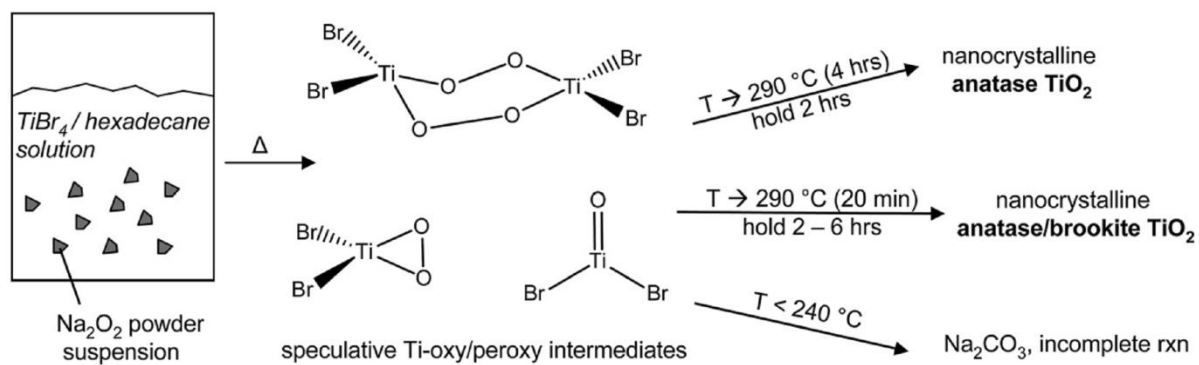


Fig. 17 TiO₂ formation pathway from TiBr₄/Na₂O₂ solvothermal system (reprinted with permission from ref. 389; Copyright @ 2008 Elsevier).

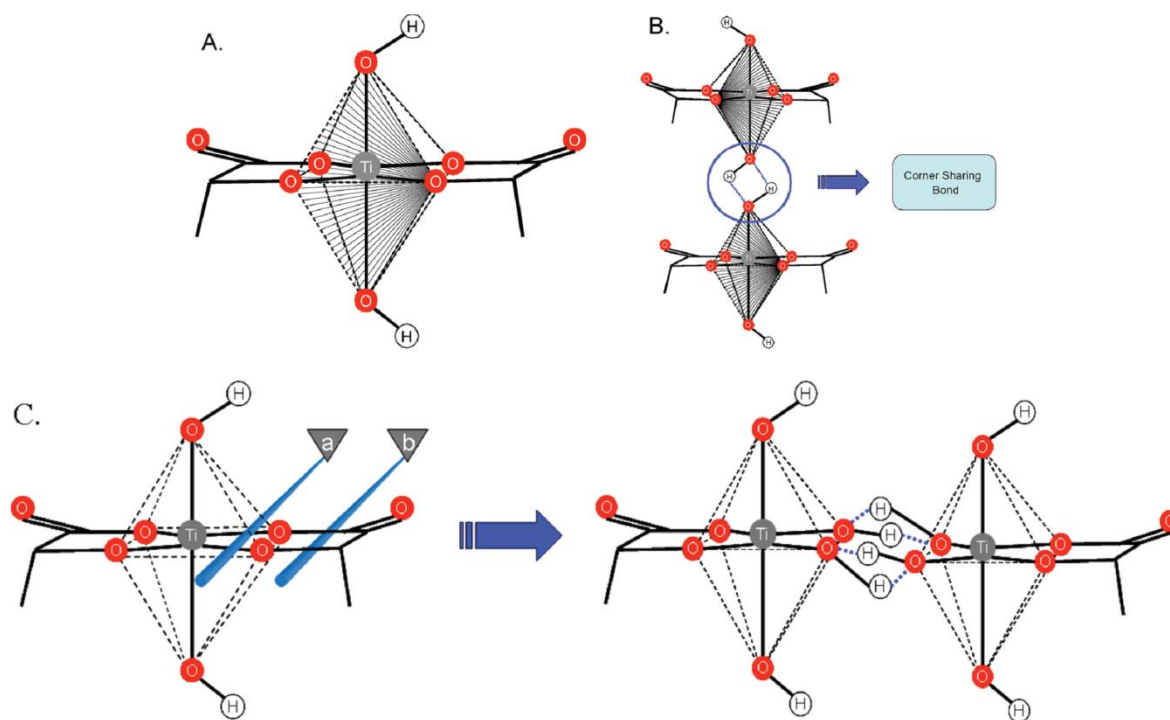


Fig. 18 (A) Structure of TiBALDH with dashed lines demonstrating its octahedral structure. (B) Illustration of the TiBALDH precursor with hydrolytically stable lactato ligands, forcing condensation along the z-axis. (C) Illustration of TiBALDH cleavage by nucleophilic attack by the OH⁻ at the (a) Ti metal center and at (b) bidentate ligands (shown by blue lines), which allows for two condensation reactions in the x-y plane of the coordination sphere to occur simultaneously yielding edge-sharing bonds. (reprinted with permission from ref. 424; Copyright © 2010 American Chemical Society).

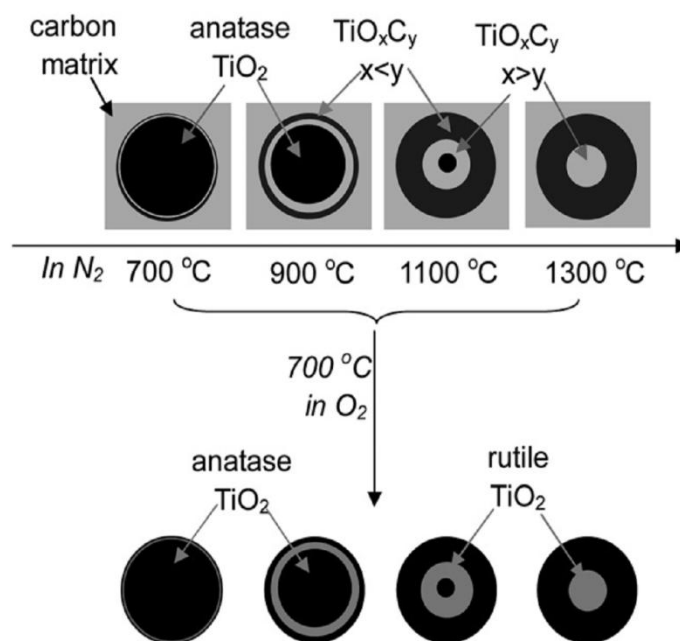


Fig. 19 Synthesis of rutile/anatase core/shell structure (reprinted with permission from ref. 428; Copyright © 2009 Royal Society of Chemistry).

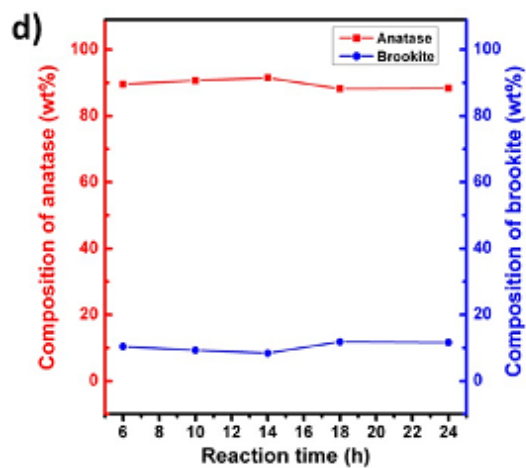


Fig. 20 Variation in anatase and brookite content with hydrothermal reaction time from TiS_2 precursor with NaOH (reprinted with permission from ref. 429; Copyright @ 2013 American Chemical Society).

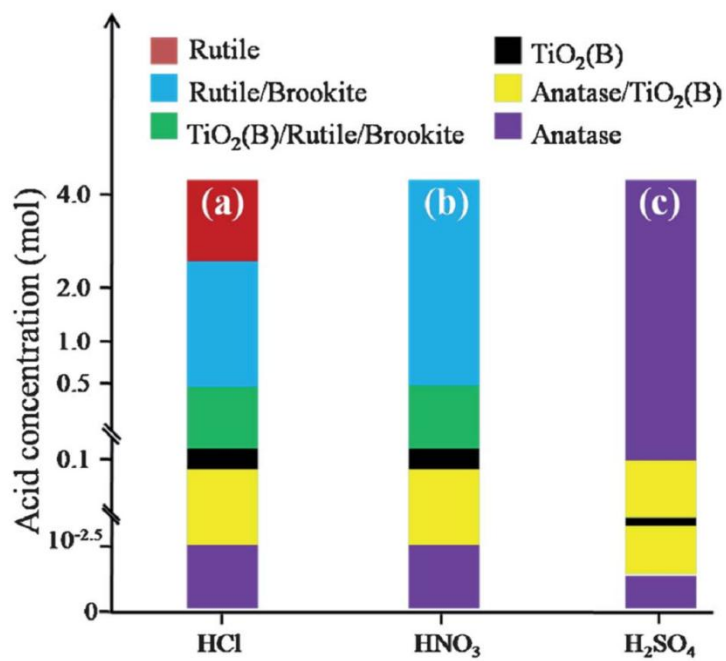


Fig. 21 Phase composition of titania with difference acid concentration from H/K titanate (reprinted with permission from ref. 442; Copyright @ 2012 Royal Society of Chemistry).

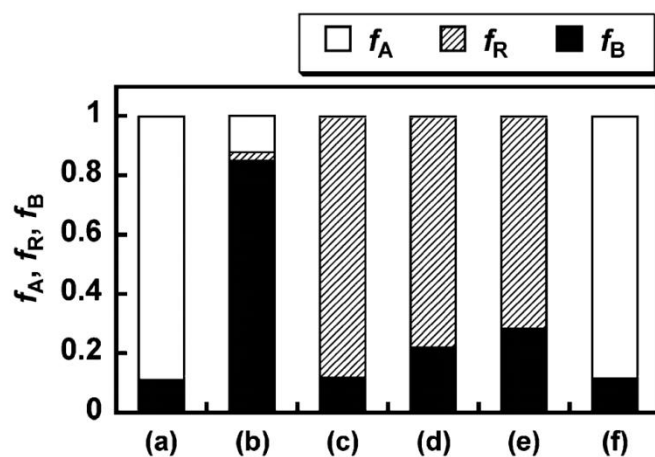


Fig. 22 Relative fraction of titania phases with various kinds of additive; (a) 2M NaClO₄; (b) 2 M HClO₄; (c) 2M HClO₄ + 2M NaCl; (d) 2M NaClO₄ + 2M HCl; (e) 2M HCl; (f) 2M NaCl (reprinted with permission from ref. 445; Copyright @ 2010 Royal Society of Chemistry).

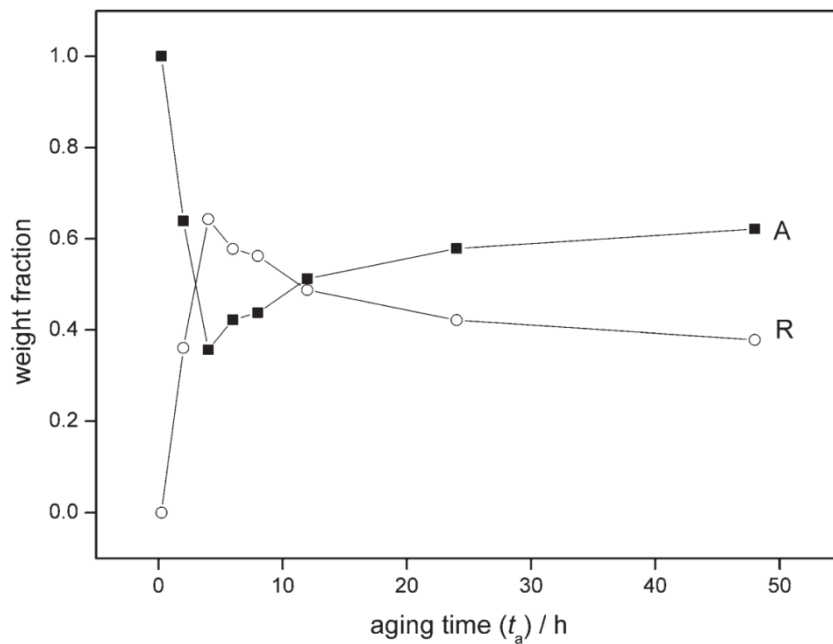


Fig. 23 Variation of anatase (A) and rutile (R) with hydrothermal aging time (reprinted with permission from ref. 128; Copyright @ 2010 American Chemical Society).

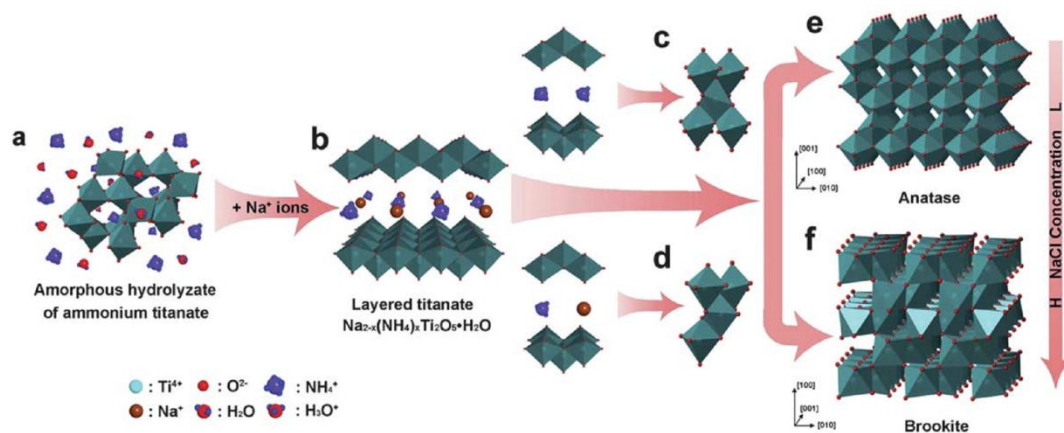


Fig. 24 Formation of anatase and brookite from ammonium titanate (reprinted with permission from ref. 450; Copyright @ 2010 Royal Society of Chemistry).

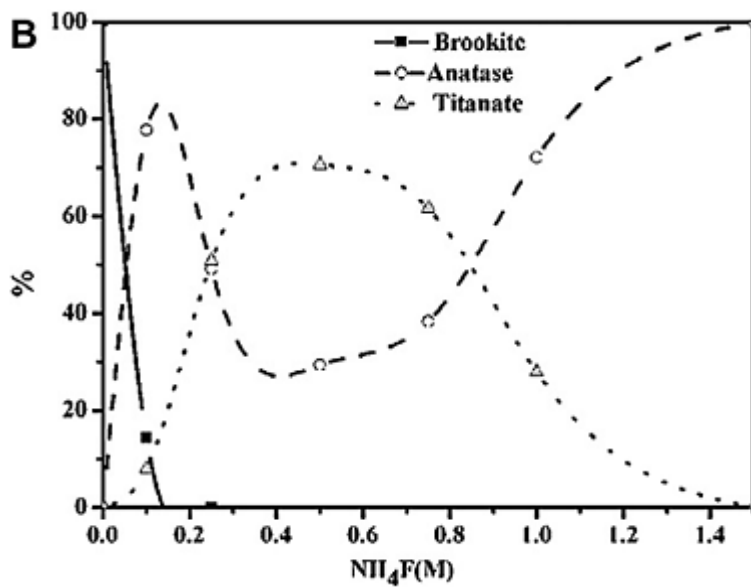


Fig. 25 Change in phase composition with varied concentration of NH_4F with 0.25 M NaF (reprinted with permission from ref. 459; Copyright @ 2013 Elsevier).

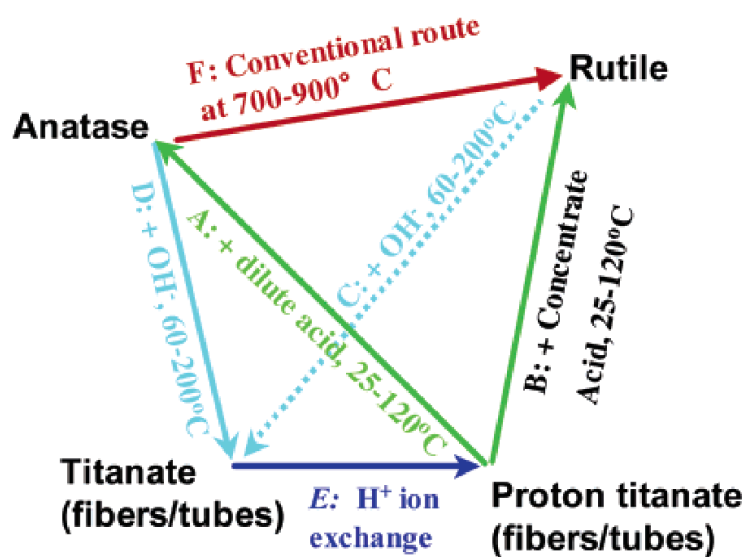


Fig. 26 Relation between titanate and other phases of titania in wet chemical approach (reprinted with permission from ref. 447; Copyright © 2005 American Chemical Society).

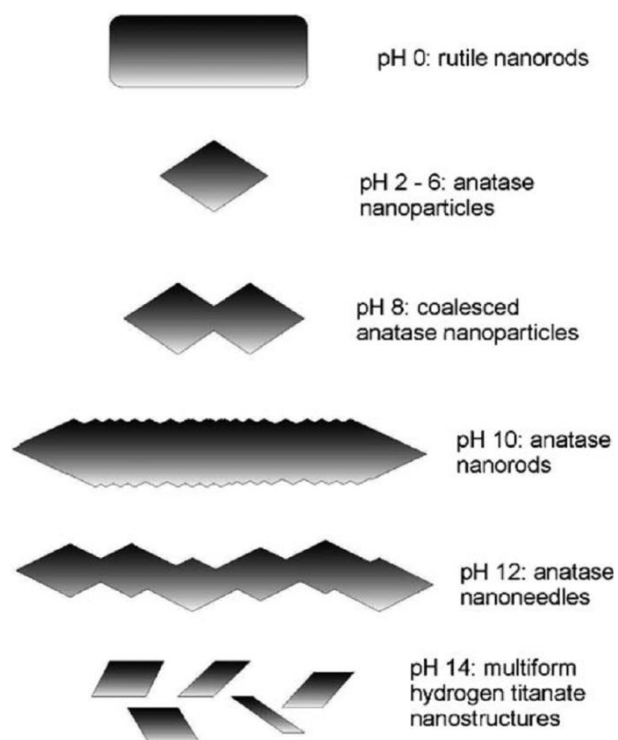


Fig. 27 Nucleation of different phases from PTC at varied pH conditions (reprinted with permission from ref. 32; Copyright 2009 Wiley-VCH Verlag).

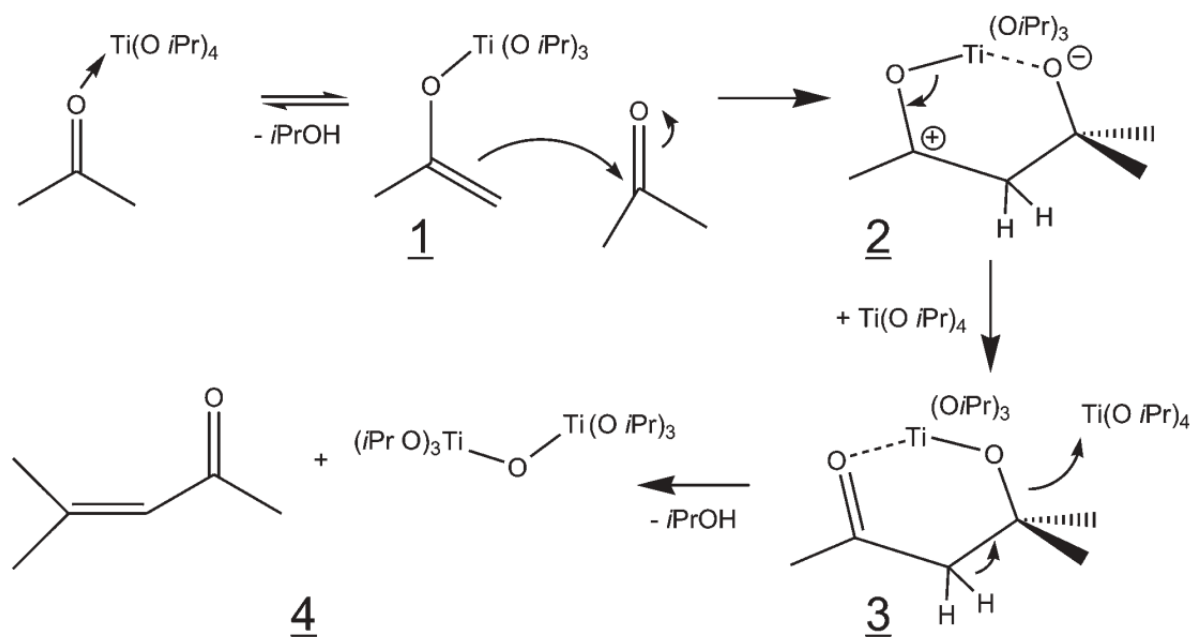


Fig. 28 Proposed mechanism pathway for TiO_2 in acetone (reprinted with permission from ref. 518; Copyright @ 2005 Royal Society of Chemistry).

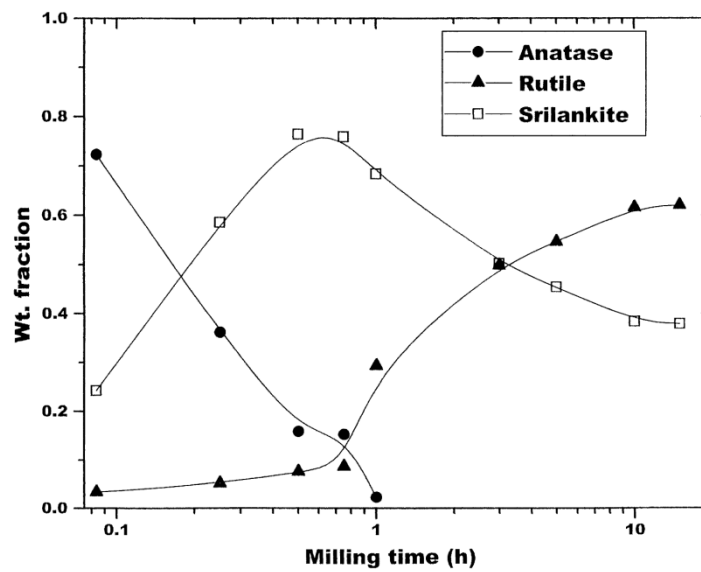


Fig. 29 Variation of phase contents with milling time (reprinted with permission from ref. 539; Copyright @ 2002 Elsevier).

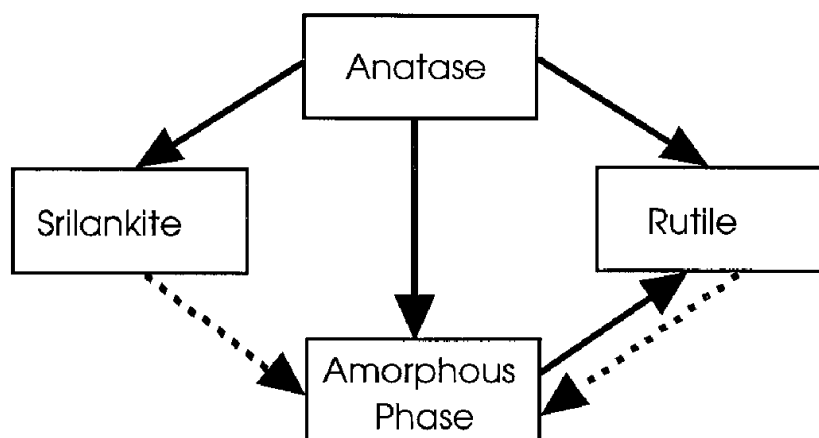


Fig. 30 TiO_2 transformations in ball milled conditions. Solid arrow(s) indicating most likely transformation, while dashed arrow(s) presenting the possible or negligible transformation (reprinted with permission from ref. 541; Copyright 2000 Springer).

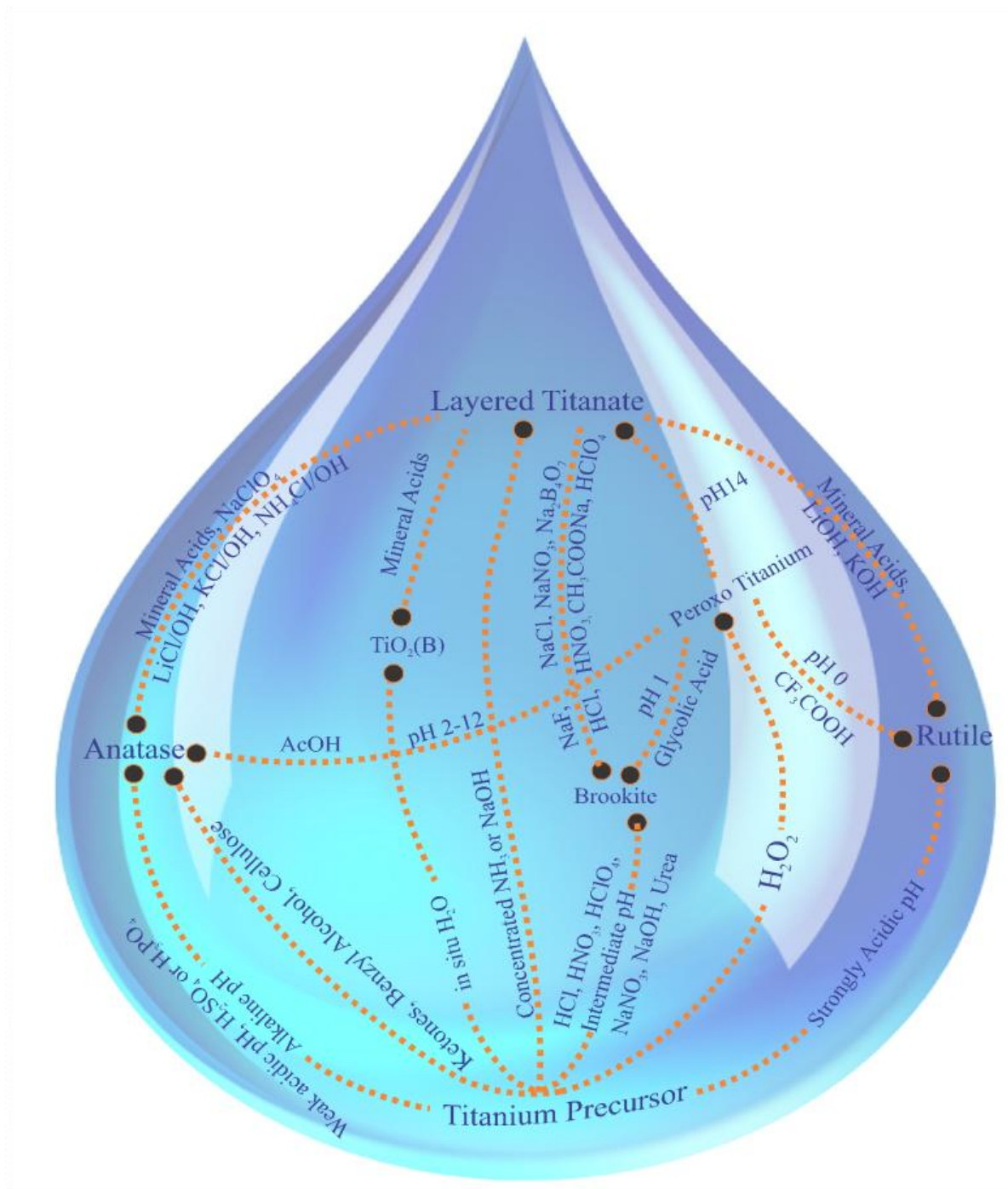


Fig. 31 Transformation of precursor to various titania polymorphs in solution based approach. Mineral Acids = HCl, HNO₃ and H₂SO₄.

Table 1: Some important results of phase transformation/stabilization of titania polymorphs under various experimental conditions.

Titanium precursor	Important results of phase stabilization/transition	Ref.
<i>Hydrothermal/solvothermal method</i>		
Ti(OBu) ₄	Polar water at HCl-toulene interface hydrolyzed titanium precursor to give Anatase-Brookite NPs decorated on Rutile NRs.	49
TiCl ₃	Pure Anatase was synthesized from (NH ₄) ₂ S ₂ O ₈ irrespective of pH and initial precursor concentration, while Rutile was observed at pH 0.44 and Brookite at pH 1.32 with oxidants like H ₂ O ₂ , HNO ₃ and HClO ₄ . The unique transformation sequence was observed via changing the precursor concentration from 0.9 to 0.05 M and pH < 0 – 1.68; rutile → anatase – brookite – rutile → anatase – brookite → brookite → anatase – brookite	67
TiCl ₄	Anatase-Rutile was observed at < 0.5 M. Brookite coexisted at intermediate concentration of 1 M. Pure Rutile at 2 M. The complex [Ti(OH) ₂ (OH ₂) ₄] ²⁺ favored Anatase/Brookite , [TiO(OH) ₅] ²⁺ promoted Rutile nucleus.	79
TTIP	Anatase was crystallized under acid free condition and Rutile with HNO ₃ . Anatase (10 nm) was thermally stable up to 800 °C compared to the samples with 6 and 28 nm particle size prepared at 80 & 240 °C respectively.	120
TiCl ₄	HF and HNO ₃ resulted in poor crystallization of Anatase compared to HCl. Addition of citric acid facilitated the formation of pure Rutile with rod like morphology (pH 0.8) and Anatase-Rutile at pH 1.09. The chelation of citrate on amorphous titania was found to dependent on pH, which influences the phase transformations.	141
Ti(OBu) ₄	Peptizing with TEAOH promoted Rutile formation at a faster rate compared to TMAOH and TBAOH.	156
TiCl ₄	Spherical Brookite-Rutile NPs were observed at 1 M, while pure Rutile NRs with {101} facet was obtained at 0.3 M. The addition of NaCl facilitated the NRs with aspect ratio close to 10.	180
TiCl ₄	<i>In situ</i> generation of water via esterification of alcohol and AcOH gave Anatase with ethylene glycol and Rutile with ethanol.	175 182

In the absence of acid, no product formed with former and **Anatase** crystallized with latter solvent.

TiCl ₃	Anatase-Brookite Observed with Brookite-Rutile Anatase-Rutile	propanol butanol octanol	183
TiCl ₄	Single phase Anatase with Rutile	propanol & butanol octanol	
TiCl ₄	Anatase , Rutile and Anatase-Rutile was observed with ethanol, water and water-ethanol systems respectively in the presence of urea and HNO ₃ .		185
Ti(OC ₂ H ₅) ₄	Anatase was observed with K ₂ SO ₄ , Na ₂ SO ₄ , KCl, NaCl, while different product was observed for NaF salt solutions. The crystallinity was very low due to adsorption of these ions on the titania surface that hinders structure reorganization.		187
TiCl ₄	<i>In situ</i> generation of water from dehydration of acetone oligomers initiated hydrolysis to form Anatase and Rutile at precursor/acetone ratio of 1:15 and 1:10 respectively.		188
TiCl ₃	Addition of tartaric acid promoted BAT and morphology changed from spindle-like to nanorod.		192
TiCl ₃	Anatase-Brookite-Rutile was transformed to pure Anatase with exposed {001} facets via the addition of ascorbic acid.		194
Ti(OC ₂ H ₅) ₄	Powder with very small crystallite size and trace Brookite content along with Anatase promoted ART at a faster rate compared to sample with only Anatase .		195
TiCl ₄	Pure Rutile NRs were observed with water, while addition of TEA as selective adjusting agent promoted Brookite formation.		202
TiCl ₃	Anatase-Brookite-Rutile was observed at pH 1, which transformed to Rutile accompanied by the formation of new corundum like titania phase that was stable up to 900 °C.		206
Ti(OBu) ₄	Anatase formed with n-butanol was stable even after calcination (800 °C) due to capping action of butoxy groups, which inhibited aggregation and reduced inter-particle contact area.		207a
TTIP	Mesoporous Anatase titania was obtained with triblock co-polymer and AcAc and was thermally stable even after calcination (700 °C).		207b
Ti(OBu) ₄	Pure Rutile microspheres were obtained on glass substrate in HCl-toulene suspension.		209
Ti(OBu) ₄	Pure Anatase and Rutile with very small crystallite size was observed from alkaline and from acid peptized gel respectively.		211
TTIP	<i>It was shown for the first time that Rutile content do not monotonically increase with increase in acidity.</i>		212

Rutile content initially increased with increase in HCl/Ti ratio and decreased thereafter

accompanied by the formation of **Brookite**.

TTIP	Anatase was observed with 1.5 M AcOH, while pure Rutile and Brookite was observed at 4 M and 3 M HCl respectively.	213
	Brookite was formed from unsymmetric $[\text{Ti}(\text{OH})_2\text{Cl}(\text{OH}_2)_3]^+$ and Rutile nucleated from symmetric $[\text{Ti}(\text{OH})_2\text{Cl}_4]^{2-}$ complexes.	
TTIP	Anatase with smaller particle size (3.1 & 3.7 nm) underwent ART at faster rate compared to other sample (6.0 & 12.7 nm).	214
	ART via dissolution of Anatase and precipitation of Rutile was observed at pH 1, while partial ART was found at pH 3.	
Ti(OBu) ₄	<i>After the hydrothermal treatment, synthesis step was followed by refluxing with ED.</i>	222
	The synergistic interaction between CTAB with TiO ₂ surface as well as amine groups of ED and TiO ₂ stabilized Brookite up to 800 °C.	
<i>Sol-Gel Hydrolysis</i>		
Ti(OBu) ₄	Hydrolysis with HNO ₃ favored ABT in preference to ART , while BAT dominated under acid free condition.	27
TiCl ₄	The E _a of ART for aged and unaged samples were 426 – 506 and 205 kJ/mol respectively. The large agglomeration number for unaged samples induces interparticle contact to promote Rutile .	31
TiCl ₄	Brookite precipitated along with Anatase at pH 5 to promote ART during calcination, due to high density of potential nucleation site at Anatase-Brookite interface.	96, 242a
TiCl ₄	Alcohol washing of precipitated powders suppressed Anatase crystallization from amorphous, while promoted ART during thermal treatment, as organic impurities on the particle surface served as nucleation sites and also created surface oxygen vacancies.	236, 237
TTIP	The slow hydrolysis of precursor with IPA prevented Rutile precipitation.	245
TTIP	Acidic hydrolysis promoted amorphous to Anatase and ART , while both transformation pathways was inhibited under basic conditions.	248
Ti(OBu) ₄	Gel obtained at pH 5 (or 9) were Anatase , while Anatase-Brookite-Rutile and Anatase-Brookite was formed at pH 3 and 7 respectively after calcination.	253
Ti(OBu) ₄	Mesoporous Anatase was observed using triblock co-polymer EO ₂₀ PO ₇₀ EO ₂₀ as structure-directing agent.	254
TTIP	Addition of Pluronic F127 promoted ABT , while addition of DEA suppressed the Brookite formation.	256
TTIP	Hydrolysis with ethanol and cellophane membrane resulted in thermally stable Anatase up to 900 °C, despite its large grain size (108 nm).	257

TiCl ₄	Low and high titanium concentration favored Rutile and Anatase due to ordered arrangement and increased random organization of octahedral units respectively.	259
TTIP	Anatase/Rutile core/shell structure was formed with PEO and AcAc, with the latter to slow down the hydrolysis rate of precursor and the former to induce nanoporosity.	263
Ti(OBu) ₄	Increase of water content in hydrolysis step favored Rutile with larger particle size during calcination.	61, 269
TTIP	Increase of hydrolysis temperature from 0 – 80 ° C shifted the crystallization and ART temperature to higher values.	271
TTIP	Hydrolysis with AcOH at pH 3 – 4 stabilized Anatase due to the chelation of acetate group on titania surface, while Rutile was favored at pH 5 – 6.	274
TTIP	Chelation of formate via syn-syn mode stabilized Anatase even at high temperature, while addition of water changed the binding mode to syn-anti to produce Rutile at low temperature.	275
TTIP	Addition of butyric acid in the hydrolysis step accelerated the crystallization of Anatase from amorphous and ART compared to AcOH and propanoic acid.	278
TTIP	Mixed Complexing agent like DEA-polyethylene glycol in the hydrolysis promoted Brookite , while AcAc-polyethylene glycol and AcAc-AcOH showed Anatase after calcination (600 °C).	279
Ti(OBu) ₄	<i>In situ</i> generated water via esterification promoted the formation of Anatase-TiO₂(B) .	280
Ti(OBu) ₄	Hydrolysis of titanium glycolate with acetone transformed to Rutile at 850 °C. The water content in acetone was the decisive factor in tuning the final size of particles.	281

Ultrasonication assisted Sol-Gel hydrolysis

Ti(OBu) ₄	Anatase and Rutile was obtained with H ₂ SO ₄ and HCl respectively.	139
	Anatase-Brookite-Rutile was obtained for 1 M HNO ₃ and only Rutile at 2 M HNO ₃ .	
TTIP-TiCl ₄	Anatase , Rutile and Anatase-Rutile was obtained with alkoxide, halide and halide-alkoxide precursors respectively.	174
TTIP	Anatase-Brookite was observed in ethanol-water systems.	297
TTIP	Mesoporous titania with Anatase crystal structure having worm-like framework was observed using long chain organic amines as structure directing agent.	298
TTIP	Mesoporous anatase was obtained under template free conditions, using AcOH as modifying agent.	299
TTIP	Anatase-Brookite was observed using triblock copolymer at neutral pH conditions.	300
TTIP	Anatase-Brookite was observed with pure water, while ethanol inhibited brookite nucleation.	302

TTIP	ABT and ART dominated during initial stages (60 min), followed by BAT (90 min) and BRT (120 min) for tip-type ultrasonication, while bath-type induced only ABT (60-120 min).	304
TTIP	Rutile fraction increased with increase in ultrasonic irradiation amplitude (40 %) and decreased thereafter.	305
TTIP	Photo-illumination during the hydrolysis with HCl promoted Anatase crystallization and ART at low temperature.	306, 307
Ti(OBu) ₄	Photo-illumination during the sol-gel hydrolysis produced Ti ³⁺ resulting in the formation of Anatase TiO ₂ -Ti ₂ O ₃ binary system.	312, 313
TTIP	Rutile was observed at high water content for photo-assisted sol-gel method, while it was obtained for intermediate water content via conventional route.	314
TiCl ₄	Anatase was obtained at very low temperature (80 °C) with t-butylalcohol via alkyl halide elimination.	323

IL assisted Sol-Gel Hydrolysis

TTIP	Increase in the volume of IL during the precursor hydrolysis enhanced the Anatase crystal growth, due to increased viscosity and decreased diffusion co-efficient.	330
TTIP	Addition of [cmim] [HSO ₄] changed the morphology from Rutile NRs to nanoflowers.	331
TiCl ₄	Addition of [emim] [Br] favored Rutile formation, as it anchored on Rutile {110} plane due to favorable geometry.	333
TiCl ₄	Addition of [bmim] [Cl] in water promoted ART , while presence of fluoride or sulfate anions stabilized Anatase .	337
Ti(OBu) ₄	Mesoporous Anatase was observed with [bmim] [BF ₄] at very low temperature (60 – 100 °C) and was stable up to 900 °C.	339
TTIP	The IL/Ti ⁴⁺ ratio of 3:1 was necessary to form crystalline titania.	344
	Porous Anatase with [bmim] [PF ₆] which served as self-assembling template like long chain surfactants.	
	Other ILs like [bmim] [PF ₄], [bmim] [CF ₃ SO ₃] and [hmim] [PF ₆] was not effective to induce mesoporous structure.	
TTIP	Pure Anatase was formed with [C ₃ mimOH] [Tf ₂ N], while Anatase-Brookite was obtained for [P ₆₆₆₁₄] [Tf ₂ N], [N ₁₈₈₈] [Tf ₂ N], [C ₄ Py] [Tf ₂ N] and [C ₄ mim] [Tf ₂ N].	354
TiCl ₄	TiO₂(B) was observed only with ILs based on imidazolium moieties.	355

Thermolysis/Thermohydrolysis

Ti powder	Brookite flowers obtained was stable up to 500 °C.	46
-----------	---	----

TiCl ₄	Anatase-Brookite-Rutile was observed with HClO ₄ (1-5 M), while Brookite-Rutile with 3 M HCl.	86
	Brookite was formed by lowering the concentration of precursor to 0.05 M and [Ti(OH) ₂ Cl ₂ (OH ₂) ₂] ⁰ was solely responsible for its formation.	
TTIP	Anatase-Brookite was obtained in hot water.	256
TiCl ₄	Pure Rutile was observed with ≤ 2 M HCl and Anatase above it.	333
TiCl ₄	Anatase-Brookite-Rutile , Anatase-Brookite , Anatase-Rutile was observed in the region of 0.25 – 0.09, 0.06 and 0.81 – 0.34 M TiCl ₄ respectively.	357
	Brookite content was scarcely affected with water, but increased with increase in aging time (48 – 76 h).	
TiCl ₄	Mesoporous Rutile titania was obtained using ocytl phenol (polyethylene oxide) as surfactant.	358
TiCl ₄	Pure Rutile NRs was obtained with ethanol, while rod-like nanoparticles was obtained with water.	359
TiCl ₄	Water to ethanol ratio	363
	Anatase-Rutile 70:0	
	Brookite-Rutile 50:20	
	Anatase-brookite 20:50	
	Anatase 10:60	
TiCl ₄	Anatase-Brookite-Rutile was synthesized with 1 M HNO ₃ and aging favored ABT and ART .	367
TiCl ₃	Phase transition pathways with increase in pH (1 – 7) followed the order; Rutile → Brookite-Rutile → Anatase-Brookite-Rutile → Anatase-Brookite .	369
TiCl ₄	Anatase with H ₂ SO ₄ or H ₃ PO ₄ , while Anatase-Rutile with HCl/CH ₃ COOH/HNO ₃ .	370
TiCl ₄	Aging the gel by simple boiling for 12 – 48 h promoted Anatase crystallinity and shifted ART to higher temperature.	371
TiCl ₄	Anatase-Brookite was observed after aging in the pH range of 2.7 – 4.0 via addition of NH ₄ HCO ₃ .	373
TiBALDH	<i>In situ</i> generation of hydroxide ion from ≥ 6.0 M urea facilitated high quality Brookite NRs.	380
TiOSO ₄	Ti ₂ O ₃ (H ₂ O) ₂ (C ₂ O ₄).H ₂ O was obtained through the addition of oxalic acid and mesoporous Brookite with high surface area was obtained from oxalate precursor.	384
TiBr ₄	Anatase-Rutile and pure Anatase was obtained with Na ₂ O ₂ depending on refluxing conditions.	389

TiOCl ₂	Addition of NbCl ₅ , NiCl ₂ and FeCl ₃ stabilized Rutile , ZrOCl ₂ favored Anatase and AlCl ₃ promoted Anatase-Rutile .	390
--------------------	---	-----

Microemulsion method

TiCl ₄	Unusual orthorhombic crystal structure was formed.	394
Ti(OBu) ₄	Finely dispersed Anatase (15 nm) nanoparticles were obtained.	403
TiCl ₄	By changing the volume ratio of oil to water in reverse microemulsion, Rutile changed its morphology from nanocluster to nanospherules, then grew into nanodumbbells and finally nanorod was obtained.	404
TiCl ₃	Pure Anatase was obtained with urea dissolved in water, while Anatase-Rutile for urea dissolved in HCl.	407
Ti(OBu) ₄	Anatase 0.5 M HNO ₃ Rutile ≥1.0 M HCl Anatase-Rutile 1 M HNO ₃ and ≤ 0.5 M HCl	410
TiCl ₄	Anatase hollow spheres were obtained and its thickness was directly proportional to precursor concentration.	411a

Preparation with various titanium precursor

[N(CH ₂ CH ₂ O) ₃ Ti-O ⁱ Pr]	Rutile was directly formed from this precursor without Anatase .	391
Water soluble titanium complexes	Anatase was selectively synthesized from citric acid, tartaric acid and malic acid, while Rutile with glycolic acid and Anatase-Rutile with lactic acid.	415
TiB ₂	Nanocone Rutile was obtained at 1 M HCl and 3 mM Na ₂ SO ₄ and Anatase with 0.5 M HCl, while Brookite was observed with HNO ₃ .	416
TiOF ₂	Anatase formed was stabilized up to 900 °C due to adsorption of fluoride ions.	418
TiBALDH	The complete hydrolysis of precursor (pH 10 – 11) resulted in Anatase , partial hydrolysis (pH 9) showed Anatase-Rutile , and extreme stability at neutral pH lead to the formation of Rutile .	424
TiO _x C _y /C	Rutile/Anatase core/shell structure was obtained.	428
TiS ₂	Layered titanate was obtained at very low concentration of NaOH (1-2 M) owing to low bond strength of Ti-S. ABT was favored at very low concentration of NaOH (0.5 M) and pure Brookite was observed at 1.2 M NaOH.	429
TiOSO ₄	Pure Anatase was observed at pH < 7, layered titanate at neutral pH and pure Brookite at alkaline conditions using 0.21 M NaOH. In contrast, Anatase-Rutile was observed	430

with LiOH and KOH. The as obtained **Brookite** flowers were thermally stable up to 900 °C.

Ti(SO ₄) ₂	Pure Rutile was observed after peptizing the precipitate with HNO ₃ at room temperature.	432i
Ti(SO ₄) ₂	Anatase , Anatase-Brookite and Brookite was obtained at pH 5, 6 – 9 and 10 – 11 respectively.	432j
Ti(SO ₄) ₂	Anatase-Rutile hollow spheres were observed with H ₂ O ₂ at pH 1.	432k
Ti(SO ₄) ₂	Pure Anatase hollow spheres were obtained with NH ₄ F-H ₂ O ₂ system.	432l

Preparation of titania from layered titanate precursor

H ₂ Ti ₅ O ₁₁ ·3H ₂ O	Unique phase transition sequence: Anatase to Rutile to Anatase was observed via increasing hydrothermal aging time under acidic peptized conditions.	128
H/K titanate	Brookite-Rutile-TiO₂(B) was observed with 0.2 – 2.0 M HCl and 0.5 – 0.15 M HNO ₃ . Pure TiO₂(B) was formed for 0.1 and 1mM HNO ₃ .	442
H ₂ Ti _n O _{2n+1}	ABT was preferred with HClO ₄ and HNO ₃ .	445
H ₂ Ti ₃ O ₇ ·xH ₂ O	Anatase and Rutile was observed with 0.05 M and 2 M HNO ₃ respectively at 30 °C. Titanate prepared at low temperature (≤ 100 °C) transformed to Anatase at 400-500 °C, while those prepared at 200 °C was thermally stable up to 650 °C.	447
(NH ₄) ₂ Ti ₂ O ₅ ·H ₂ O	Anatase was formed in alkaline medium due to deintercalation of NH ₄ ⁺ ions. Presence of NaCl (or NaF) results in Brookite Presence of NaNO ₃ , Na ₂ B ₄ O ₇ and CH ₃ COONa also favored Brookite depending on its concentration and hydrothermal aging time. Mixture of NH ₄ F and NaF favored pure Anatase , although it was not observed with only NH ₄ F or NaF.	450-454
K ₂ Ti ₂ O ₅	Anatase core was stabilized up to 900 °C, due to the presence of TiO₂(B) shell.	467
H ₂ Ti ₄ O ₉ ·1.2H ₂ O	Anatase-Rutile was observed with varied concentration of mineral acids.	468
H ₂ Ti ₄ O ₉ ·nH ₂ O	Pure Anatase was observed with water and TiO₂(B)-Anatase with methanol and ethanol.	473

Preparation of titania from PTC

PTC	Pure Rutile at pH 0, Anatase in wide pH range 2 – 12 and lamellar hydrogen titanate was formed at pH 14.	32
-----	--	----

PTC	Brookite-Anatase was observed at pH 1.	33
PTC	Addition of AcOH yields Anatase-Rutile .	483
PTC	Modification with H ₂ O ₂ resulted in thermally stable Anatase up to 900 °C because of increased Ti-O-Ti bond strength.	489
PTC	PTC derived from TiCl ₄ showed Anatase , while Anatase-Rutile from TTIP.	491
PTC	Pure Brookite was obtained with glycolic acid and transformed to Rutile at 1125 °C, with critical size for BRT was found to be 24 nm.	493
PTC	Rice like Rutile was observed via addition of CF ₃ COOH.	495

Preparation of titania via non-aqueous route

TiX ₄	Rutile was favored with increase in nucleophilicity of halide in the precursor.	506
TiCl ₄ - Ti(OBu) ₄	Mesoporous Anatase-Rutile was obtained and Anatase content decreased with increase in [TiCl ₄].	507
TiCl ₄ -TTIP	The gel obtained with CCl ₄ at low hydrothermal temperature (140 °C, 3 h) showed maximum Rutile content compared to sample obtained at high temperature (160 °C, 3 h) after thermal treatment.	511
TiCl ₄	<i>In situ</i> generation of water due to condensation of BA at Ti centers initiates nucleation and growth of titania NPs.	513, 514
	The reaction was illustrated from the prospect of S _N 1 mechanism.	
TiCl ₄	Reaction medium containing TiCl ₄ and BA seeded with ST21 (commercial Anatase) resulted in Anatase-Rutile .	515
TTIP	Anatase nanoplatelets were observed with benzyl amine or m-xylene diamine.	517
TTIP	Anatase was observed in the presence of various ketones as oxygen donors.	518
TiCl ₄	Rutile content decreased with increase in carbon chain length of primary alcohols, while Anatase-Rutile and Brookite-Rutile was observed for secondary and tertiary butanol respectively.	519
TiCl ₄	Anatase NPs and Rutile NRs was obtained at high and low mole ratio of TiCl ₄ /n-butanol respectively, while only Anatase was observed with ethanol irrespective of its concentration.	521
TiCl ₄	Anatase was obtained with natural cellulosic material as oxygen donors.	523

Preparation of titania via mechanical activation (ball milling method)

Anatase (70 nm)	ABT dominated for the milling speed of 500 rpm, while ART and BRT prevailed at 600 rpm.	109
TiOSO ₄ . xH ₂ O	The Rutile was observed with Na ₂ CO ₃ .	529
Anatase	Smaller particle size (22 nm) transformed to Srilankite and Rutile at a faster rate compared to large crystallites (96 nm).	533
Anatase (270 nm)	High pressure polymorph of titania (orthorhombic; α-PbO ₂) was observed.	538
Anatase-Rutile (34.3:43.1 nm)	Anatase-Rutile-Srilankite was observed at initial stages of ball milling. Anatase transformed to Srilankite rather than to Rutile .	539
Anatase-Rutile (17 nm)	Anatase-Rutile transformed to Srilankite or became amorphous at later stages of milling. Increase of temperature during milling in air cooled conditions destabilized Anatase , while milling under water cooled conditions inhibited Rutile .	541
Anatase (30 nm)	Transformation rate of Anatase to Srilankite and Rutile increased with decrease in oxygen partial pressure of milling atmosphere.	542
Anatase (136±51 nm)	Anatase to TiO ₂ II phase transformation rate was faster for high powder to ball weight ratio.	543
Anatase (70 nm)	Increasing milling time did not affected phase transformation, but milling speed and ball to powder ratio leads to high energy release for each particles to facilitate phase transition.	544
(TiOSO ₄ .xH ₂ O .yH ₂ SO ₄)	Rutile formation was suppressed in the presence of NaCl as diluents phase.	546

Note: For detailed experimental conditions, readers are requested to follow the corresponding references.